MECHANISTIC STUDIES OF ELECTROCATALYTIC PROCESSES: UPGRADING OF LIGNIN MONOMERS TO BIOFUELS (PROBING SUBSTRATE SYNERGY); ALKYLATION OF AMINES WITH ALCOHOLS VIA BORROWING HYDROGEN MECHANISMS; AND REDUCTION OF THE CARBOXYLIC ACID FUNCTIONALITY IN AMINO ACIDS

By

Benjamin Appiagyei

A DISSERTATION

Submitted to
Michigan State University
in partial fulfilment of the requirements
for the degree of

Chemistry—Doctor of Philosophy

2020

ABSTRACT

MECHANISTIC STUDIES OF ELECTROCATALYTIC PROCESSES: UPGRADING OF LIGNIN MONOMERS TO BIOFUELS (PROBING SUBSTRATE SYNERGY); ALKYLATION OF AMINES WITH ALCOHOLS VIA BORROWING HYDROGEN MECHANISMS; AND REDUCTION OF THE CARBOXYLIC ACID FUNCTIONALITY IN AMINO ACIDS

By

Benjamin Appiagyei

Electrochemical synthesis of organic compounds provides a means to revolutionize synthetic industrial chemistry by developing green, cost-effective processes that compete with traditional synthetic routes. For instance, bio-oil, the liquid product from biomass pyrolysis, can be reductively stabilized with electrocatalytic hydrogenation (ECH) using Raney™ Nickel as the cathode under very mild conditions (75 °C, 1 atm, H_2O as electrolyte). This process can be achieved via traditional catalytic hydrogenation protocols, but under harsher conditions of pressurized hydrogen gas and elevated temperature. Electrocatalysis also enables amines to be directly alkylated with low cost and readily available alcohols as electrophiles, where water is the solvent and the only byproduct. Classical alkylation of amines employs alkyl halides or their analogues as electrophiles which leads to a side stream of acids or wasteful salt byproducts. In a third application, ECH provides a means to reduce the carboxylic functionality of amino acids to form amino alcohols. Carboxylic acids are conventionally converted to alcohols using strong reducing agents such as $LiAlH_4$ and BH_3. Not only are these reagents costly for large scale production, but they are also hazardous and, like the alkylation above, produce substantial waste byproducts. The outstanding nature of these electrocatalytic methods is the ability to use clean electrons from electricity and protons from water to achieve mild organic transformations using easily prepared heterogenous electrocatalysts, which also allows easy separation and catalyst reusability.

This dissertation investigates the mechanisms of three processes: (1) Acknowledging the fact that though a complex mixture of lignin monomers may polymerize under catalytic acid or base and high temperature conditions, we envisage that they may also mutually interfere in the catalytic reduction processes, so the understanding of such interactions is essential to success in moving from model systems to real bio-oil. (2) Abstracting hydrogen (H_2) from the CHOH moiety of an alcohol generates a carbonyl group, a good electrophile which enables reductive alkylation of an amine to the corresponding alkylamine via the so-called borrowing hydrogen mechanisms. (3) Electrocatalytic *in-situ* generation of hydrides on an electrode surface can reduce the carboxylic acid functionality, while retaining the stereochemistry on the amino position of the amino acids.

ACKNOWLEDGEMENTS

I would like to sincerely express my profound gratitude to God for watching over me in my journey through life and for this achievement. I was blessed with a wonderful advisor Dr. James (Ned) Jackson who is an outstanding scientist and a mentor. He understood me from where I was and allowed me to grow both professionally and personally during my time here in MSU. Ned entrusted me with over 15 undergraduate and high school researchers who worked under my supervision and mentorship. Through this and many other experiences, I have refined my critical thinking and communication skills and gained intellectual freedom to develop my profession. I would like to express my profound gratitude to him and his family for their continuing friendship. I would also like to thank my parents, Cecilia and Raphael Ampomah for their unconditional love and financial support in my life and allowing me to pursue my dreams. To my most favorite people, my Godparents, Victoria and John Amoah, I cannot be thankful enough for your selfless love and the life's examples you showed me while I was living with you. I would like to honestly thank my dearest wife, Michelle and our children Madison, Macey, Cash and Kelvin for allowing me to take time away from them to focus on my research.

My time at MSU has been full of new experiences and fun; the snow, the freezing rain, the colors of the leaves during fall, the football games (Go Spartans!) and the amazing friends. I am grateful to the graduate school and the MSU Chemistry department for the financial support through graduate assistantship. I would like to thank Dr. Robert Maleczka Jr. for recruiting me during his trip to West Africa and his research presentation delivered at University of Ghana in 2014. This academic achievement would not have been possible if it wasn't for him and his diligence in recruiting young African scholars to pursue Ph.D. in chemistry. I am forever grateful to him.

I would like to thank the past and present lab members of the Jackson group for listening to my presentations in group meetings over the years and offering me their constructive critics: Dr. Tayeb Kakeshpour, Dr. Pengchao Hao, Dr. Souful Bhatia, Dr. Greg Spahlinger, Dr. Fang Zhen, Gracielou, Yuting, Cesar, Monique and Sophie.

The completion of this dissertation would not have been possible without the assistance of my guidance committee; Dr. William D. Wulff (second Reader), Dr. Greg Swain and Dr. Christopher M. Saffron. Thank you all for your time and assistance over the years. Finally, thanks to Dr. Dan Holmes for his training and assistance with the NMR instruments, Dr. Kathryn Severin for her training with the department GC-MS and lastly, Zhongyu and Meheryar in the Saffron group for their assistance in using their lab GC-MS.

TABLE OF CONTENTS

LIST OF TABLES

LIST OF FIGURES

LIST OF SCHEMES

CHAPTER 1: LITERATURE REVIEW ON FOSSIL CARBON REPLACEMENT WITH BIOMASS CARBON VIA ELECTROCATALYSIS

Introduction

Organic electrosynthesis, though a minor part of electrochemistry, has demonstrated an outstanding potential to revolutionize classical industrial organic synthesis protocols due to its environmental compatibility. Most importantly, electrochemistry provides tools that can replace toxic oxidizing or reducing reagents and reduce energy consuming processes. This dissertation has focused on developing green electrochemistry methodologies for organic synthesis. Electrochemistry provides a means to tap directly into non-fossil alternative sources of energy such as from wind, sun, water etc. (electrons are inherently clean reagents) as the driving force for chemical processes. Reaction monitoring in real-time is also possible in electrochemical processes, thereby enhancing mechanistic studies and identifying errors in the early stages of reactions. Electro-synthetic methods are not only associated with less or no pollutant byproducts; they are also promising methods for removing dangerous pollutants from the environment. For example, a current concern is the need for removal of Poly- or Per-fluoroalkyl Substances (PFAS) from drinking water. It must be noted that electrochemistry process cannot be considered completely clean unless the source of electricity is produced from an alternative source rather than combustion of fossil carbon.

A Brief History of Organic Electrosynthesis and Recent Advances

The development of organic electrosynthesis has progressed based on the wealth of ideas and discoveries made by some scientists in the early 1800s. In 1833 Faraday discovered Faraday's law (Q = *nNF,* where Q = charge consumed, *n* = moles of electrons involved per mole of compound being transformed, *N* = moles of compounds being transformed, *F* = Faraday's constant) and in 1834 discovered that hydrocarbons could be formed by electrolysis of acetic acid salts.[1] Though the nature of the product was unidentified, in 1849 Herman Kolbe discovered the Kolbe electrolysis reaction which was the oxidation of a carboxylic acid (RCOOH) with a platinum electrode to form the dimeric alkane (R-R) and CO_2.[2]

The Kolbe reaction opened the door to electrosynthesis which led to several variations of the reaction process. In 1902, Hofer and Moest modified the Kolbe reaction by converting aliphatic carboxylic acids to alcohols with loss of CO_2 by electrolytic decarboxylation in a neutral or alkaline solution in the presence of inert anions such as sulfate, phosphate, carbonate or bicarbonate. The *Hofer-Moest* reaction[3] suggested that the addition of the inert anion favored the formation of the carbocation intermediate rather than the radical intermediate. The normal stable radical intermediates lead to hydrocarbon formation via the *Kolbe reaction,* whereas the carbocation favors the *Hofer-Moest* reaction, a non-Kolbe reaction.

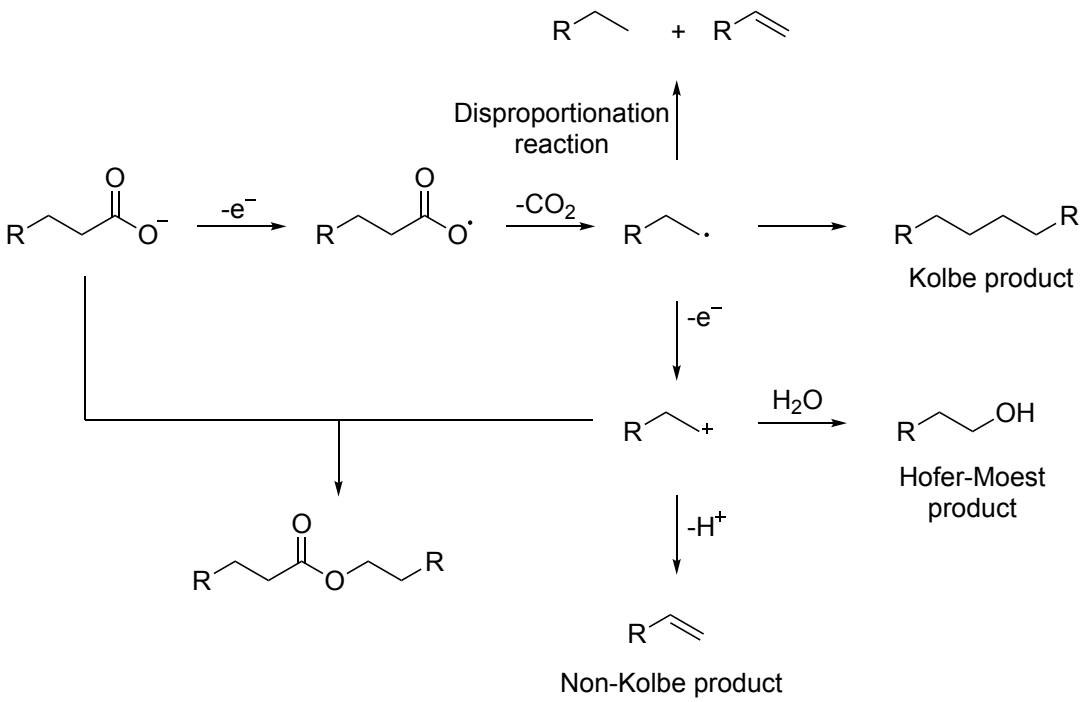

Figure 1.1. Reaction mechanism for the formation of Kolbe, Non- Kolbe and Hofer-Moest products.[4]

The second variation of the Kolbe reaction was the Crum Brown–Walker oxidation which demonstrated the oxidation of a monocarboxylate monoester to a diester. This process was adopted for the commercial preparation of sebacates from adipates. These processes, however, release the carboxylate carbon as CO_2 from each acid.[5]

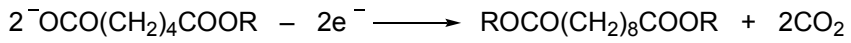

Figure 1.2. Crum Brown–Walker reaction for the synthesis of sebacates from adipates

The large scale electrosynthesis of the Nylon precursor adiponitrile via electrohydrodimerization from acrylonitrile was developed by Baizer in 1980, bringing about a revolution in electro-synthetic methods.[6] During the 20th century to present, there have been a series of developments in

organic electrosynthesis that are captured in the historical reviews of Lund[7] and Palkovits[4]. In the Kolbe reaction mechanism, the dimerization process is successful with radicals which may be resistant to further oxidation. The reported threshold for the ionization potential is about 8 eV hence methyl (8.75 eV), isobutyl (8.35 eV), cyanomethyl (10.87 eV), and dimethylcyanomethyl (9.15 eV) radicals resist ionization and follow the Kolbe reaction. On the other hand, radicals with lower ionization potentials such as isopropyl (7.90 eV), *t*-butyl (7.32 eV), cyclohexyl (7.60 eV) and benzyl (7.76 eV) readily undergo further oxidation to form carbenium ions which may follow reaction processes such as polymerization, rearrangement, deprotonation or reaction with nucleophiles.[8]

Electrocatalysis Functional Group Interconversions

Oxidation

Oxidation of Alcohols

Oxidations of alcohols to aldehydes, ketones, carboxylic acids or the fully oxidized form, CO_2[9] are among the main reactions of organic chemistry. These functional group interconversions allow the alcohols to be converted from nucleophilic species to electrophilic ones (aldehydes, carboxylic acids and carbon dioxide). The classical alcohol oxidation such as Swern oxidation uses oxalyl chloride in DMSO followed by triethylamine. Also, reagents such as pyridinium chlorochromate (PCC) and pyridinium dichromate (PDC) are used to convert primary alcohols to aldehydes. Jones reagents (CrO_3) and nitric acid transform primary alcohols to their carboxylic acid congeners.

An example of an electrocatalytic alcohol oxidation that has gained interest recently is the use of *N*-hydroxyphthalimide (NHPI) and (2,2,6,6-tetramethylpiperidin-1-yl)oxyl (TEMPO) as catalysts.

Rafiee *et. al* have explored the power of NHPI and TEMPO as catalysts for electrocatalytic oxidation of alcohols to aldehyde. This reaction works well when a double mediated system of Br^{-}/Br_2 and $TEMPO_{(red)}/TEMPO_{(ox)}$ are used.[10]

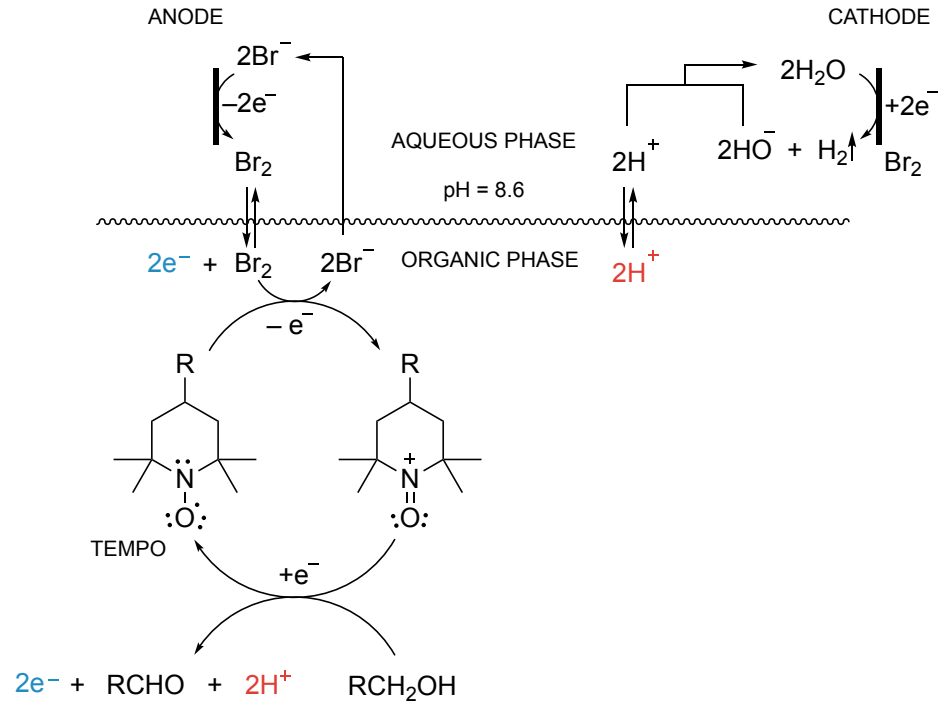

Figure 1.3. The general mechanism for the electrooxidation of alcohols with a double mediator $R_2N{=}O^{+}/R_2N{-}O^{\bullet}$ and Br_2/Br^{-} in a two-phase system.

As a tool, TEMPO oxidation of alcohols has been reported to be favored in mild alkaline solution whereas the NHPI worked best in dilute acetic acid. NHPI generates the phthalimide-N-oxyl (PINO) radical in-situ, where it then acts as an active oxidizing agent through a radical chain pathway. [11]

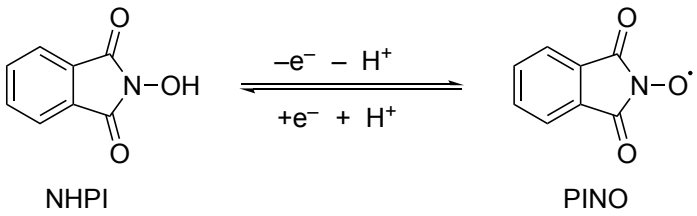

Figure 1.4. Electron-transfer reactions of TEMPO and PINO.

Oxidation of Aromatic Compounds

Mechanistically, aromatic electro-oxidation occurs via electron transfer to the anode giving rise to a cationic species which may react with the solvent. Aromatic ethers follow this mechanism quite readily due to the well stabilized cationic intermediate formed. For instance, the oxidation of hydroquinone dimethyl ether to benzoquinone may follow a mechanism whereby the overall loss of two electrons (simultaneously or stepwise) might occur followed by the reaction of the cationic species (cationic radical or dication) with water to form the unstable bis-hemiacetal hydroquinone. The latter readily decomposes to benzoquinone and methanol.[8]

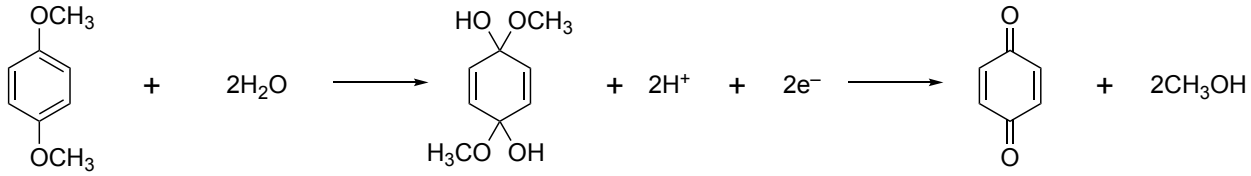

Figure 1.5. Electrocatalytic oxidation of bis-hemiacetal hydroquinone

Oxidation of Amines

Amine oxidation has been the way to degrade complex amine compounds for identification and proof of structure. Although all amines can be oxidized by first, loss of electron on the nitrogen followed oxidation of the alkyl group. Only tertiary amines form amine oxides with peroxide. The reaction of a tertiary amine with peroxide occurs by a nucleophilic attack of the nitrogen on the oxygen resulting in the formation of hydroxy ammonium ion and hydroxide anion. The hydroxide ion subsequently picks up the proton from the hydroxy ammonium ion releasing amine N-oxide.[12] Arylamines tend to be easily oxidized with oxidation occurring at the amine group as well as on the ring.

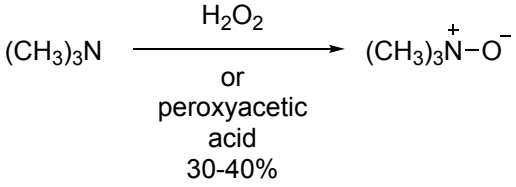

Figure 1.6. Oxidation of trimethylamine

Reduction

Aldehydes and Ketones

The reductions of ketones and aldehydes are classically achieved using hydrides, catalytic hydrogenation, and in some cases baker's yeast. In 1937, the electrochemical synthesis of sorbitol and mannitol from glucose was officially practiced by Atlas Powder Co. in the United States. The electrochemical reactor was an open-top divided cell fitted with an amalgamated-lead cathode and a lead anode. The catholyte was an aqueous solution of sodium hydroxide and the anolyte was dilute sulfuric acid. In the basic solution D-glucose isomerized partially to mannose and both D-glucose and mannose were reduced to sorbitol and mannitol.[14]

Reduction of Carboxylic Acids

Selective electroreduction of carboxylic acid to aldehyde or alcohol is a challenging process. Strongly reducing hydride reagents such as $LiAlH_4$ and BH_3 are mostly employed for the reduction of carboxylic acid to primary alcohols whereas the specialized reagents DIBAL-H is employed for reduction to aldehyde. Though $NaBH_4$ does not reduce carboxylic acids under ambient conditions, Periasamy et al. have reported selective reduction with $NaBH_4$ and I_2 to alcohols. A selective reduction of cinnamic acid to the corresponding α,β-unsaturated alcohol was reported.[15]

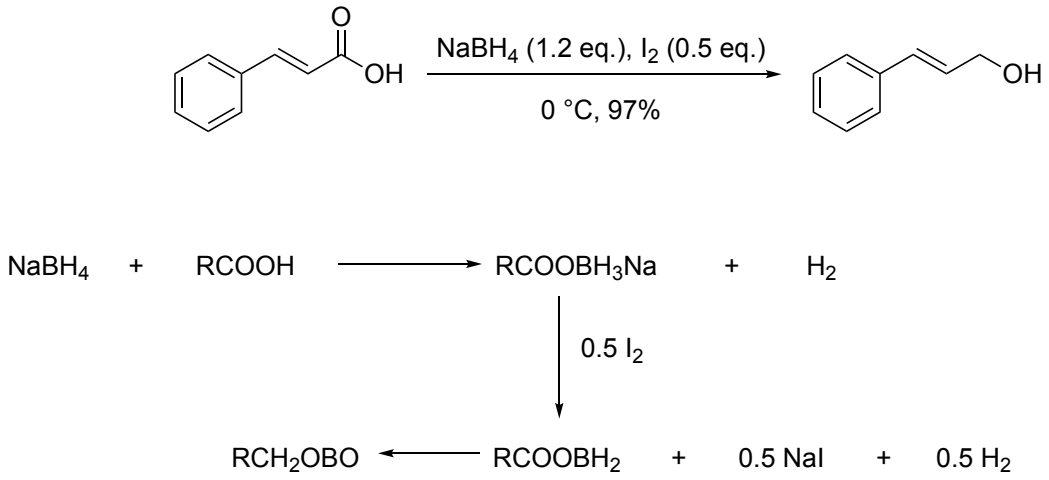

Figure 1.7. Reduction of α-β unsaturated carboxylic acid to allylic alcohol

Formation of aldehydes from carboxylic acid is hard to achieve but Brookhart et al. reports a more attractive method in which hydrosilylation of a carboxylic acid occurs with the aid of a Lewis acid $B(CF_5)_3$ to form a disilyl acetal which is easily converted to aldehyde by acid hydrolysis.[16]

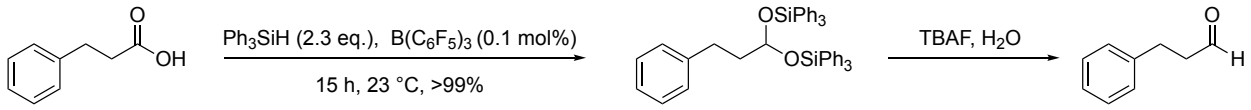

Figure 1.8. Selective reduction of carboxylic acid to aldehyde

Electroreduction of Aromatic Carboxylic Acids

Electrolytic reduction of aromatic acids has been studied under atmospheric pressure and in open vessels. Carl Mettler in 1905 demonstrated the electroreduction of benzoic acid to benzyl alcohol in aqueous alcoholic sulfuric acid at 6-12 Am/cm^2 on lead electrodes at 20-30 °C and yielded 70-90% product. [17] Stein et al. also demonstrated similar selective electroreduction of benzoic acid to benzyl alcohol with 20% sulfuric acid in ethanol with 4-20 Am/cm^2 on cylindrical lead electrodes at 30°C and had over 80% yields.[18] Presumable an *in-situ* formed ester intermediate is more susceptible to electroreduction than a plain carboxylic acid. However, at that acid concentration, the R-COOH is protonated, so may be good at accepting an electron from Pb, which is bad at reducing protons to make H_2.

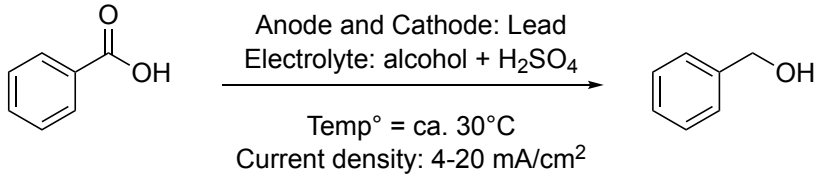

Figure 1.9. Selective electrocatalytic reduction of benzoic acid to benzyl alcohol

Selective electroreduction of benzoic acid and salicylic acid to benzaldehyde and salicylaldehyde respectively have been studied with mercury cathodes as well. The electrolytes used here were boric acid and sodium carbonate solution with hot benzene or toluene as a co solvent. Using benzene as co-solvent removed the aldehyde from the aqueous solution to prevent its further conversion to the alcohol. It was proposed that it was the formation of sodium amalgam that converted the acid to aldehyde.[19,20]

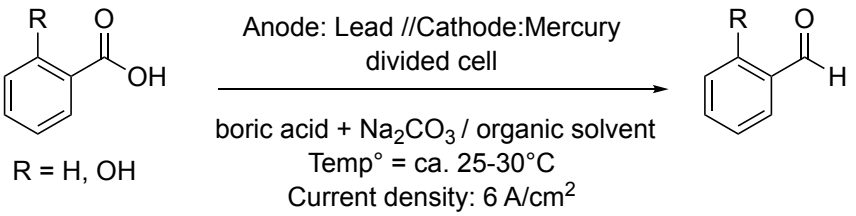

Figure 1.10. Electrocatalytic reduction of benzoic acid and salicylic acid to benzaldehyde and salicylaldehyde

Electroreduction of aromatic acids under pressurized hydrogen and carbon dioxide gases have also been explored, investigating the effect of pressure on the electrolytic system. The reactions were performed at 6 A/dm^2 with pressure of 1-30 atm with temperature maintained at 50°C using water bath. It was observed that the yield and current efficiency increased with increasing pressure. Thus, over the range of 1-30 atm yielded 50-81.3% and current efficiency of 44.6% to 71.4% respectively. It was observed that the gas used had no effect on the yield and C.E at 1 am but a very significant effect on the results at high pressures. For instance, individual reactions at 1 atm with H_2 or CO_2 gave 44.6% yield and at 30 atm gave 71.4% to 54% yields respectively. The effect of pressure was also investigated for electrochemical conversion of benzoic acid to benzaldehyde. Here, a mercury cathode was used in a mixture of sulfuric acid and ethanol. The reaction was conducted at 20-25 °C at 1-30 atm. Similar to the effect of pressure on the benzoic acid to benzyl alcohol reduction, at 1 atm, H_2 or CO_2, yielded 16.3% each with C.E of 7.6% whereas at 30 atm 43% yield was achieved with H_2 and only trace reduction was observed for CO_2. [21]

Nitro-compounds

Electrocatalytic reduction of aromatic nitro compounds may be the most studied organic reduction process. Electrochemical synthesis of quinolone and quinoxaline have been achieved on

Raney Nickel electrodes via intramolecular amide formation from the hydroxylamine formed through electrohydrogenation of the corresponding nitro-compounds by Lessard et al.[22]

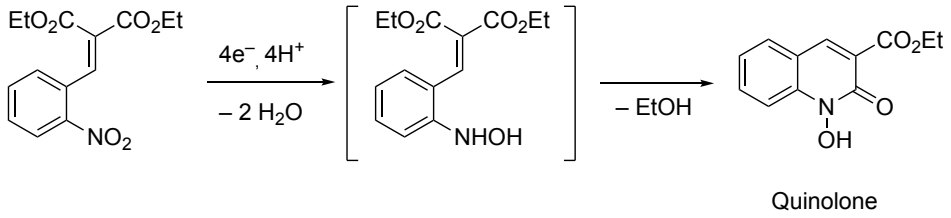

Figure 1.11. Electrochemical synthesis of quinolone

Similarly, the electrosynthesis of (ethyl 4,5-dihydro-4-oxo-5-hydroxy-1,2,4-triazolo [1,5-a] quinoxaline-2 -carboxylate) was achieved with 85%, whereas the classical synthesis was reported to have yielded 65%.[23]

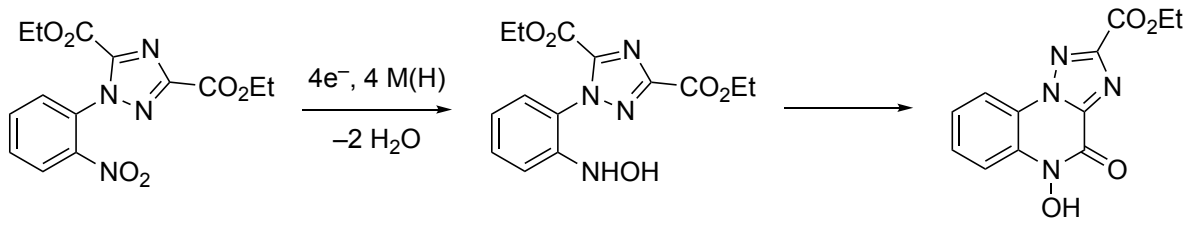

Figure 1. 12. Electrochemical synthesis of quinoxaline

Nitriles

The electrochemical reduction of organic nitriles in acidic medium gives amines whereas in alkaline or neutral medium the C-CN bond is cleaved. However, α,β-unsaturated nitrile undergo electrohydrodimerization in an alkaline medium.[24] The extent of dimerization is affected by factors such as reduction potentials, electronic and steric effects. Reduction with cobalt-based molecular electrocatalysis was reported to convert acetonitrile to ethylamine. Two cobalt bis-iminopyridines, $[Co(DDP)(H_2O)_2](NO_3)_2$ (1, DDP = cis-[1,3-bis(2-pyridinylenamine)] cyclohexane) and [Co(cis-

DDOP)(NO_3)](NO_3) (2, cis-DDOP = *cis*-3,5-bis[(2- Pyridinylenamine]-*trans*-hydroxycyclohexane)[25] were explored for their HECs potential and high selectivity for acetonitrile reduction. Also, the electrochemical reduction of adiponitrile to hexamethylenediamine using nickel electrode has been studied

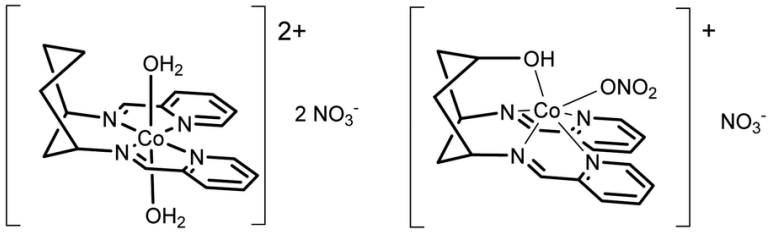

Figure 1. 13. Cobalt catalysts for electrocatalysis of nitrile reduction.

Imine

Reductive amination or reductive alkylation reactions of ketones or aldehydes with amines proceed via formation of an imine intermediate which is then reduced by mild reducing agents such as $NaBH_3CN$. Electrocatalytic reductive aminations of electron-deficient aldehydes and ketones have been developed by Zhou et al. which were applied to the synthesis of (±) clopidogrel, a medication for reducing the risk of heart disease and stroke in patients with high risk.[26]

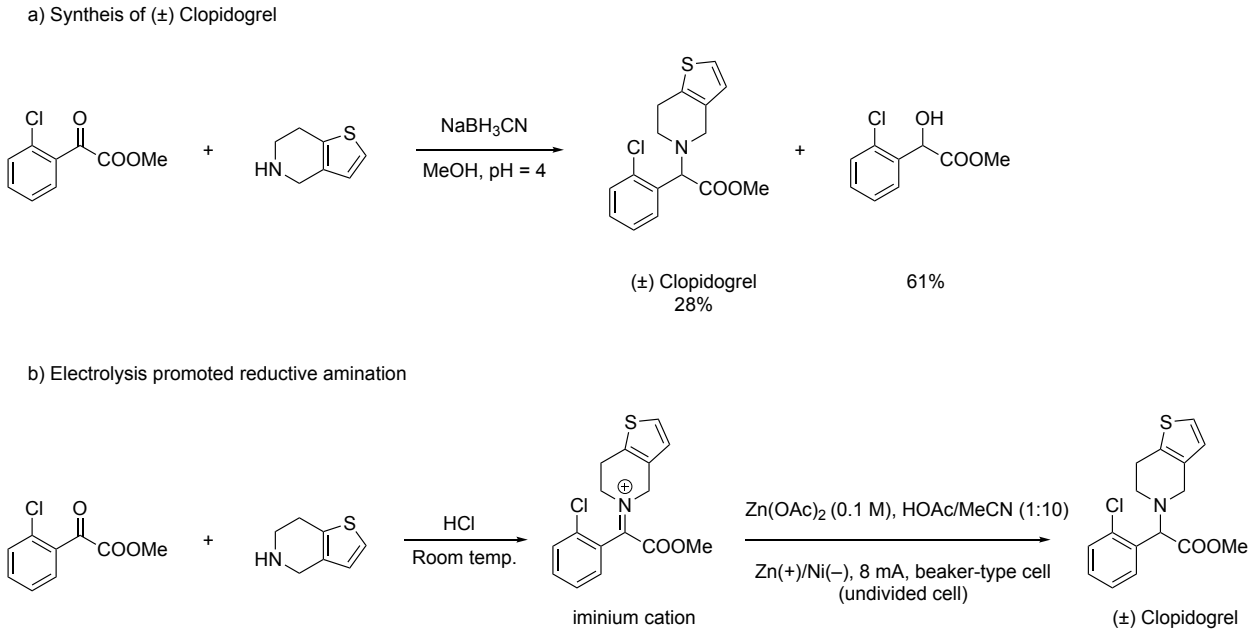

Figure 1. 14. a) The traditional synthesis and b) electrocatalytic synthesis of (±) clopidogrel

Replacement of Fossil Carbon with Biomass Carbon

Biomass Conversion to Fuels

Due to the non-renewable nature of fossil carbon (petroleum, coal, natural gas) fuel and the increasingly urgent threat of global warming and sea level rise due to greenhouse gas emission, there is a pressing need for scientists to explore alternative fuel sources based on cycling carbon. This problem has a major impact on a country's economic and political strength. Biomass, the most abundant and cost-effective form of carbon (plant source), if effectively tapped could replace a significant fraction of the fossil carbon used today. Biomass basically is the organic material on earth that has stored the solar energy in the form of chemical bonds. The first generation of biomass conversion to fuel focused on bioethanol formation via conversion of sugars from corn starch and sugar cane through enzymatic and fermentation processes. The challenges facing these methods are; (1) the use of food plant consumed by humans and other animals, putting fuel formation into conflict with food supply; (2) the cost of obtaining enzymes in pure form to enable the needed digestion reactions; and (3) the use of arable lands reserved for the growing of the starting materials. These standing challenges have led to a second generation of biomass conversion efforts that focus on non-edible biomass such as trees, grass and agricultural waste, materials referred to as *lignocellulosic biomass*. This route also comes with major challenges, the most significantly, the much more heterogenous nature of biomass and the need for harsher conditions to effective convert it into fuel and platform chemicals. Thermochemical conversion is by far the most effective and promising method for utilizing lignocellulosic biomass. The advantage of this method lies in its simplicity, its feedstock flexibility, and its potential to be integrated into the oil-refinery industries, connecting it to with the current fuel distribution infrastructures.

Gasification is another possible route for fuel production from biomass, which entails biomass conversion at high temperature to syngas, a mixture of CO and H_2. The hydrogen can be isolated for fuel cell reactors or the mixture could serve as feedstock for a Fischer-Tropsch reactor to form liquid hydrocarbon fuels. Another promising method is fast pyrolysis; Here a rapid of heat of the biomass to an intermediate temperature (5-600°C) in an anaerobic atmosphere. This process converts it to bio-oil (liquid), biochar (solid), non-condensable gases and heat. The liquid bio-oil is relatively acidic and unstable (reactive), and hence requires prompt to upgrading to stabilize and increase its energy content (i.e. fuel value). In sum, lignocellulosic biomass provides an alternative source of energy and a favorable effect on global warming since the carbon introduced into the environment is recycled by plants, avoiding the introduction of additional fossil carbon (new carbon) into the atmosphere and environment.

Biomass Fast Pyrolysis

The 2010 techno-economic analysis of Anex et al. suggested that fast pyrolysis is the least costly method for biomass upgrading compared with gasification and biochemical methods.[27] Biomass pyrolysis is achieved at high temperature (400-700 °C) and a heating rate of 50-1000 °C/min in an inert atmosphere. The purpose of fast pyrolysis is for bio-oil production though more solid char is formed at lower temperature slower heating and CO, CO_2 and CH_4 increase at higher temperatures. The liquid bio-oil is usually dark-brown, oxygen rich and suffers from; (1) high viscosity, (2) high-reactivity and (3) low specific energy. The high viscosity is due to the incomplete breakdown of lignin leaving behind dimers, trimers, and oligomers. The high reactivity is associated the low pH = 2.5, large due to the presence of acetic acid, which can catalyze polymerization processes with other components such as formaldehyde, furfural, phenolic

compounds, carboxylic acids and derivatives. Bio-oil has a low energy content due to the high content of oxygen in contrast to petroleum. The specific energy for petroleum fuel is about 45 MJ/kg whereas bio-oil is about 18 MJ/kg. It is this high oxygen functional group composition that justifies the need for stabilization and energy upgrading.

Boateng et al. investigated the elemental composition of switchgrass and alfalfa stems and compared it to the elemental composition of the bio-oil obtained from these feedstocks by fast pyrolysis.[28] The results in both cases similar with slightly higher carbon content in the alfalfa bio-oil.

Table 1.1. Analysis of biomass samples before pyrolysis[28]

db = dry basis

	switchgrass	Alfalfa early bud	Alfalfa-full flower
Proximate (wt %, db)			
Volatile matter	83.41	73.39	75.29
Ash	2.61	8.74	5.83
Fixed carbon	13.98	17.87	18.88
Ultimate (wt %, db)			
C	47.53	44.30	45.97
H	6.81	5.43	5.52
N	0.51	2.52	1.60
S	0.00	0.22	0.088
Cl	—	0.59	0.41
O	42.54	38.20	40.58

Table 1.2. Analysis of bio-oil from biomass pyrolysis[28]

Wt %, db	switchgrass	Alfalfa early bud	Alfalfa-full flower
C	47.47	53.88	56.84
H	6.96	8.47	7.86
N	0.36	4.59	3.73
S	—	0.05	0.07
Cl (ppm)	—	249	242
O	45.19	32.73	31.30
Ash	0.01	0.28	0.30

Upgrading Fast Pyrolysis Oil

The reported yield of liquid for bio-oil to be used for upgrading is typically is ca. 60% for the most optimized methods. These low yields are due to the bio-oil's high oxygen content and viscosity. Therefore, more effective methods are needed to raise the yields of bio-oil upgrading to biofuel. Advances in the methods such as hydrogenation, hydrodeoxygenation, catalytic pyrolysis and catalytic cracking have been the most studied.

Hydrogenation is the traditional process for stabilizing bio-oil, resulting in the reduction of the organic acids and aldehydes to less reactive alcohols. This is usually achieved under elevated pressure of 10-20 MPa hydrogen gas high temperatures and appropriate catalysts. In the upgrading process the carbon:hydrogen ratio increases as well as the pH and the water content whereas the viscosity decreases. The properties of bio-oil from pyrolysis are generally improved by hydrotreatment and esterification of the organic acids over catalyst. A novel one-step hydrogenation–esterification method has been designed by Zheng which converts organic acids and aldehydes to stable combustible components. This method uses a platinum catalyst and acidic supports such as HZSM-5 or amorphous aluminum silicate. Here the main unstable acids of bio-oil such as acetic acids are converted to esters.[29]

Hydrodeoxygenation (HDO) is a hydrogenolysis process for reducing or removing the oxygen content from the bio-oil. This process is carried out under high pressure hydrogen with the appropriate catalyst. Components containing functional groups such as ketones, aldehydes, acids, esters and phenols are deoxygenated while increasing the carbon–hydrogen content by weight of the molecules is increased. Catalysts explored in depth for this process are NiMo or CoMo sulfide–supported hydrotreating catalysts. Recent studies by Wang et al. have shown that Pt supported on mesoporous ZSM-5 (Zeolite Saucony Mobil–5) gives better results than the previous reports of Pt/Al_2O_3 in hydrodeoxygenation of dibenzofuran. The good performance of Pt/ZSM–5 was attributed to the combination of the strong acidity and the mesoporous nature of the ZSM-5.[30] HDO is very promising for bio-oil upgrading due to the excellent hydrodeoxygenation activity and selectivity but it

usually requires noble metal catalyst. Exploration for novel, low cost catalysts has led to several amorphous catalyst candidates that tested for their stability and performance in bio-oil upgrading. Wang et al. developed and compared three amorphous catalyst; Co–W–B, Ni–Co–W–B and Ni–W–B and showed that the activity of the catalysts for HDO reaction. Co–W–B was the discovered to be the most thermally stable of them.[31]

Catalytic pyrolysis has demonstrated promising potential for biomass liquefaction. Incorporation of catalyst in-situ or ex-situ to pyrolysis of biomass has the advantage that it can stabilize the formed bio-oil. The method does not require the need for pressurized hydrogen for bio-oil upgrading and has the advantage of operating under atmospheric pressure. This process is classically carried out on the biomass in a fixed bed reactor or fluid bed with catalysts such as HZSM–5, ZSM–5, Cu or alumina and a stream of nitrogen gas. Several catalysts have been studied and screened for activity and selectivities and the influence of temperature. Hong et al. explored three catalysts; ZSM–5, Al–SBA–15 and alumina on pyrolysis of herb residue in a fixed–bed for the quality of the bio-oil formed the catalysts lowered the oxygen content of the bio-oil. The highest yield of bio-oil obtained was at 450 °C was 34.26% with 10 wt% of the alumina catalyst and 9.21% without catalyst. The product of the pyrolysis was studied for the fuel values which were ca. 26 $MJKg^{-1}$ with and 19 $MJKg^{-1}$ without catalyst.[32] Hu et al. have also reported that catalytic pyrolysis saturated the aromatic rings in bio-oil under HZSM–5 or alumina catalysts. [32,33] Addition of CaO[34] and $CaCl_2$ to pyrolysis has also been reported to show catalytic dehydration and catalytic effects on elephant grass.

Catalytic cracking is basically the thermal conversion process applied to bio-oil under conditions of pressurized hydrogen with appropriate catalyst such as HZSM–5 at temperature ca 350 °C. It has been traditionally applied towards bio-oil upgrading resulting in products of solid, liquid and gas states. Recent advances in this method has been its combination/coupling with catalytic a pyrolysis process. This recent process required the design of a sequential biomass reactor that consisted of the traditional pyrolysis reactor and apparatus with a further supported catalytic decomposition of gaseous intermediate. Using Fe/γ-Al_2O_3 as the secondary catalyst the products obtained from the latter method were high in gaseous products of H_2, CH_4, and Co.[35]

Lignin

Structure, Property, and Nomenclature

Lignocellulose consists of about 30-50% cellulose, 20-35% hemicellulose and 20-35% lignin. Lignin is a co-polymer, composed of three (hydroxyphenyl, guaiacyl and syringyl) arylpropane units (also known as monolignols) linked via strong ether (C-O) and C-C linkages.[36] The linkages in lignin are described by the carbon atoms in the aliphatic side chains of the monolignols which are labeled as α, β, and γ while those in the aromatic moieties are numbered 1–6 from where the propyl group is attached. For example, the α-O-4 linkage represents a bond between the α carbon of the aliphatic chain and the oxygen attached to the carbon 4 of the aromatic ring. The major linkages between the structural units of lignin are β-O-4 (β-aryl ether), β–β, and β-5. Other linkages include α-O-4 (α-aryl ether), 4-O-5 (diaryl ether), 5–5, α-O-γ (aliphatic ether), and β-1 (spirodienone), as shown

in Figure 4. Specific cleavages of these linkages are needed to valorize lignin into useful chemicals. The linkages between monolignols basically determine the reactivity of lignin. As β-O-4 (β-aryl ether) is the most frequent linkage in lignin, its chemical reactivity dictates considerably the resistance of lignin to chemical digestion.

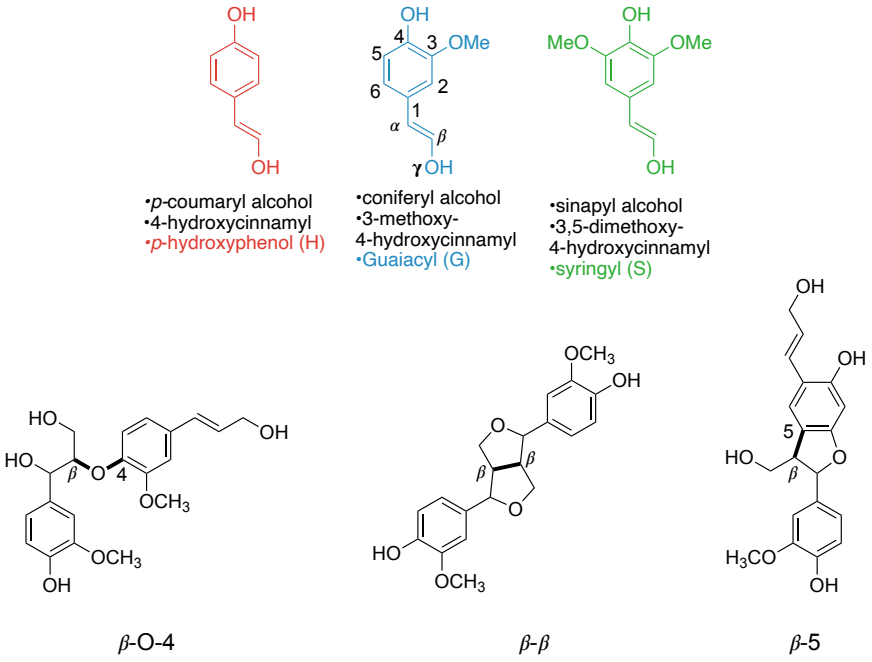

Figure 1. 15. Arylpropane units of lignin and some common linkages in lignin

Findings in literature suggest that the mechanism of polymerization in which phenolic radicals are formed from oxidation of monolignols. These radicals undergo coupling reactions with themselves (forming dimers, trimers etc.) or with analogous radicals formed on the growing lignin chain[37]. This process is catalyzed by peroxidases and laccases. Polymerization is also known to be affected by non-enzymatic oxidation. The monolignol derived radicals are also reactive at C1, C3, C5 and Cβ sites due to the delocalization of spin throughout the conjugated π-system. Steric hindrance on the aromatic moiety is known to

limit reactivity on these sites but the presence of the multiple reactive sites leads to the numerous possible interunit bonds.

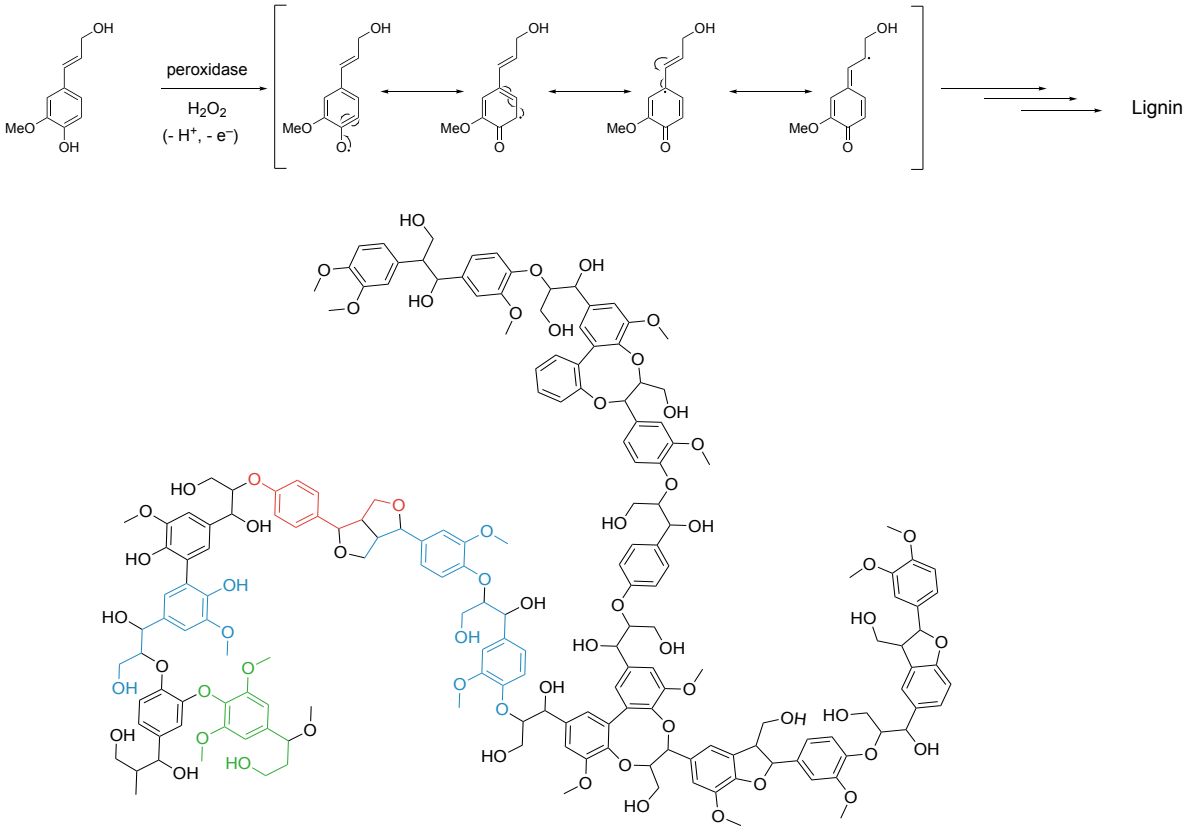

Figure 1. 16. Mechanism of polymerization[37] of monolignol to the structure[38] of Lignin in Softwood.

Due to the recalcitrant nature of lignin, lignin-containing woods are traditionally simply used for their high heating values[39] and burned to produce heat (which may generate steam) to generate electricity.[40] To replace fossil carbon, it is important that all components of the finite biomass carbon supply be tapped. The US alone annual energy consumption for transportation is ca. 29 EJ (29 x 10^{18} J) since 2015. The increase rate in the fuel consumption is 0.1%< per year. With specific energy of petroleum at 48 $MJKg^{-1}$ in the

year 2030 the annual consumption would be ca. 0.6 billion tonnes. The DOE Billion-ton study optimistically suggest a 1.04 billion dry tonnes of harvested biomass in 2030 which would be ca 21 EJ.[41] So, the effective utilization of all the biomass carbon would not be able to solve the transportation demand completely in the near future. The established methods for biomass conversion employs fermentation process which leads to loss of 1/3 of carbon content to CO_2. So effective methods to utilize all the carbon content in lignocellulosic biomass (cellulose, hemicellulose and lignin) to liquid fuel are sorely needed.[42]

Research Rationale

Concerns Regarding Electrocatalytic Hydrogenation

Electrocatalytic hydrogenation (ECH) provides a new approach for upgrading of bio-oil to biofuel. For instance, (ECH) can be reductively stabilized fragments of bio-oil using Raney™ Nickel as the cathode under very mild conditions (75 °C, 1 atm, H_2O as electrolyte).[43] A general concern with ECH is the possibility of generating of cross-linkages in lignin fragments via acid or base catalyzed step growth polymerization from their complex mixture. These cross-linker could form a phenolic resin or tar that could occlude the surface of the catalyst (Raney™ Nickel). Bakelite, a classical thermoset material, is an example of a phenolic resin synthesized from phenol and formaldehyde by heating under acid or base conditions. For lignin-based phenolic resin, the phenol-rich structure of lignin lends itself quite readily to replace phenol in the traditional synthesis protocol. Bio-oil

produced from fast pyrolysis is known to be very reactive due to the presence of acetic acid, formaldehyde, acetaldehyde, furfural, phenolic compounds and other carboxylic acid derivatives. Cross-linking polymerization reaction can easily occur between the phenolic compounds and the aldehydes (figure 1.17) but would be disfavored if these fragments could be effectively reduced in the ECH cell. They may also mutually interfere in the catalytic reduction processes, so an understanding of such interactions is essential to success in moving from model systems to real bio-oil.

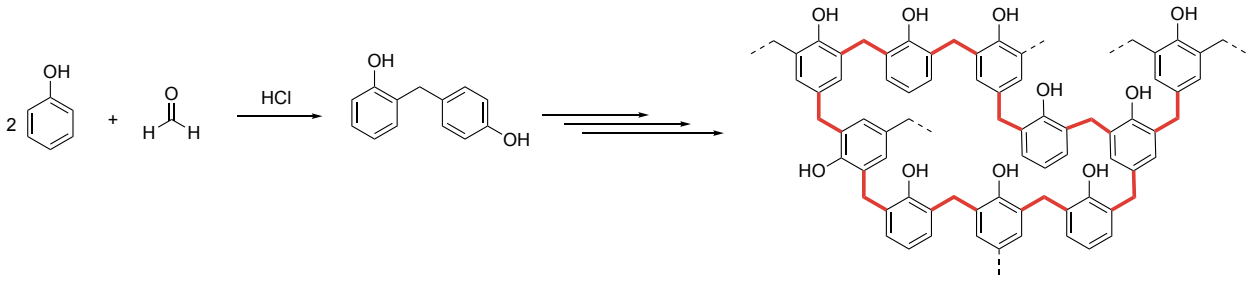

Figure 1. 17. Phenol-formaldehyde resins[37]

Aim and Objectives

In the previous ECH studies of lignin monomers (positional isomers of 2-methoxyphenol) by Dr. Lam et al, two competing reactions were revealed; path (1) C-O hydrogenolysis, immediately followed by aromatic saturation to form cyclohexanol and path (2) direct aromatic saturation, forming methoxycyclohexanols. Importantly, these saturated products do not undergo further ether cleavage under the ECH conditions. The reactivity pattern of the three isomeric methoxyphenols suggested that demethoxylation was strongly favored by proximity between the alkoxy and the hydroxy groups. Thus, 2-methoxyphenol underwent almost complete ether cleavage, whereas the 3- and 4-methoxyphenols followed paths 1 and 2 roughly equally. [44]

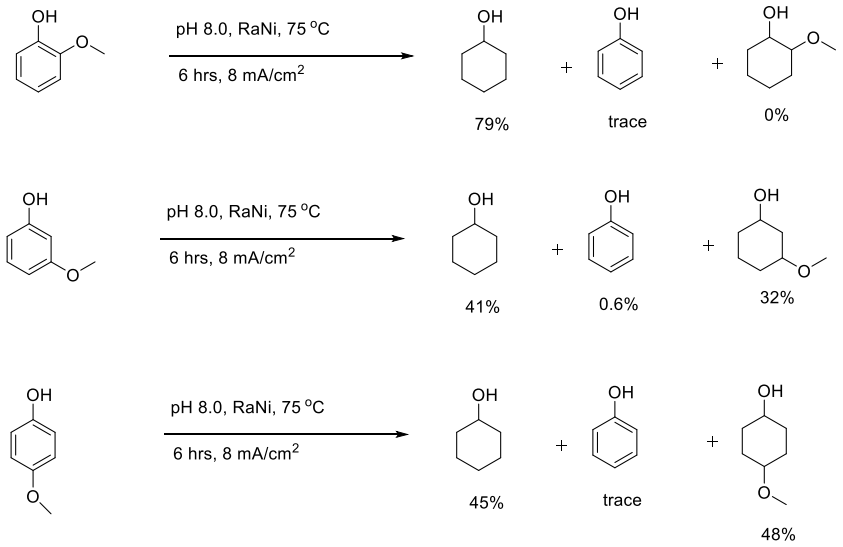

Figure 1. 18. ECH reactivity of 2-, 3- and 4-methoxyphenol showing effect of substituent positions. [44]

In that earlier report, Lam et al. explored the reactions of these three substrates starting from one solution concentration (10 mM). Importantly, when anisole (methoxybenzene) was subjected to these reaction conditions, essentially no reaction was observed.

We hypothesized that if intramolecular hydrogen bonding as in guaiacol was able to activate ether cleavage, perhaps also an *inter*molecular association of phenolic O-H sites with aryl ethers could enable ether cleavage. The ability to probe selectivity is essential to the understanding of reaction mechanisms. Herein, we report hydrogen-bonding (H-B) within monomers (*intra*-molecular H-B) or between molecules (*inte*r-molecular) as a contributory factor for these reaction pathways. The ab initio study of the adsorption energetics and geometries of phenol on Nickel [111] by Delle Site et al. suggest that the benzene ring adsorbs flat on the nickel metal while the peripheral C-H bonds and especially the C-OH site tilt from the surface. In effect the C-Ni bond bearing the oxygen appears to be weakened.[45] This arrangement suggests that this oxygen atom may be available for external (not through bonds) interactions with solvent or other substrate molecules, and might be able to assist in their activation. Meanwhile, it also implies that direct ether cleavage through oxidative insertion into an Aryl-OR bond is unlikely. Also, H/D exchange study which revealed that there is no C-H activation of the alkoxyl group. So, a more likely explanation would be partial saturation of the ring and re-aromatization via elimination of HOR. Following this line of thinking, we envision that the -OR is activated to function as a leaving group through the H-bonding interaction. [3]

CHAPTER 2: MECHANISTIC STUDY OF ELECTROCATALYTIC UPGRADING OF LIGNIN MONOMERS TO BIOFUELS (PROBING SUBSTRATE SYNERGY VIA HYDROGEN-BONDING)

Introduction

Green and cost-effective applications to produce platform chemicals and fuels from biomass have remained a challenge in sustainable Chemistry.[46] Utilizing feedstocks especially from agricultural (wood) or municipal waste resources that do not compete with the food supply is seen as the most promising route to replacing fossil carbon. Woody (lignocellulosic) biomass comprises three basic components: cellulose, hemicellulose, and lignin.[47,48] There are established paths [49] to process cellulose (the most abundant natural polymer) into bio-ethanol and other platform chemicals on an industrial scale. Economically viable means to utilize lignin (the most abundant natural aromatic polymer), however, have lagged. Lignin is the "glue" in lignocellulosic biomass that holds cellulose and hemicellulose together.

Electrochemistry has recently gained attention for its utility in "green" organic transformations, minimizing byproducts, and using electricity from non-fossil energy sources such as wind, solar, hydroelectric, geothermal. With a platinized Pt electrode, hydrogen equivalents from water electrolysis can be used to effect ElectroCatalytic

Hydrogenation/hydrogenolysis (ECH), reducing organic compounds at ambient pressure and at temperatures below 100 °C.[50] For instance, in electrochemical reduction of benzene and tetrahydronaphthalene (tetralin), the reduced products were formed with a yield of 53-81% and a current efficiency of 61-87% in ethylenediamine saturated with lithium chloride as the electrolyte. In contrast, classical catalytic hydrogenation (CH), a well-established method used in oil refineries, requires harsher conditions such as H2 gas at 300 °C and 20 atm to hydrogenate benzene. [51]

In principle, ECH bypasses the kinetic barrier of splitting the hydrogen molecule and avoids the pressures demanded by the poor solubility of hydrogen gas in aqueous media. Mechanistically ECH entails several steps as shown in Scheme 1: (1) reductive chemisorption of protons on the catalytic metal (M) cathodes to form surface-bound hydrogen atoms; (2) adsorption of organic substrate (Y=Z) on the catalyst surface; (3) reduction of substrates with the adsorbed hydrogen, increasing their fuel value through hydrodeoxygenation; (4) desorption of the reduced product, opening up the catalyst sites. In a competing process, the adsorbed hydrogens react via Heyrovsky (5) or Tafel (6) mechanisms to form hydrogen gas which bubbles out of the aqueous solution. Reaction efficiency depends on the catalyst's ability to favor incorporation of the metal-bound hydrogen into the organic substrates over production of hydrogen gas. [52].

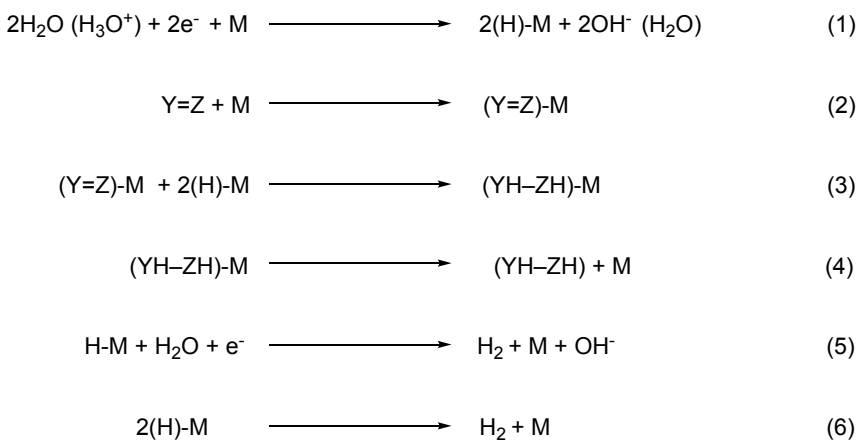

Scheme 2.1. Mechanisms of hydrogenation/hydrogenolysis and competing hydrogen evolution in aqueous media.

As shown in Figure 1a, previous ECH studies of lignin model methoxyphenols showed two competing reactions: (1) C-O hydrogenolysis, followed immediately by ring saturation to form cyclohexanol; and (2) direct aromatic saturation to methoxycyclohexanols. Importantly, the saturated products do not undergo further ether cleavage under the ECH conditions. The reactivity pattern of the three isomeric methoxyphenols suggested that demethoxylation was favored by proximity between the alkoxy and the hydroxy groups. Thus, 2-methoxyphenol underwent almost complete ether cleavage, whereas the 3- and 4-methoxyphenols followed paths 1 and 2 (Figure 1a) above roughly equally (Figure 1b). In that earlier report, Lam et al. explored the reactions of these three substrates starting from one solution concentration (10 mM). Importantly, when anisole (methoxybenzene) was subjected to these reaction conditions, essentially no reaction was observed. We hypothesized that if intramolecular hydrogen bonding as in guaiacol was able to activate

ether cleavage, perhaps also an intermolecular association of phenolic O-H sites with aryl ethers could enable ether cleavage.

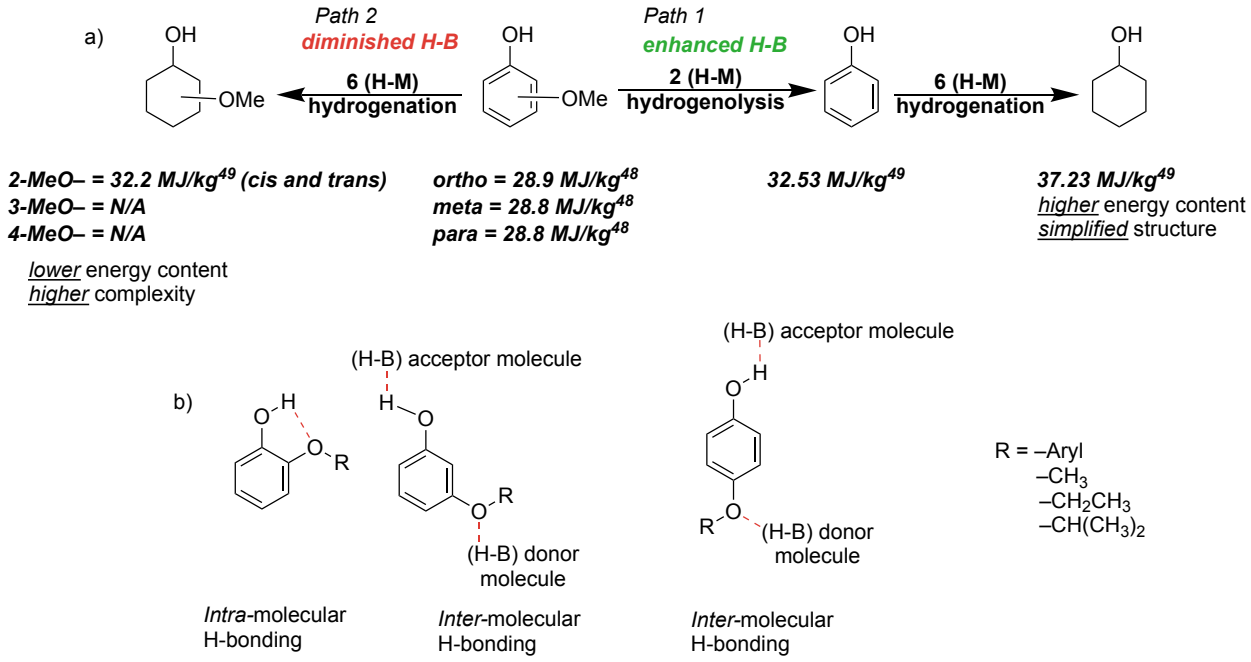

Figure 2.1. (a) Reaction pathways of ECH of guaiacol isomers illustrated with the specific energies of relevant molecules.[53,54] b) Speculated H-bonding interactions activating aryl or alkyl ether cleavage of most stable rotational isomers of methoxyphenols. [55]

Such bimolecular chemistry should be sensitive to reactant concentrations. Herein, we explore hydrogen-bonding (HB) within monomers (intra-molecular HB) or between molecules (inter-molecular HB) as a contributory factor for these reaction pathways.

The ab initio study of the adsorption energetics and geometries of phenol on Nickel [111] by Delle Site et al. suggest that the benzene ring adsorbs flat on the nickel metal while the peripheral C-H bonds and especially the C-OH site tilt from the surface. In effect the C-Ni bond bearing the oxygen appears to be weakened.[45] This arrangement suggests that this

oxygen atom may be accessible for external interactions with solvent or other substrate molecules, and might be able to assist in their activation. Meanwhile, it also implies that direct ether cleavage through oxidative insertion into an Aryl-OR bond is less likely[8] than partial saturation of the ring and re-aromatization via elimination of HOR. Following this line of thinking, we envisioned that the -OR group might be activated to function as a leaving group through the H-bonding interaction.

Experimental

Catalyst Preparation

The electrochemical setup and conditions used in this work are essentially similar to those employed by Lam et al. The working side (cathode) uses Lessard's Raney™ Nickel[52] to effect ECH of the organic substrates, while the Kanan-Nocera cobalt phosphate (Co-P) [56] water splitting catalyst anode oxidizes water, acquiring the electrons needed for the cathodic reduction. The Raney™ Nickel cathode was prepared from a square of stainless 314 screen (50 mesh, 3 x 2.5 cm; only 2.5 x 2.5 cm was exposed) that was submerged in a 50 mL plating bath in an open cell and connected to a plain solid nickel sacrificial anode. The plating solution was made from 213 g of $NiCl_2 \bullet 6H_2O$, 200 mL of 30% NH_4OH, and 30 g of NH_4Cl in 1 L of deionized water. Powdered Ni-Al alloy (2.5 g) was suspended in this bath by vigorous magnetic stirring. At a plating current of 375 mA, the powder was trapped onto the stainless-steel mesh cathode as the dissolved nickel plated out. The mesh was flipped 180° after every 30 mins of the 2 h plating treatment to ensure uniform deposition on both

faces. The prepared electrode was then etched with 6 M NaOH at 75 °C for 8 hours to leach out the aluminum and activate this “skeletal nickel” catalyst. The activated catalytic electrode was stored in 4% NaOH or isopropyl alcohol until it was used as the catalytic cathode in ECH experiments.

The Co-P anode was made by rolling a stainless-steel 314 screen (8 mesh, 12 × 4 cm) into a cylindrical shape. This cylinder was then immersed in 50 mL of a solution of 0.50 mM $Co(NO_3)_2$ in 0.10 M pH 7 potassium phosphate buffer and subjected to current at 50 mA for 8 h in an open cell connected to a stainless steel cathode.

Reaction Procedure

The Co-P anode and the Raney™ Nickel cathode were placed in a divided electrochemical cell separated by a Nafion® membrane. The cathodic chamber was charged with 50 mL of a 0.1 M pH 8 potassium borate aqueous buffer solution (in some cases isopropyl alcohol (IPA) or a mixture of IPA and *n*-butanol were added) and the anodic chamber contained 50 mL 0.1 M pH 7 potassium phosphate buffer solution. Following Lam et al., reactions were studied at 75 °C and 50 mA (8 mA/cm^2) with periodic extraction of aliquots for analysis.

Results and Discussion

ECH of 2-methoxyphenol (Guaiacol)

Time course plots for reductions of guaiacol (2-methoxyphenol) at 50 mA and 75 °C with initial concentrations of 18 mM and 60 mM are shown in Fig 2. As previously reported, guaiacol completely prefers demethoxylation over ring saturation; no 2-methoxycyclohexanol was observed at either concentration. The resulting phenol was rapidly saturated to cyclohexanol, an overall 8-electron reduction from guaiacol. The overall rate of total product formation rose from 1.3 mM to 3.8 mM/hour, with current efficiency increasing from 18% to 55%, essentially the same factor as the 18 to 60 mM increase in substrate concentration. We speculate that this preference for demethoxylation reflects activation of the OCH_3 moiety as a leaving group via the intra-molecular $OH^{\cdots}OCH_3$ H-bonding.[55]

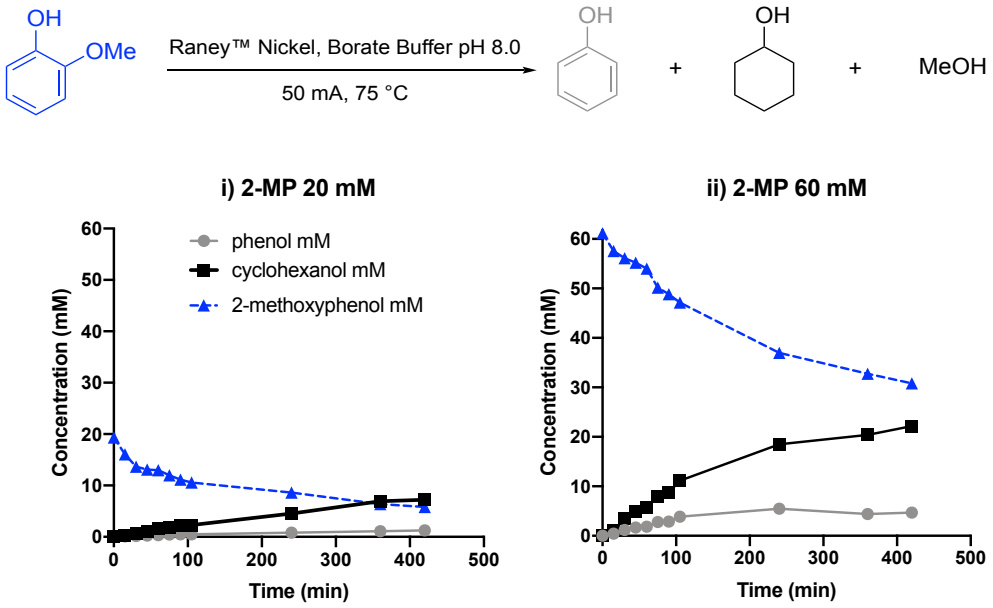

Figure 2.2. ECH of (i) 20 mM and (ii) 60 mM 2-methoxyphenol solution (50 mL) at 50 mA and 75 °C for 7 h.

ECH of 3-methoxyphenol: Selectivity vs Concentration

Like guaiacol, 3-methoxyphenol showed increased rates of substrate conversion at higher concentrations. However, no significant variations in selectivity between C-O cleavage to form phenol (and ultimately cyclohexanol) (path 1) and direct ring saturation (path 2) (figure 2.2) were found. Specifically, as shown in Figure 2.2a(i)-(v), over 20-60 mM runs, the rate of reaction shifted from 1 to 2 mM products/hour. The selectivity for path 2 over path 1, however, showed a negligible shift, from 2.8:1 to 3.1:1. Thus, the selectivity for demethoxylation vs. direct ring saturation appears insensitive to substrate concentration.

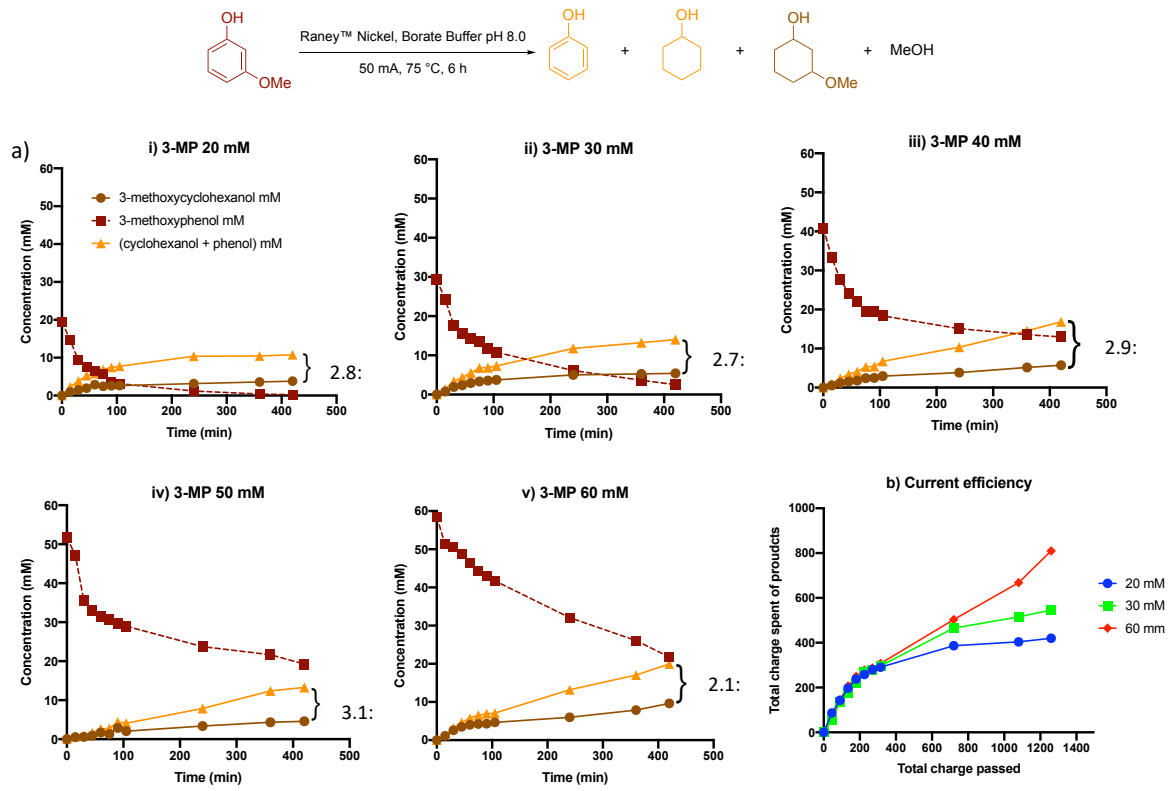

Figure 2.3. (a) The ECH reaction of (i) 20 mM, (ii) 30 mM, (iii) 40 mM, (iv) 50 mM and (iv) 60 mM 3-methoxyphenol solution (50 mL) of solution at 50 mA. Note that the orange line and triangles represent the sum of the demethoxylation products phenol and its hydrogenation product, cyclohexanol; (b) The current efficiency showing the quantity of charge consumed in ECH reactions vs the quantity passed for runs at 20, 30, and 60 mM 3-methoxyphenol.

As expected for the faster conversion at higher substrate concentrations, overall reaction current efficiencies also increased from 33 to 64%. Thus, as in the guaiacol case, higher substrate concentrations compete with hydrogen production more effectively, increasing current efficiency (figure 3b). The instantaneous current efficiency (eq. 1) was then calculated at each sampled time to reveal the fraction of charge passed that accomplished ECH (Figure 3b). Values above 100% (i.e. slope > 1) in the first hour reflect the residual

reducing power left in the skeletal nickel electrodes after activation by NaOH etching to remove the aluminum component.

$$CE\% = \frac{(Mol_{prod} \times n \times F)}{C_{total}} \times 100\% \qquad \text{(eq. 1)}$$

where Mol_{Prod} = moles of product (phenol, cyclohexanol, methoxycyclohexanol) formed; F = Faraday's constant, 96,485 $Cmol^{-1}$; n = number of electrons per reaction; and C_{total} = total charge passed.

Turning attention to the low selectivity between paths 1 and 2, we speculated that it might reflect the composition of the adsorbed layer of the fairly hydrophobic 3-methoxyphenol substrate on the catalyst surface. To test this idea, we explored the effects of including isopropyl alcohol (IPA) and n-butanol (BuOH) in the ECH reactions at 20 mM 3-methoxyphenol. With 10% IPA added to the borate buffer, there was no significant shift in selectivity suggesting that the IPA, which is completely miscible with water, does not significantly modulate the substrate's interaction with sites on the catalyst. However, with 1% BuOH added to the 10% IPA/borate buffer, path 1 was substantially favored, leading to a 6.4:1 selectivity. Increasing to 2% *n*-BuOH essentially completely favored the demethoxylation (path 1) products phenol and cyclohexanol; only traces of the methoxy-cyclohexanol products from pathway 2 (figure 2.4 (ii & iii)) were seen. However, the reactions with *n*-BuOH were slowed and showed poor mass recoveries (ca. 50%), which were tentatively attributed to BuOH worsening the extraction efficiency in the sample analyses. We note here that BuOH is only soluble in water up to 8%; the presence of

electrolyte salts and of IPA likely modify this value but not enough to exceed the electrolyte's solubility limits here. Control experiments were performed with synthetic mixtures containing 10 mM each of 3-methoxyphenol, 3-methoxycyclohexanol, cyclohexanol and phenol with 10% IPA and 1% BuOH in the borate buffer electrolyte to check the extraction efficiency. Using the same extraction process as in the main experiments the results indicated a quantitative (>99%) extraction of all components except the 3-methoxycyclohexanol of which about 27% was lost.

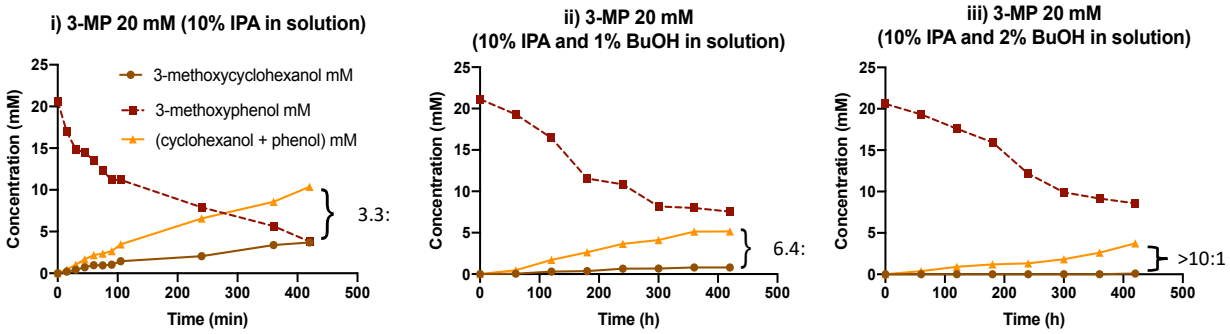

Figure 2.4. The ECH reactions of 20 mM 3-methoxyphenol with (i) 10% IPA, (ii) 10% IPA and 1% n-BuOH and (iii) 10% IPA and 2% n-BuOH added to the borate buffer electrolyte and run at 50 mA for 7 hours. Note that the orange line and triangles represent the sum of the demethoxylation products phenol and its hydrogenation product, cyclohexanol. See also Fig. 2.3a(i) for the 20 mM instance with neither alcohol additive.

ECH of 4-methoxyphenol: Selectivity vs Concentration

4-methoxyphenol showed reactivity similar to that of 3-methoxyphenol but its selectivity did vary significantly with concentration. Thus, the selectivity for C-O cleavage vs direct ring saturation shifted from ca. 2.5:1 to 5.1 as substrate initial concentration rose from 20 to

60 mM. The rate of reaction shifted from 1.8 to 4.5 mM products/hour with overall current efficiency from 28% to 67%. Again, 10% IPA and 1% *n*-BuOH were introduced with the electrolyte into a 20 mM run and the selectivity shifted to 7:1, consistent with the effect seen in the case of 3-methophenol.

Literature reports on spectroscopic properties of 3- and 4-methoxyphenols reveal slight differences which may be relevant for the selectivity patterns of the two in our surface electrocatalytic reactions. The IR stretch of the O-H in 3-methoxyphenol is reported at 3657 cm^{-1}, and 4-methoxyphenol as 3662 cm^{-1} compared to 3657 cm^{-1} of phenol.[55] This implies that 4-methoxyphenol has a slight effect on the O-H bond, possibly enhanced on catalytic surfaces for *inter*molecular HB. Also, the reported enthalpies of formation in the gas phase for 3- and 4-methoxyphenol are –240.8 and –234.3 kJ/mol respectively at 298 K and 0.1 MPa.[57] The slightly greater stability of 3-methoxyphenol may conceivably lower its ECH reactivity relative to 4-methoxyphenol.

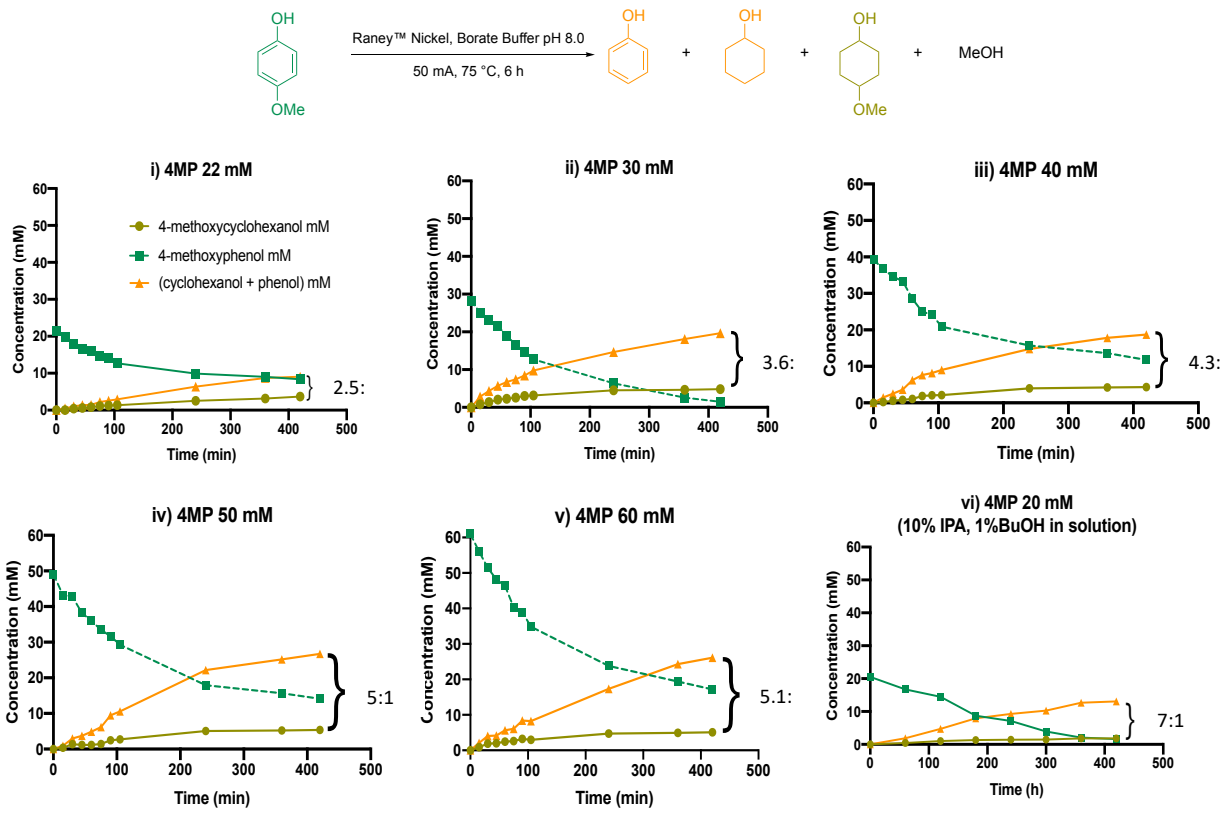

Figure 2.5. The ECH reaction of (i) 20 mM, (ii) 30 mM, (iii) 40 mM, (iv) 50 mM (v) 60 mM and vi) 20 mM (10% IPA and 1% n-BuOH) of 4-methoxyphenol at 50 mA for 7 h. The selectivity for direct ring saturation vs C-O cleavage is denoted with the half bracket '}'.

Substrate Synergy (Interaction Between Different Molecules)

The ultimate question to address is whether the hydroxyl group of the substrate or of other additives can activate ether cleavage on another molecule. Justified by the *n*-BuOH experiment we also explored methoxy cleavage of anisole with phenol or catechol. Though anisole alone was unreactive upon ECH, an equimolar mixture of anisole (H-bonding acceptor) and phenol or catechol (H-bonding donor) gave up to 6% yield of benzene, while a 5% yield of toluene was observed from an equimolar mixture of 4-methyanisole and phenol after 24 hours of ECH. It should be noted that an octane layer on top of the

electrolyte was introduced to trap the volatile substrates and products (anisole, 4-methylanisole, benzene, toluene).

^{1}H-NMR Studies of H-bonding Association

To explore the question of self-association via hydrogen bonding in the methoxyphenols, ^{1}H-NMR studies of their solutions were conducted at various concentrations and temperatures in $CDCl_3$. Though the ECH reactions were run in aqueous solutions, the initial ^{1}H-NMR studies in D_2O did not show any significant variations in chemical shift as the concentration and temperature were varied. Presumably, the much more abundant water (D_2O) itself satisfies the H-bonding sites of the methoxyphenols, disrupting any self-association in solution. The initial hypothesis to explain the concentration-dependent activation envisaged that the substrate would associate on the hydrophobic surface of the catalyst. Following this logic, we adopted $CDCl_3$ for the H-bonding NMR studies. As expected, the 2-methoxyphenol showed no change in the —OH chemical shift with varied temperature and pressure. However, as shown in the ^{1}H-NMR spectra of 3- and 4-methoxyphenol, the —OH chemical shifts showed significant changes of 0.4 and 0.5 ppm, respectively, over the range of 1-60 mM concentrations and temperatures from -10 to 20 °C (fig. 5). The results confirm association by H-bonding in $CDCl_3$. However, relative to $CDCl_3$, the hydrophobicity of the catalyst surface is unknown.

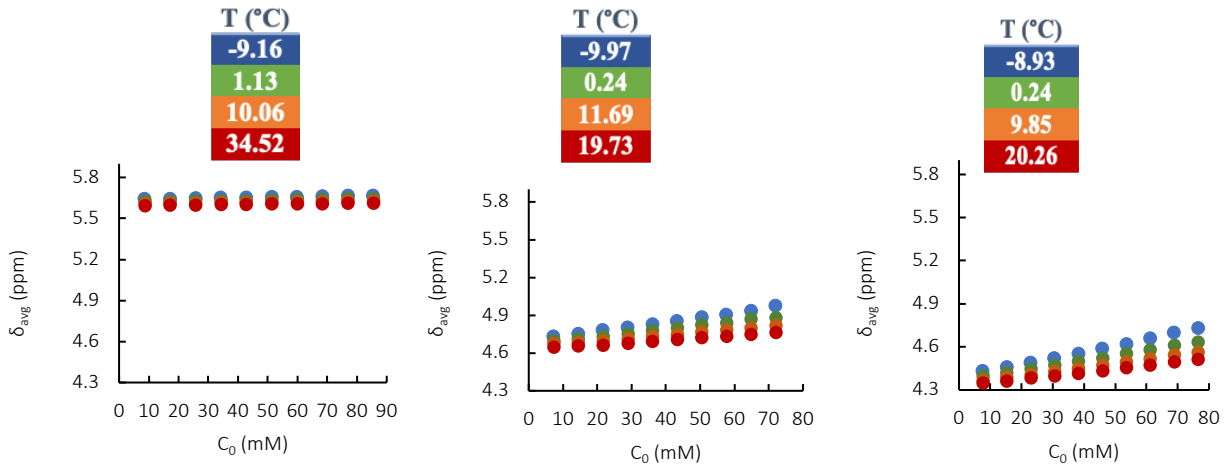

Figure 2.6. The chemical shift of the hydroxy hydrogen (Ar-OH) at varied concentrations (6 mM to about 80 mM) and temperatures (-9 to 20 °C) extracted from ^{1}H-NMR of (i) 2-methoxyphenol, (ii) 3-methoxyphenol and (iv) 4-methoxyphenol in $CDCl_3$

Probing Aggregation of Lignin Model Monomers by Using DOSY NMR

As a second tool to evaluate concentration-dependent association, we employed Diffusion Ordered SpectroscopY (DOSY)-NMR. DOSY is a pseudo 2D-NMR method that is often used to augment 1D-NMR in analyzing complex mixtures. This technique measures the diffusion coefficients of the mixture's components based on their molecular size and shape according to the Stokes-Einstein equation (eq.2).

$$D = \frac{kT}{6\pi\eta r_s} \qquad \text{(eq. 2)}$$

where k is the Boltzmann constant, T is temperature, η is the viscosity of the liquid and r_s is the hydrodynamic radius of the molecule.

Hydrogen bonded dimers' or other oligomers' size and shape, and thus diffusion rates in concentrated solutions should differ from those of isolated monomers in dilute solutions.

Ideally, the spectra would also provide insight into the nature of the associations and shapes of the complexes in solution, suggesting how they might interact on a hydrophobe-coated Raney™ Nickel catalyst surface during ECH. Figure 2.7 shows the hydrodynamic radii of the methoxyphenols in dilute 6 mM and the concentrated 60 mM solutions extracted from the DOSY-NMR spectra. The hydrodynamic radii at the different concentrations of the 2- and 3-methoxyphenols showed negligible variation with concentration, but the changes for 4-methoxyphenol were slightly larger, suggesting that it may be slightly more susceptible to hydrogen bonding, perhaps due to the lower steric congestion around its donor and acceptor substituents. This findings is also consistent with the slightly greater chemical shift sensitivity to concentration seen in Figure 2.6 for 4-methoxy isomer The experimentally determined hydrodynamic radii of ca. 5 Å are a bit high, relative to the density-derived molecular volumes of the methoxyphenols, all close to 130 $Å^3$, which would predict radii of 3.1 Å, and 4.0 for the dimer. However, the melting points of the three methoxyphenols vary widely, at 28, -17, and 53 ˚C, and the crystal structure of 4-methoxyphenol shows all of its -OH sites involved in chains of hydrogen bonds. These values highlight possibly contrasting propensities of the 3-methoxy- and 4-methoxyphenols for intermolecular hydrogen bonding.

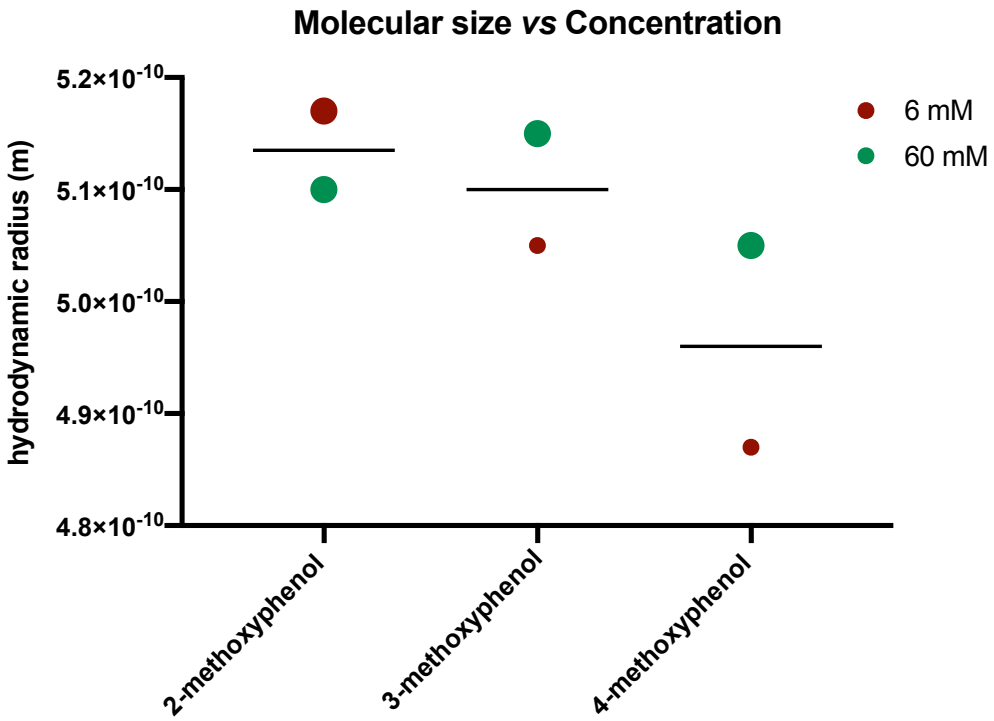

Figure 2.7. Concentration vs diffusion coefficient extracted from explicit DOSY-NMR of the lignin model compounds in $CDCl_3$.

Conclusion and Outlook

Studies of ECH with variable concentrations and additives point to a modest amount of synergistic interaction between model molecules relevant to those found in biomass pyrolysis oils. We propose the possibility of intermolecular activation via H-bonding on the partially hydrophobic surface of the Ni catalyst. Though the mechanism remains incompletely defined, we have uncovered factors that enhance desired C-O cleavage selectivity over direct ring saturation of methoxyphenols on the skeletal Nickel electrocatalyst. Future studies will explore a broader range of additives and more complex substrate candidates. The insights gained in this work may aid in understanding and

predicting the pathways of ECH upgrading and product funneling in the much more complex mixtures obtained from biomass fast pyrolysis.

Acknowledgements

Thanks to Dr. Tayeb Kakeshpour for his dedication in learning and working on Dosy-NMR with me on this project and for these hard-working undergraduate researches who came along to dedicate their time and knowledge to push this research forward: Mr. Chris McAllister, Mr. Jack Walch, Mr. Julian Palmer-Ingram, Ms. Zahra Almisbaa and Mr. Chris. D. Klap.

APPENDIX

GC-MS

2-methoxyphenol (20 mM)

a)

b)

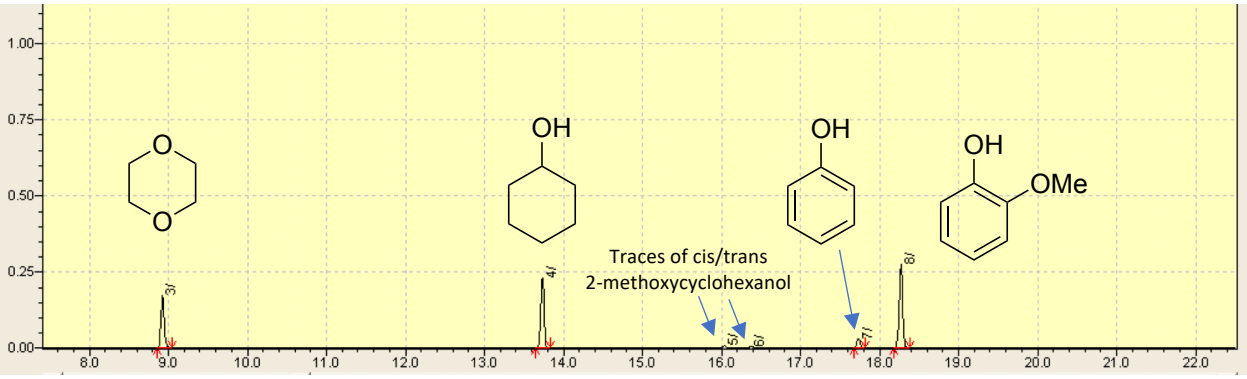

Figure 2.8. GC results with p-dioxane as internal standard (I.S) showing 20 mM of 2-methoxyphenol at a) 0 h and b) 7 h at 75 °C and constant current of 50 mA.

2-methoxyphenol (60 mM)

a)

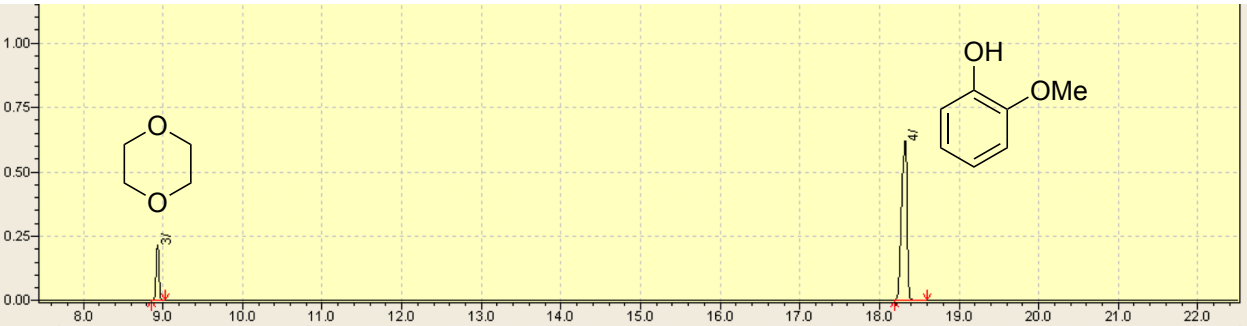

b)

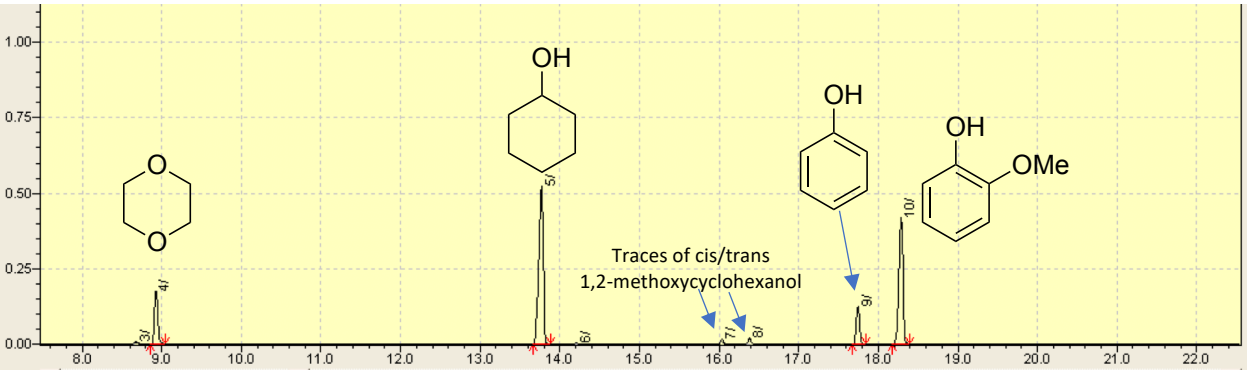

Figure 2.9. GC results with p-dioxane as internal standard (I.S) showing 60 mM of 2-methoxyphenol at a) 0 h and b) 7 h at 75 °C and constant current of 50 mA.

3-methoxyphenol (20 mM)

a)

b)

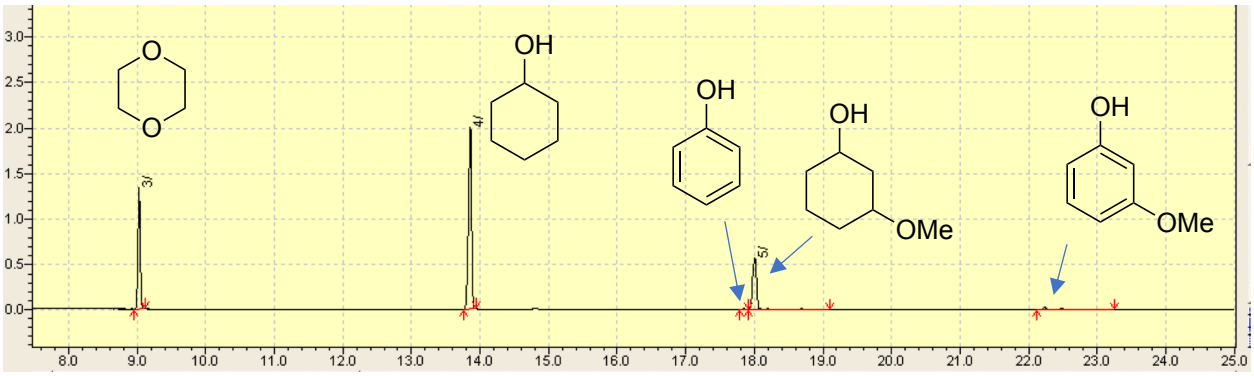

Figure 2.10. GC results with *p*-dioxane as internal standard (I.S.) showing 20 mM of 3-methoxyphenol at a) 0 h and b) 7 h at 75 °C and constant current of 50 mA.

3-methoxyphenol (60 mM)

a)

b)

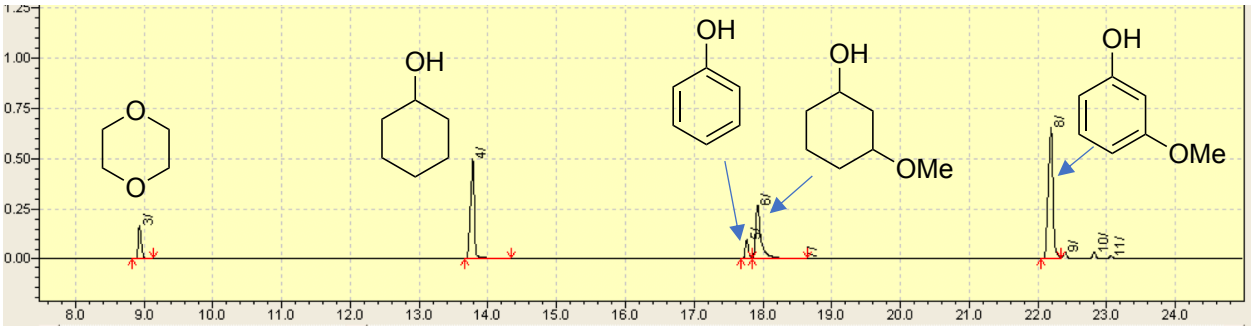

Figure 2.11. GC results with *p*-dioxane as internal standard (I.S) showing 60 mM of 3-methoxyphenol at a) 0 h and b) 7 h at 75 °C and constant current of 50 mA.

4-methoxyphenol (30 mM)

a)

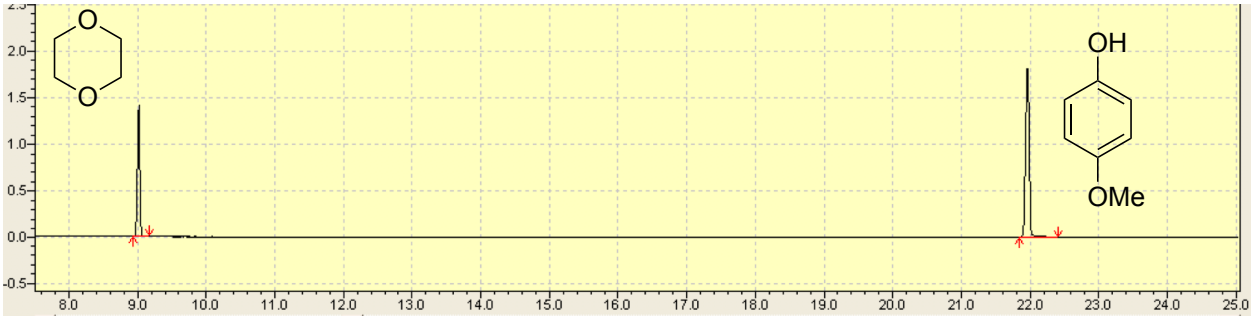

b)

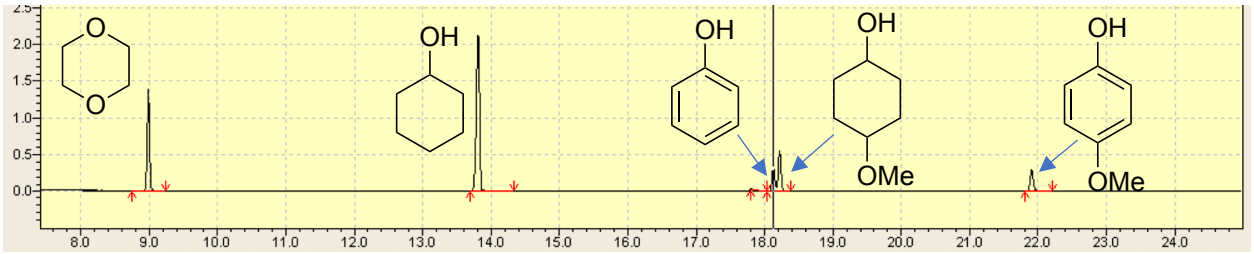

Figure 2.12. GC results with *p*-dioxane as internal standard (I.S) showing 30 mM of 4-methoxyphenol at a) 0 h and b) 7 h at 75 °C and constant current of 50 mA.

4-methoxyphenol (60 mM)

a)

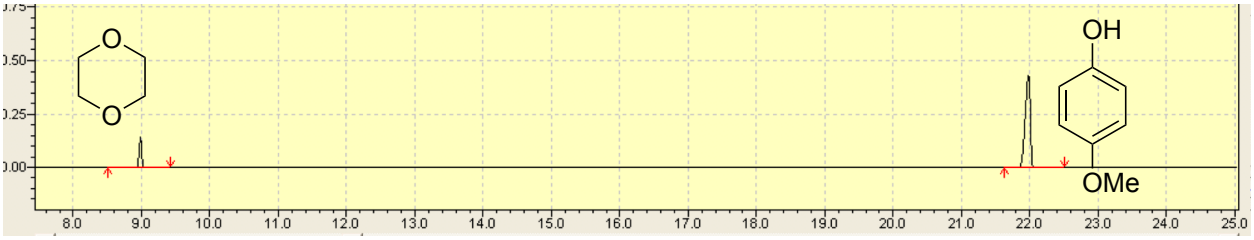

b)

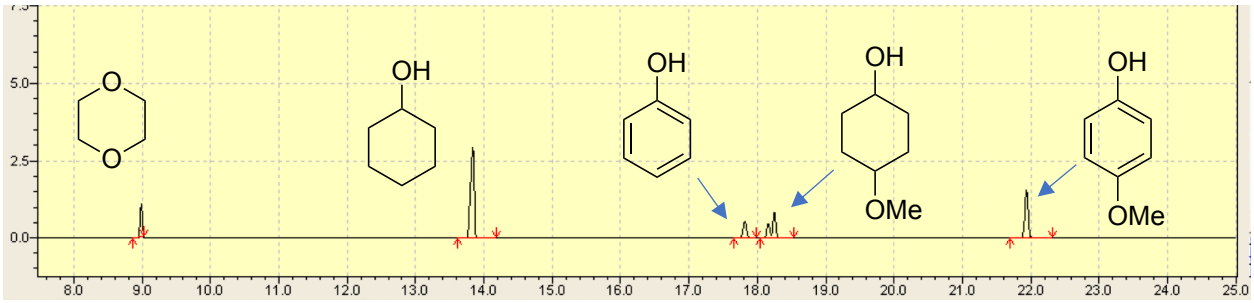

Figure 2.13. GC results with *p*-dioxane as internal standard (I.S) showing 60 mM of 4-methoxyphenol at a) 0 h and b) 7 h at 75 °C and constant current of 50 mA.

^{1}H–NMR Kinetic

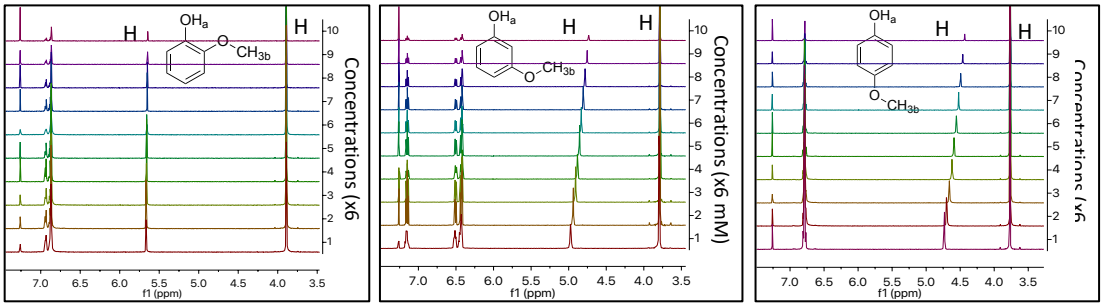

Figure 2.14. Kinetic ^{1}H-NMR of 2-, 3- and 4-methoxyphenol in $CDCl_3$ from 6 mM to 60 mM at-10 °C revealing association of 3- and 4-methophenol through the phenolic OH interaction hence the change in chemical with varying concentration.

CHAPTER 3: ELECTROACTIVATED ALKYLATION OF AMINES WITH ALCOHOLS VIA BOTH DIRECT AND INDIRECT BORROWING HYDROGEN MECHANISMS

Introduction

A green, efficient *N*-alkylation of amines with simple alcohols has been achieved in aqueous solution via an electrochemical version of the so-called "borrowing hydrogen methodology". [58] Alkylamines play essential roles in industry, medicine, and the life sciences;[59–61] they are the building blocks of proteins, while various cofactors, vitamins, neurotransmitters, and alkaloids, not to mention the nucleic acids, bear alkylated amino moieties. Amines are classically synthesized via amide or nitrile reduction, by S_N2 alkylation with alkyl halides or their analogues, or via reductive alkylation with carbonyl species.4–7 However, these methods may suffer from various disadvantages: (a) reducing agents such as LiAlH4 and alkylating agents such as alkyl halides typically generate by-product salts, raising material and disposal costs; and (b) strong alkylating agents often over-alkylate to form quaternary ammonium ions. We describe here two modes of heterogeneous electrocatalytic amine alkylation with low cost, readily available alcohols: direct and indirect "borrowing hydrogen" paths. In this reaction (Scheme 2.1), an alcohol undergoes temporary hydrogen removal to give an aldehyde or ketone (I). Condensation with an amine forms an imine (II) or iminium intermediate which is then reduced to the alkylated amine product, replacing the hydrogen "borrowed" in the alcohol oxidation. This path avoids the low

electrophilicity of alcohols and the poor atom economy of classical alcohol activation methods, with their stoichiometric waste streams. For instance, Hünig's base (diisopropylethylamine) is made by reacting diisopropylamine with diethyl sulfate, a toxic, alcohol-derived alkylating agent.[66] The atom economy of the reaction is low (50%) due to the bulky ethylsulfate byproduct. Our net use of aqueous alcohol as alkylating agent forms water as the only by-product, making this process "green" and atom efficient.

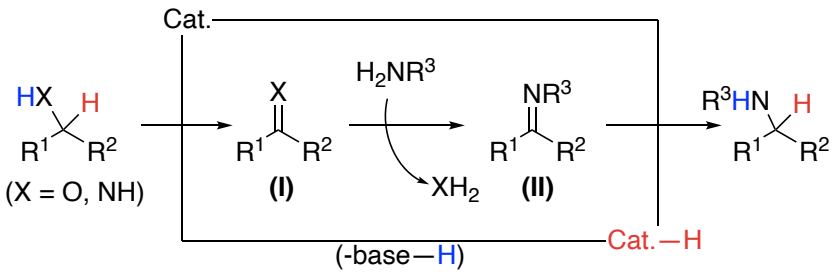

Scheme 3. 1. Mechanistic pathway of hydrogen auto-transfer ("borrowing hydrogen") process with amines and alcohols.

Literature Review

Stereoretentive H/D exchange has been achieved via chemical (Jere et al.)[67] and electrochemical (Bhatia et al.)[68] heterogeneous ruthenium activation at sp^3 C-H sites bearing amine or alcohol moieties. There we envisaged oxidative insertion of Ru at the sp^3 C-H geminal to the alcohol -OH, to form a surface-bound sp^2 intermediate which is then back reduced by surface-bound deuterium formed from D_2O (scheme 2.2). Building on these findings, in this manuscript, we exploit the electrophilicity of the sp^2 carbon intermediate to *N*-alkylate amines.

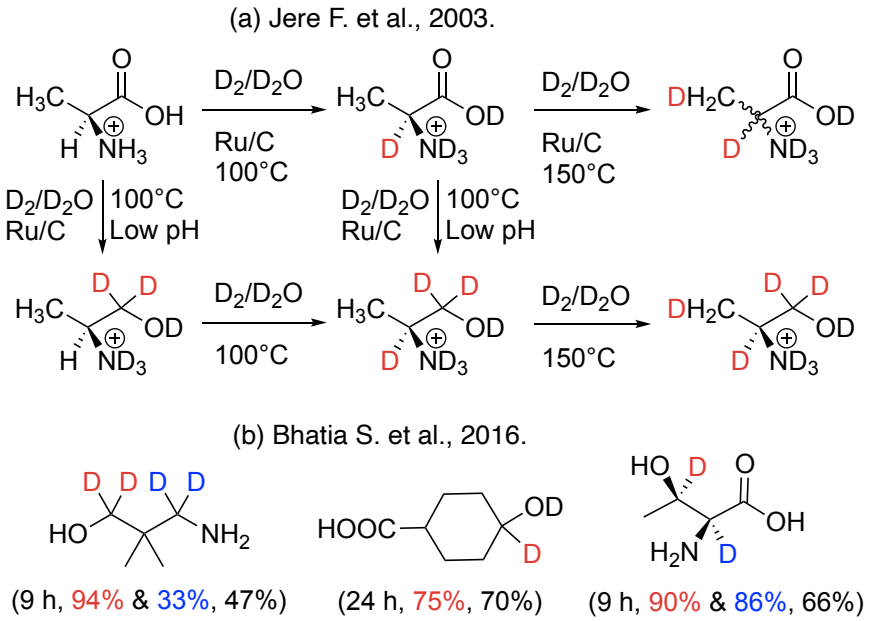

Scheme 3. 2. (a) Stereoretentive C–H bond activation in the aqueous phase catalytic hydrogenation of amino acids to amino alcohols (b)Electrocatalytic stereoretentive H/D exchange at sp3 sites bearing alcohols and amines.

Ammonia alkylation by alcohols is thermodynamically favored, largely due to the exothermicity of water loss. Scheme 2.3 shows the uniformly favorable energetics for stepwise conversion of ammonia and ethanol to triethylamine and water.

								Energy Changes Gas Phase[a] and (aqueous phase)[b] (kcal/mol)
	NH_3	+	EtOH	⟶	$EtNH_2$	+	H_2O	
ΔH_f	-11.0		-55.9		-13.8		-57.6	-4.5
$+\Delta G_{hyd}$	(-15.3)		(-60.9)		(-18.3)		(-63.9)	(-6.0)
	$EtNH_2$	+	EtOH	⟶	Et_2NH	+	H_2O	
ΔH_f	-13.8		-55.9		-23.9		-57.6	-11.8
$+\Delta G_{hyd}$	(-18.3)		(-60.9)		(-28.0)		(-63.9)	(-12.7)
	Et_2NH	+	EtOH	⟶	Et_3N	+	H_2O	
ΔH_f	-23.9		-55.9		-34.2		-57.6	-12.0
$+\Delta G_{hyd}$	(-28.0)		(-60.9)		(-37.4)		(-63.9)	(-12.4)

Scheme 3. 3. Energy changes for stepwise ammonia ethylation to form triethylamine. [a]Data from NIST Webboo[69]; [b]Aqueous phase energies = $\Delta H_f + \Delta G_{hyd}$.[70]

N-Alkylation of Amines with Alcohols

N-alkylation of amines with alcohols was first reported by J.U. Nef in 1901. Achieved simply with sodium ethoxide at high temperature, this work showed that a transition metal catalyst was not necessary.[71] Homogenous catalysis of such processes was first reported in 1981 by Grigg *et al*.[72] who used rhodium, ruthenium and iridium catalysts to achieve selective mono *N*-alkylation of pyrrolidine with primary and secondary alcohols, and formed heterocyclic rings via inter- and intramolecular *N*-alkylations. In similar work, Watanabe *et al*. used the ruthenium complexes $[RuCl_2(PPh_3)_3]$ at 150-200 °C to N-alkylate aminopyridines with primary alcohols.[73] In 2009, William *et al*. alkylated various amines regioselectively with 1° and 2° alcohols using $[Ru(p\text{-cymene})Cl_2]_2$ and the bidentate phosphines dppf or DPEphos. In refluxing toluene for 24 h, this approach converted primary to secondary and secondary to tertiary amines. It was then used to synthesize Piribedil and Tripelennamine, anti-Parkinsonism and antihistamine drugs.[74] The team's 2011 microwave-promoted solvent-free update achieved similar *N*-alkylations of 1° and 2° amines with 1° and 2° alcohols.[75] In 2016, Takacs *et al.* demonstrated regioselective mono and sequential amination of diols with several ruthenium (II) complexes via a bifunctional borrowing hydrogen mechanism.[76]

Direct synthesis of alkyl amines from ammonia and alcohols is also a growing field. The water-soluble $[Cp^*Ir(NH_3)_3][I_2]_2$ catalyst of Yamaguchi *et al*. enabled reaction of 1° and 2° alcohols such as *n*-hexanol and cyclohexanol in aqueous ammonia to yield trihexylamine (96%) and dicyclohexylamine (84%) respectively. The size of the alcohol controlled the selectivity of the reaction to the 2° or the 3° amines.[77] Deutsch *et al*. also reported a new homogeneous catalyst, $[Ru(CO)ClH(PPh_3)_3]$, which enables mono-alkylation of NH_3 with

secondary alcohols in toluene.[78] Overall, Ruthenium- and Iridium-based homogeneous catalysts appear most effective in *N*-alkylation of amines with alcohols.

Heterogenous catalysis for alcohol amination has been known since 1924, when Brown and Reid demonstrated the use of silica gel as an effective catalyst for *N*-alkylation of aniline with methyl, ethyl, *n*-propyl and *n*-butyl alcohols over a temperature range of 300-500 °C.[79] In recent studies Shi and Deng have used an iron oxide immobilized palladium catalyst under base and solvent free conditions to achieve *N*-alkylation of aniline with several primary alcohols to ca. 99% yield.[80] Also, Jaenicke *et al*. found Ag/Al_2O_3 promoted with Cs_2CO_3 or K_3PO_4 to be active and selective catalysts for *N*-alkylation or acylation of amines with several primary alcohols at 120 °C in xylene.[81] Thus, with secondary amines, piperidine and pyrrolidine, the hemiaminal intermediate underwent dehydrogenation as well as dehydration/rehydrogenation to give amides and amines, respectively. Mizuno *et al*. have developed heterogeneous Ru[82] and Cu[83] catalysts for polyalkylation of aqueous ammonia (or urea) by alcohols to form secondary and tertiary amines. The same group have also used ruthenium hydroxide to heterogeneously catalyze *N*-alkylation of various aromatic and heteroaromatic amines, forming secondary amines in moderate to excellent yields without need for co-catalysts or promoters.[84] Both homogeneous and heterogeneous catalysis of hydrogen autotransfer processes have recently been extensively reviewed.[85–88]

Most directly relevant to the work herein, electrocatalytic *N*-alkylation of amines with alcohols was reported by Kagiya in 1986.[89] Using Pt as electrodes and lithium nitrate as electrolyte with Pt black powder stirring in neat alcohol, aromatic amines and aniline were

alkylated with methanol and ethanol with 65% current efficiency at ambient temperatures. Here, the platinum black was the key to the high current efficiency in reducing the Schiff base with the generated free hydrogen, which was soluble in the alcohol electrolyte. (Scheme 3.4).

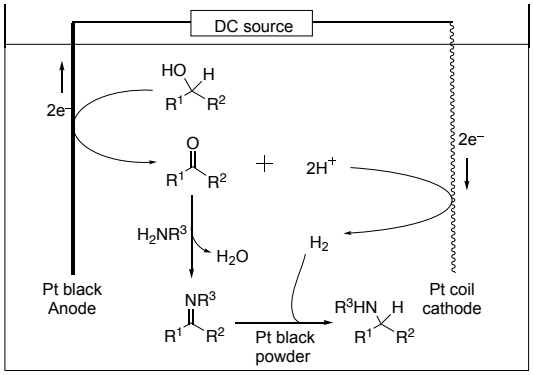

Scheme 3. 4. Electrolytic *N*-alkylation of amines with alcohol by Kagiya et al.

Though the methods above did achieve alcohol amination with attractive yields, many used conditions of high temperature and pressure, organic (non-green) solvents, or costly homogeneous catalysts requiring later separation. Here, we describe two different mechanisms for net electrocatalytic alkylation of ammonia and other amines, in water at temperatures below the boiling point over an easily prepared and mechanically removable catalyst of ruthenium on activated carbon cloth.

Experimental

Catalyst Preparation

An electrodeposited Ru/ACC catalyst was developed and optimized[90] based on the activated carbon cloth (Zorflex® ACC FM100) used in our earlier studies on electrocatalytic reduction by Li

et al.[91] and H/D isotopic exchange by Bhatia *et al.*[68] The ACC (3 cm x 1.5 cm) was initially washed in de-ionized (DI) water and then allowed to dry in an oven overnight at 105 °C. It was then soaked in a solution of Ru $(NH_3)_6Cl_3$ (1.0089 g) dissolved in ammonium hydroxide (1.98 mL) and water (13.02 mL). The damp ACC was dried on the laboratory bench for 24 h, then under vacuum at room temperature. The Ru-impregnated ACC was then electrochemically reduced in an H-cell with 0.2 M HCl as electrolyte at a constant current of 150 mA for 30 mins (about 3 times the quantity of charge required). This catalyst showed similar reactivity to the H_2 reduced counterpart described by Li *et al.* and Bhatia *et al.* Figure 3.1 (i & ii) shows the SEM images of the Ru/ACC before and after electrochemical reduction.

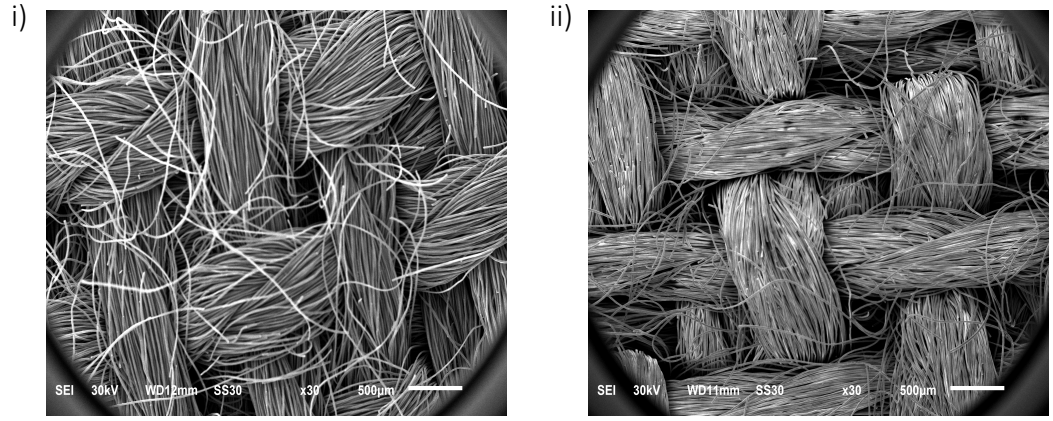

Figure 3.1. SEM images of (I) ACC and (II) electrochemically reduced Ru/ACC in a divided H-cell. The white coating represents the reduced Ru as revealed by EDX in SI.

Reaction Optimization

The reaction was initially performed in a divided two-chamber (2-C) electrochemical cell with Ru/ACC as cathode and Pt as anode, separated by a Nafion®117 membrane. Preliminary investigations examined methylation of the secondary amine pyrrolidine with

methanol. Conversion of 20 mM of pyrrolidine to 3° amine (1-methylpyrrolidine) would theoretically require only 20 mM of methanol, but at this low alcohol concentration, conversion was negligible at 33.3 mA/cm^2 over 6 hours.

Alcohol Concentration

Optimizing alcohol concentration to achieve practical reaction times, we studied a range from 1% v/v (250 mM) to 30% v/v (7.25 M) methanol in 0.01 M phosphate buffer at pH 7; rates rose with methanol concentration up to a saturation point at 20% v/v (Figure 3.2a).

Current Density

Using 20% v/v alcohol, we then studied the effect of varying current density on the rate of the reaction, exploring values ranging from 0.4 mA/cm^2 to 44.4 mA/cm^2 (Figure 3.2b). Initially, we hypothesized that the reaction would follow the borrowing hydrogen process at the cathode where Ru/ACC would catalyze C-H activation of alcohol to form a surface-bound aldehyde or ketone. This carbonyl species would condense with amine to generate surface imine or iminium species which would in turn undergo back reduction to amine. The current in this scenario should only be that needed for the electroactivation of Ru, ≥ 2.2 mA/cm^2, as seen in our earlier H/D exchange studies. But the alkylation rate showed a direct relationship to current density, reaching a maximum at 44.4 mA/cm^2, indicative of a true oxidation/reduction process. Further optimization studies used currents of 33.3 mA/cm^2.

Temperature

As expected, increasing temperature accelerated the reaction. However, at temperatures as low as 36 °C, alkylation still proceeded at useful rates, demonstrating the reaction's mildness (Figure 3.2c).

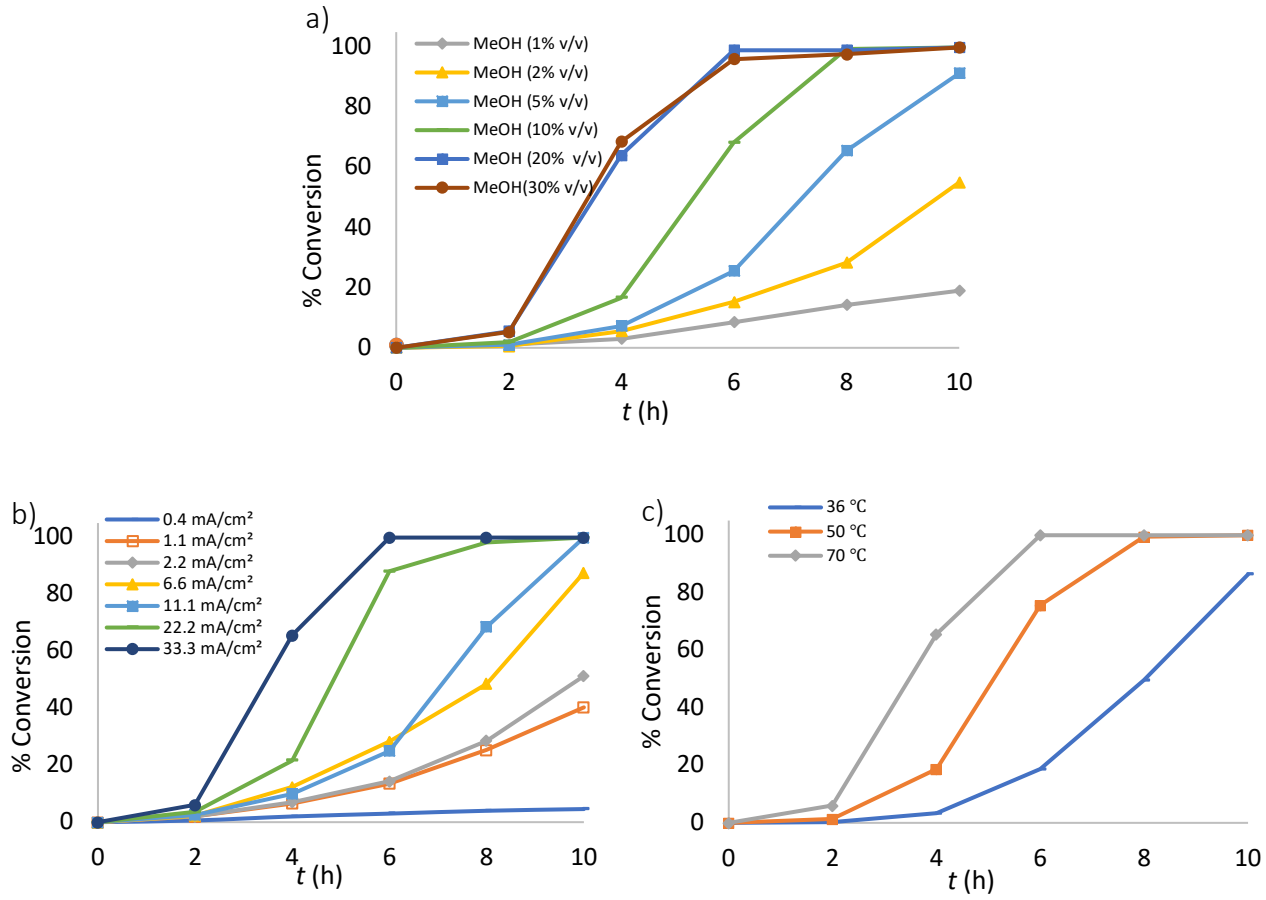

Figure 3.2. (a) effect of alcohol concentration; (b) effect of current density and (c) effect of temperature. Conditions: Pyrrolidine (20 mM in 20 mL) with alcohol added to the cathodic chamber. Standard conditions when not varied: 20% v/v methanol; 33.3 mA/cm^2; 70 °C.

Mechanistic Investigation and The Role of The Catalyst

To explore the importance of current density, an experiment using Ru/ACC (cathode) and Pt (anode), was run with pyrrolidine and methanol added to the cathodic chamber. Though the Ru/ACC electrode was activated by passing current prior to addition of the organics, no current was passed afterward. No alkylated product was formed, confirming the need for current to enable the reaction. Most importantly, simple ACC without Ru as the cathode gave alkylation results and rates similar to those with Ru/ACC. To confirm that this finding did not arise via reductive deposition of catalytic metal contaminants on the cathode, we conducted two experiments: (a) the divided H-cell was rinsed with aqua regia for 96 h, and (b) a brand-new H-cell was used to eliminate the possibility of the presence of even minute amounts of remaining Ru that could catalyze the reaction. Both scenarios yielded alkylated product. Together with the above current requirement, these results pointed to simple anodic oxidation, imine formation, and reduction at the ACC cathode. Even higher alkylation rates were seen if the carbonyl species was supplied directly. Thus, with a Ru/ACC cathode and a Pt anode at 33.3 mA/cm^2, we found 92% alkylation of pyrrolidine to 1-isopropyl pyrrolidine in the presence of 20% v/v acetone over 4 h as compared to 62% in the same period with isopropyl alcohol (figure 3.3).

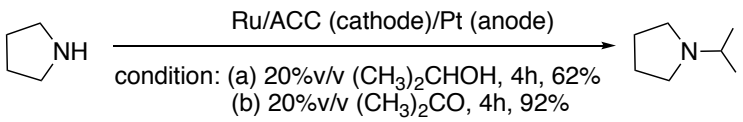

Figure 3.3. Comparison of reactions of pyrrolidine with isopropyl alcohol *vs* acetone, confirming the corresponding carbonyl species as an intermediate.

The above findings implied that methanol had permeated through the Nafion®117 membrane to the Pt anode, gotten oxidized to formaldehyde, permeated back to the cathodic chamber, condensed with pyrrolidine to form iminium, and undergone reduction on the ACC. To test this hypothesis, a cell with ACC (cathode) and Pt (anode) was charged with amine (pyrrolidine) and methanol respectively in the cathodic and anodic chambers. If methanol was indeed oxidized by the Pt anode, amine methylation should be, and indeed was, faster than the case with methanol on the cathode side (Figure 3.4b, green line). Thus, Ru was unnecessary for the alcohol activation in this case (Figure 3.4b, red line). This finding also explained the observed 2 h induction periods seen in our initial studies, which we had earlier attributed to electroactivation of ruthenium.[68]

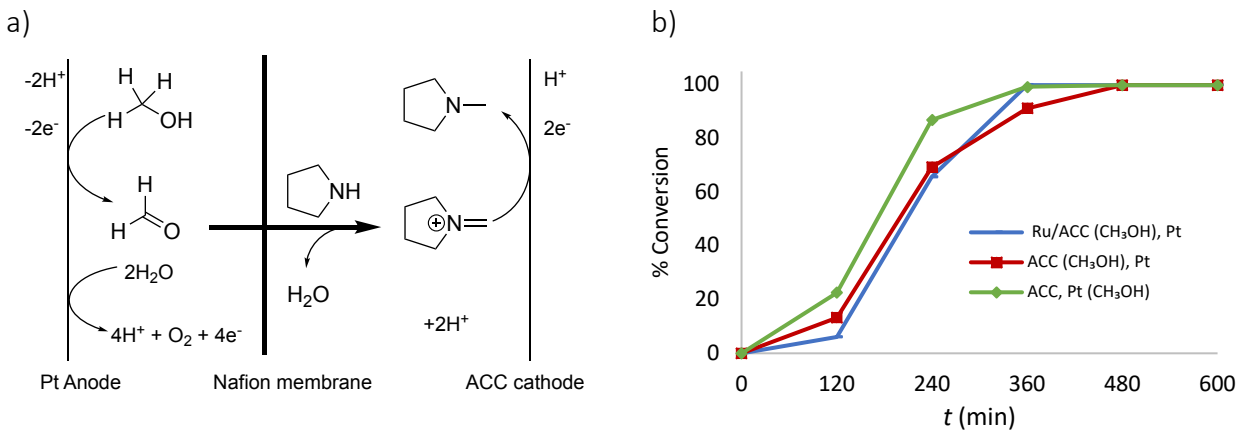

Figure 3.4.(a) Pyrrolidine methylation with methanol in the anode chamber. (b) Alkylation with varied electrode (cathode, anode) pairs with methanol. In the case of the (—blue line) and (—red line) runs, methanol was added to the cathodic side with pyrrolidine. In the last (—green line) example, methanol was added to the Pt anode side. Conditions: Pyrrolidine (20 mM in 20 mL) and 20% v/v methanol in a divided cell with 33.3 mA/cm^2 at 70 °C.

Substrate Scope in Divided 2-chamber (2-C) Cell

Using ACC as cathode and Pt as anode at 33.3 mA/cm^2 and 70 °C, we explored the reaction's substrate scope by methylating additional secondary amines to give 1,4-dimethylpiperazine, 1-methylmorpholine, 1-methyldicyclohexylamine, and 1-methyl-piperidine-4-carboxylic acid. Except for morpholine, these 8 h runs, with methanol in the cathode chamber, gave relatively low yields but did demonstrate the ability of the 2-C cell to effect alkylation with more diverse substrates (Figure 3.5).

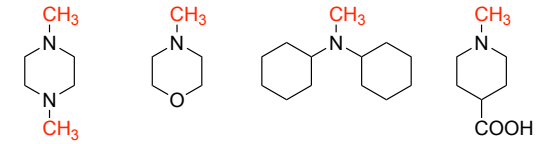

Figure 3.5. Methylation products from alkylation with ACC/Pt in 2-C Cell. Conditions: Substrate (20 mM in 20 mL), 33.3 mA/cm^2, 70 °C & CH_3OH (20% v/v added to anodic chamber).

The Undivided 1-chamber (1-C) Cell

Noting that the above alkylations entailed alcohol oxidation at the Pt anode rather than hydrogen auto-transfer at a Ru/ACC cathode, the process was reoptimized in a 1-chamber (1-C) cell with ACC cathode and Pt anode. This new context enabled reaction at lower current density (2.2 mA/cm^2), alcohol concentration (5% v/v), and temperature (60 °C) values, substantially improving over the 2-C conditions. Based on a flow of 2e- per molecule to oxidize methanol to formaldehyde, and to reduce the iminium species, the optimized current efficiency (CE%, defined in equation 1) for 1-C pyrrolidine methylation was 22%, ignoring any losses due to adsorption of organic substrates into the ACC cloth electrode.

$$CE\% = \frac{(Mol_{prod} \times n \times F)}{C_{total}} \times 100\%$$

where Mol_{Prod} = moles of products formed, F = faraday's constant, 96,485 C mol^{-1}, n = number of electrons per reaction, and C_{total} = total charge passed in coulombs.

Several cathode-anode catalyst combinations (Figure 3.6) were explored in the 1-C context, again using pyrrolidine methylation as the test reaction. Use of ACC as cathode but

replacing Pt with Ru/ACC at the anode gave improved conversion (98.3% vs. 83.3% in 6 h) and CE% (30% vs. 22%). Use of Ru/ACC for both electrodes yielded similar results.

Importantly, no reaction was observed when ACC was used as both cathode and anode (Figure 5). As a check, the inability of the ACC to activate alcohols was further explored via experiments in D_2O with ACC as both anode and cathode electrodes; no C-H exchange was seen. Literature confirms the inertness of carbon electrodes for alcohol oxidation. For instance, glassy carbon (not competent) has been studied with boron-doped diamond (BDD) (competent) for the oxidation of methanol and benzyl alcohol.[30] The inertness of common carbon electrode materials makes them ideal as catalyst and electrocatalyst supports. Examples include ultrathin Co_3O_4 supported on carbon paper and carbon cloth for ethanol oxidation,[31] platinum on graphite for benzyl alcohol oxidation,[32] and indium tin oxide (ITO) on reticulated vitreous carbon[92] electrodes for ethanol oxidation.

Most intriguing was the case with Ru/ACC as the cathode and ACC as the anode, where methylation still occurred, albeit slowly, even with an anode unable to oxidize alcohol. This observation indicates that the electroactivated Ru/ACC cathode is capable of alkylation via actual hydrogen auto-transfer, the classic “borrowing hydrogen” mechanism.

For the two-electrode process, substrate scope was explored with the ACC cathode and Ru/ACC anode combination in a 1-C cell (Figure 3.6). Reaction of pyrrolidine in 5% methanol at 60 °C gave a 98% yield of 1-methylpyrrolidine in 6 h at pH 7.5. Though the ACC-Pt combination had given only modest yields (≤ 30%) upon pyrrolidine alkylation with ethanol and 2-propanol, at pH 8.5 these substrates, as well as cyclohexanol and benzyl alcohol, now yielded 1-ethylpyrrolidine (99%), 1-isopropylpyrrolidine (92%), 1-cyclohexylpyrrolidine

(20%), and 1-benzylpyrrolidine (30%) respectively (Table 3.1). The slightly alkaline pH increases the free amine concentration, presumably accelerating imine formation. Pyrrolidine alkylations with two alcohols incapable of oxidation to carbonyl species, phenol and *t*-butanol, were also attempted, but as expected, they yielded no alkylation products, consistent with the borrowing hydrogen mechanism.

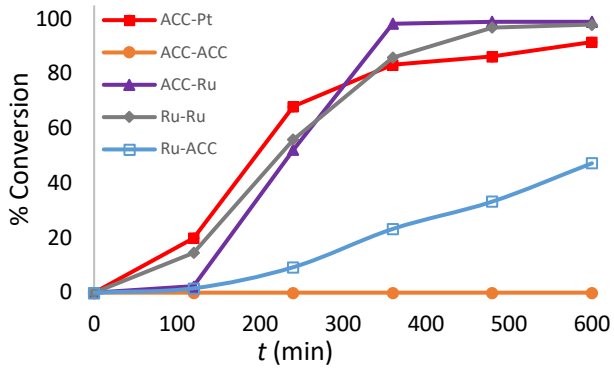

Figure 3.6. Pyrrolidine methylation in 1-chamber cell (1-C, open cell) with various cathode-anode electrode combinations. Conditions: Pyrrolidine (20 mM in 20mL), 2.2 mA/cm^2, 60 °C and CH_3OH (5% v/v).

Table 3.1. Alkylation of pyrrolidine with 1° and 2° alcohols

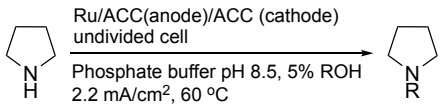

Entry	Alcohol	product	Conversion %	Yield %	C.E %
1	CH_3OH		99 (100)	42 (98)[a]	18
2		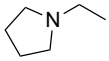	99 (100)	49 (99)[a]	18
3		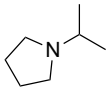	96 (98)	39 (92)[a]	16
4	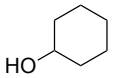	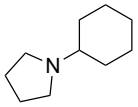	55 (65)	8 (20)[b]	4
5	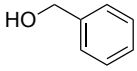	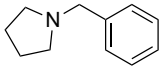	90	30[b]	8

C.E % = current efficiency, [a] yield at 6 hours, [b] yield at 10 h. Values in parentheses includes species in solution and extracted from the electrodes using 5 mL *t*-BuOH. Conversion values are based on pyrrolidine.

Computational Justification

To explain the falling yields of the pyrrolidine reactions with increasing alcohol size, we calculated the electronic energies of the individual species for the process of alkylated pyrrolidines. As expected, oxidation of alcohol to aldehyde or ketone favored the secondary over the primary alcohols in both gas phase and water. The intermediate iminium ion formation favored the larger cationic species in gas phase and the reverse is true in water phase. We suggest that this observation reflects the stronger water stabilization of smaller vs larger cations. The imine reduction was not significantly different among the models as they were all very strongly stabilized upon

the reduction in this last step. Overall, the alcohol oxidation is computed to be the rate determining step which agrees with our experimental results (Table 3.2).

Table 3.2. DFT calculation of the reaction steps from alcohol oxidation to iminium formation and then iminium reduction in gas phase (top values) and aqueous phase (values in brackets) at B3LYP/6-31G*

Electronic energy (kcal/mol)				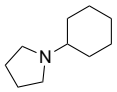	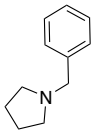
Alcohol oxidation	24.1 **(27.8)**	18.02 **(20.6)**	14.6 **(16.1)**	14.8 **(16.8)**	13.6 **(16.3)**
Iminium formation	1.1 **(3.1)**	-1.3 **(5.6)**	-3.1 **(7.1)**	-5.4 **(8.3)**	-4.1 **(10.1)**
Iminium reduction	-32.2 **(-34.0)**	-23.2 **(-26.6)**	-17.0 **(-20.9)**	-15.6 **(-21.3)**	-18.2 **(-26.1)**

Amine Substrate Scope

Extending the amine substrate scope led to yields of 4-methylmorpholine (46%) and 1-methylpiperidine (55%) respectively after 10 h reactions with methanol at pH 7.5. These efforts were extended to ethanol at pH 8.5, yielding 4-ethylmorpholine (69%) and 1,6-diethylpiperazine (47%) respectively (Table 3.3). Methylations worked best at pH 7.5 whereas the 1° and 2° alcohols gave excellent results at pH 8.5. Traces of hydrocarbon-range resonances in the ^{1}H-NMR are attributed to the possible formation of branched Guerbet alcohols[93] .

As seen in Table 3.3, the system tolerated the carboxylic functional groups in isonipeconic acid and sarcosine (*N*-methylglycine). Though slow, methylation of the strongly sterically hindered 2° amine dicyclohexylamine gave (34%) 1-methyldicyclohexylamine. Turning to aniline as the simplest aromatic amine, we attempted ethylation, but even after substantial optimization efforts, lowering the pH to 3 to minimize aniline oxidation, we still only obtained small amounts of the monosubstituted *N*-ethylaniline.

Table 3.3. Alkylation of 2° amines with methanol and ethanol

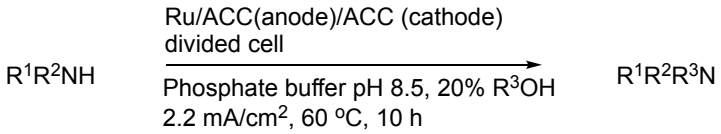

Entry	Alcohols	R_2NH	Products	Conversion %	Yield %
1	CH_3OH		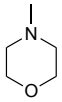	86	46
2			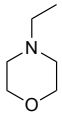	91	69
3	CH_3OH			71	55
4		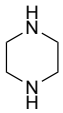	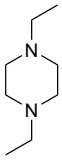	67	47
5		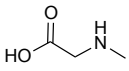	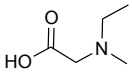	48	17
6	CH_3OH	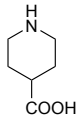	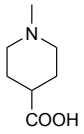	68	33
7	CH_3OH	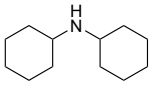	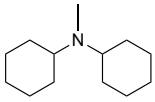	58	34

Alkylation of Ammonia

Attempting direct alkylation of ammonia with ethanol (Table 3.4), a 9% yield of triethylamine was obtained in 10 hours at 60 °C. This low yield was attributed to loss of

ammonia by evaporation. We then studied the reaction at room temperature (25 °C) and observed a decreased yield to 7% but still suspected loss of ammonia by evaporation. Use of ammonium acetate[94] (to provide aqueous ammonia *in situ*) at 60 °C with a Teflon cap to partially seal the electrochemical cell yielded 36% triethylamine. Reaction progress, monitored by 1H NMR, showed the formation of ethylamine (b.p. = 16 °C) and diethylamine (b.p. = 55 °C) in small quantities, supporting the expected stepwise formation of triethylamine. To explore the possibility of intermediate disproportionation to mono and triethylated products, diethylamine was subjected to the reaction with ethanol, yielding 92% triethylamine; ethylamine was not observed, indicating no disproportionation as expected from the thermodynamic data in Scheme 2. Two different paths to diethylbutylamine were explored: (1) a 1° amine (*n*-butylamine) and 5% ethanol and (2) a 2° amine (diethylamine) and 5% *n*-butanol, with yields of 32% to 52% respectively. As expected, the reaction requiring two sequential alkylations gave the lower yield. The low solubility of *n*-butanol (8% v/v in H_2O)[95] compared to ethanol (fully miscible with H_2O) could also have contributed to its lower yield.

With isopropyl alcohol, only diisopropylamine was formed, regardless of reaction time. Consistent with the literature report on cyclohexylation,[77] this result is presumably due to the bulky isopropyl groups hindering the formation of the final imine intermediate. However, alkylation of diisopropylamine with ethanol, a primary alcohol, did give a 28% yield of Hünigs base (Table 3.4).

Table 3.4. Synthesis of triethylamine and diisopropylamine

Entry	Alcohols	Substrates	Products	Temp. °C	Yield %
1		NH_3		60	9
2		NH_3		r.t	7
3		NH_4OAc		60	36
4				60	39
5				60	26
6		NH_3		60	20
7				34	30
8				34	28
9		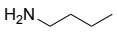	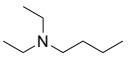	70	32
10	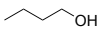		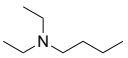	69	52

Single-electrode Alkylation

Returning to the relatively slow amine alkylation achieved on the cathode alone, a new mechanism must be considered. Here no free carbonyl species is seen or expected. Our previously reported finding of stereoretentive C-H activation and H/D exchange in alcohols and amines on the Ru/ACC cathode suggested that in the amine alkylation reactions, the stereochemistry of the original alcohol might be carried over to the resulting amine. We explored the stereochemical outcome of the single-electrode alkylation with the *cis*/*trans* isomers of 4-methylcyclohexanol and with 4-methylcyclohexanone reacting with pyrrolidine. Using *t*-butanol as co-solvent to improve the solubility of the cyclohexyl systems, reactions were conducted in a series of membrane-separated and open electrochemical systems, with yields and product stereochemistry evaluated.

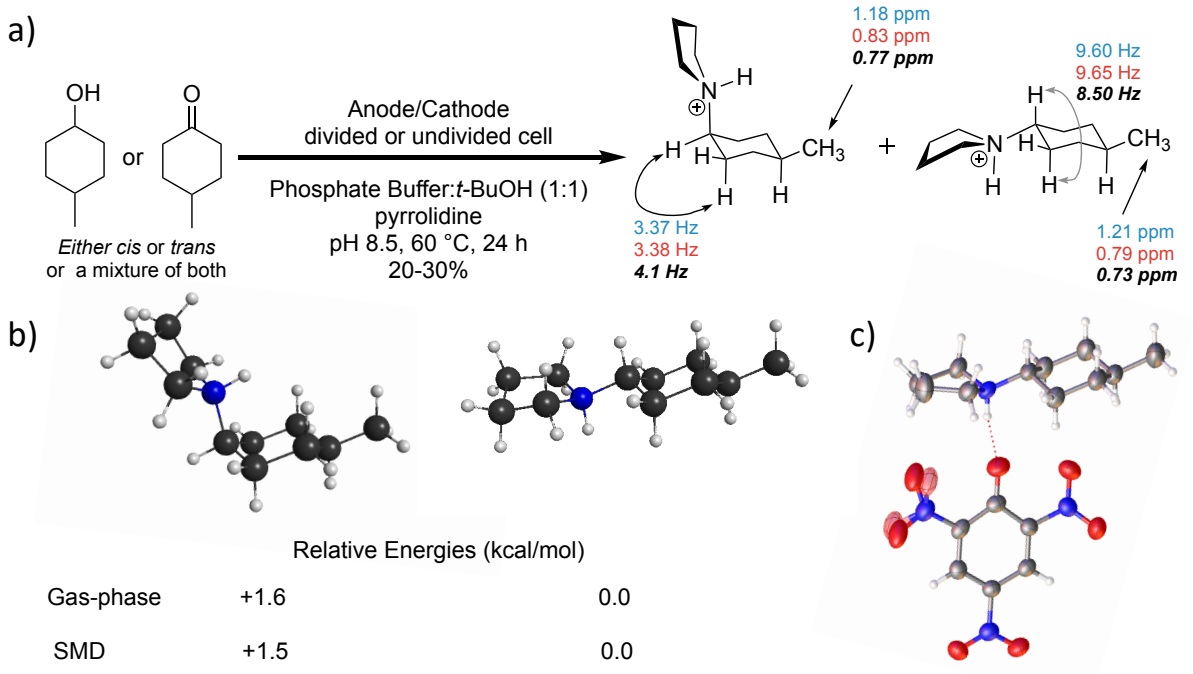

Figure 3.7. (a) Reactions of pyrrolidine with *cis*-4-methylcyclohexanol, *trans*-4-methylcyclohexanol, a mixture of *cis/trans*-4-methylcyclohexanol or 4-methylcyclohexanone. (b) Relative energies of the most stable conformers and coupling constants of (left) *cis*-4-methylcyclohexylpyrrolidine and (right) *trans*-4-methylcyclohexylpyrrolidine computed with Gaussian16 at the B3LYP[96]/6-31G(d,p)[97] level. For NMR chemical shift and coupling constant calculations, the GIAO method in Gaussian16 was used with the above geometries at the MPW1PW91[98]/6-311+G(2d,p)[99] level of theory, with chemical shifts referenced against tetramethylsilane (TMS) calculated at the same level of theory. Coupling constant values shown are experimental (blue) and computed "aqueous phase (SMD)" (red) and "gas phase" (black). (c) Crystal structure of the picrate salt of *trans*-4-methylcyclohexylpyrrolidine (m.p = 189-191 °C) obtained from amination of 4-methylcyclohexanol.[100]

Stereochemistry of One- and Two-electrode Alkylation

As seen in Table 3.5 (entries 1, 2), no alkylation product was observed with ACC for the two electrodes, with or without a membrane divider. This finding is consistent with the earlier noted inability of ACC alone to oxidize alcohols to the corresponding carbonyl compounds; as expected, no direct reaction is seen between alcohol and pyrrolidine. On the other hand, with cyclohexanone, regardless of membrane, the expected alkylation did occur. The resulting 1:1 ratio of cis and trans pyrrolidinyl cyclohexanes was essentially like that seen from classical sodium borohydride reduction (entry 5). As expected with the ketone substrate, the nature of the anode was unimportant (entries 6, 7). Significantly, with an oxidation-competent Ru/ACC anode, reaction with the cis isomer of the alcohol did yield the same 1:1 amination ratio, consistent with formation of ketone at the anode (entry 8), enabling the 2-electrode amination process.

A different pattern emerged with ACC anodes and Ru/ACC cathodes. Here the amination must have occurred only at the activated ruthenium cathode, as the ACC anode is not able to oxidize the alcohol. With or without membrane present, this one-electrode process effects amination of the ketone or either of the 4-methylcyclohexanol isomers with a 2:1 cis:trans ratio of aminated cyclohexane. Disappointingly, no direct reflection of the initial alcohol's stereochemistry is seen in the product ratio, but the Ru/ACC reduction does have a different stereochemical selectivity than reduction by ACC alone. Evidently the alcohol undergoes C-H activation at the cathode (a process known to retain stereochemistry) but undergoes release at some point in the process of forming the imine intermediate and undergoing the final reduction. In sum, the Ru/ACC cathode does activate and aminate

alcohols but is not able to retain a trace of their original stereochemistry under the present reaction conditions.

Table 3.5. Stereochemical outcome by electrode pairing in 1-C and 2-C reactor configurations

Exp.	Cathode	Membrane	Anode	Alcohol	Product; Cis/trans-Selectivity
1	ACC	Yes	ACC	Alcohol[a,b] (cis/trans)	No Reaction
2	ACC	No	ACC	Alcohol[a] (cis/trans)	No Reaction
3	ACC	No	ACC	Ketone[c]	1:1
4	ACC	Yes	ACC	Ketone[b,c]	1:1
5	$NaBH_4$/TFE/40 °C	N/A	N/A	Ketone[c]	1:1
6	ACC	Yes	Ru/ACC	Ketone[b,c]	1:1
7	ACC	No	Ru/ACC	Ketone[c]	1:1
8	ACC	No	Ru/ACC	Alcohol[a] (cis)	1:1
9	Ru/ACC	No	ACC	Alcohol[a] (cis)	2:1
10	Ru/ACC	Yes	ACC	Alcohol[a,b] (trans)	2:1
11	Ru/ACC	Yes	ACC	Alcohol[a,b] (cis/trans)	2:1
12	Ru/ACC	Yes	ACC	Ketone[b,c]	2:1

[a]Alcohol = 4-methylcyclohexanol; [b]Substrate placed in cathode compartment; [c]Ketone = 4-methylcyclohexanone

Notably, no re-equilibration of the above cis/trans ratios was observed after amination. Product mixtures with the 1:1 ratio obtained from the ACC reductive amination reactions remained the same when re-exposed to any of the electrode combinations. Products were

identified by melting point,[100] GC/MS and 2D-NMR, but most significantly confirmed by the X-ray structure of the *trans*-N-(4-methylcyclohexyl)pyrrolidine, which we obtained in the form of the picrate salt (Figure 3.7). This isolated material enabled unambiguous assignments of the NMR spectra, enabling easy analysis of product mixtures. To estimate the energetics of the cis and trans aminated isomers, we also ran B3LYP/6-31G(d,p) calculations in gas and simulated aqueous[101] phases on both neutral and protonated forms of the 4-methylcyclohexyl pyrrolidine. For the latter, which are expected to dominate at a pH of 8.5, the *trans* isomer was calculated to be 1.5 kcal/mol lower in free energy than the *cis* isomer, when solvation and vibrational analyses are included. However, it was the cis product that dominated in the Ru/ACC-reduced product mixtures. This apparent deviation from the purely thermochemical ratio presumably reflects imine adsorption on the catalyst surface and hydrogen delivery to the less sterically hindered face of the cyclohexane ring, opposite to the methyl substituent.

For product analysis, fortunately, the chemical shifts of the methine hydrogens on the carbon bearing the nitrogen were distinct in the experimental ^{1}H-NMR with coupling constants of 8.50 Hz for the *trans*-isomer and 4.10 Hz for *cis*. The calculated NMR coupling constants in gas-phase/simulated solvent were 9.60 Hz/9.65 Hz and 3.37/3.38 Hz respectively (figure 3.7). Also, the 4-methyl protons were distinctly separated in the experimental NMR. Computing the theoretical NMR chemical shifts (CS) of the 4-methyl groups in the two isomers relative to that of TMS,[102,103] our results were consistent with experimental data, finding the 4-methyl group of the trans isomer to be upfield from that of the cis by 0.3 (gas phase), 0.3 (SMD[104], water) and 0.4 (experimental) ppm.

Conclusions and Outlook

In conclusion, we have developed an electrocatalytic system that achieves amine alkylation with alcohols via two differing "hydrogen borrowing" pathways: an indirect, two-electrode path in which the hydrogen "borrowed" at the anode is returned via regeneration from H^+ and e^- at the cathode; and a direct C-H activation, condensation, and re-reduction scheme taking place at the cathode alone. We have found that for imine reduction to *N*-(4-methylcyclohexyl)pyrrolidine, the Ru/ACC cathode has a (*trans/cis)* selectivity of 1:2 whereas the plain ACC cathode forms a 1:1 product ratio, essentially the same as the classical reductive amination with $NaBH_4$. Investigating the use of various cathode-anode pairings, we have found Ru/ACC as anode and ACC as cathode to be the optimal system for amine alkylation via electrocatalytic oxidation at the anode and reduction at the cathode in an undivided one-chamber H-cell (open cell). The reaction is most readily accomplished using smaller primary and secondary alcohols, but bulkier alcohols such as benzyl alcohol and cyclohexanol can also be used successfully. The chemistry has been applied to synthesis of laboratory reagents such as triethylamine, diethylbutylamine and *N,N*-diisopropylamine (Hünig's base) in good yields. Looking ahead, we continue to pursue more effective ways to alkylate aromatic amines, and to extend these electrocatalytic strategies to the classes of C-C bond forming reactions observed in more conventional catalytic settings.[85–87]

Acknowledgements

Thanks to Dr. Souful Bhatia for getting me started on this project before he finished his Ph.D. and to Ms. Gabriela Keeney for working alongside with me during her undergraduate studies at Michigan State University.

APPENDIX

Characterization of Compounds

^{1}H NMR: Reaction of pyrrolidine with methanol

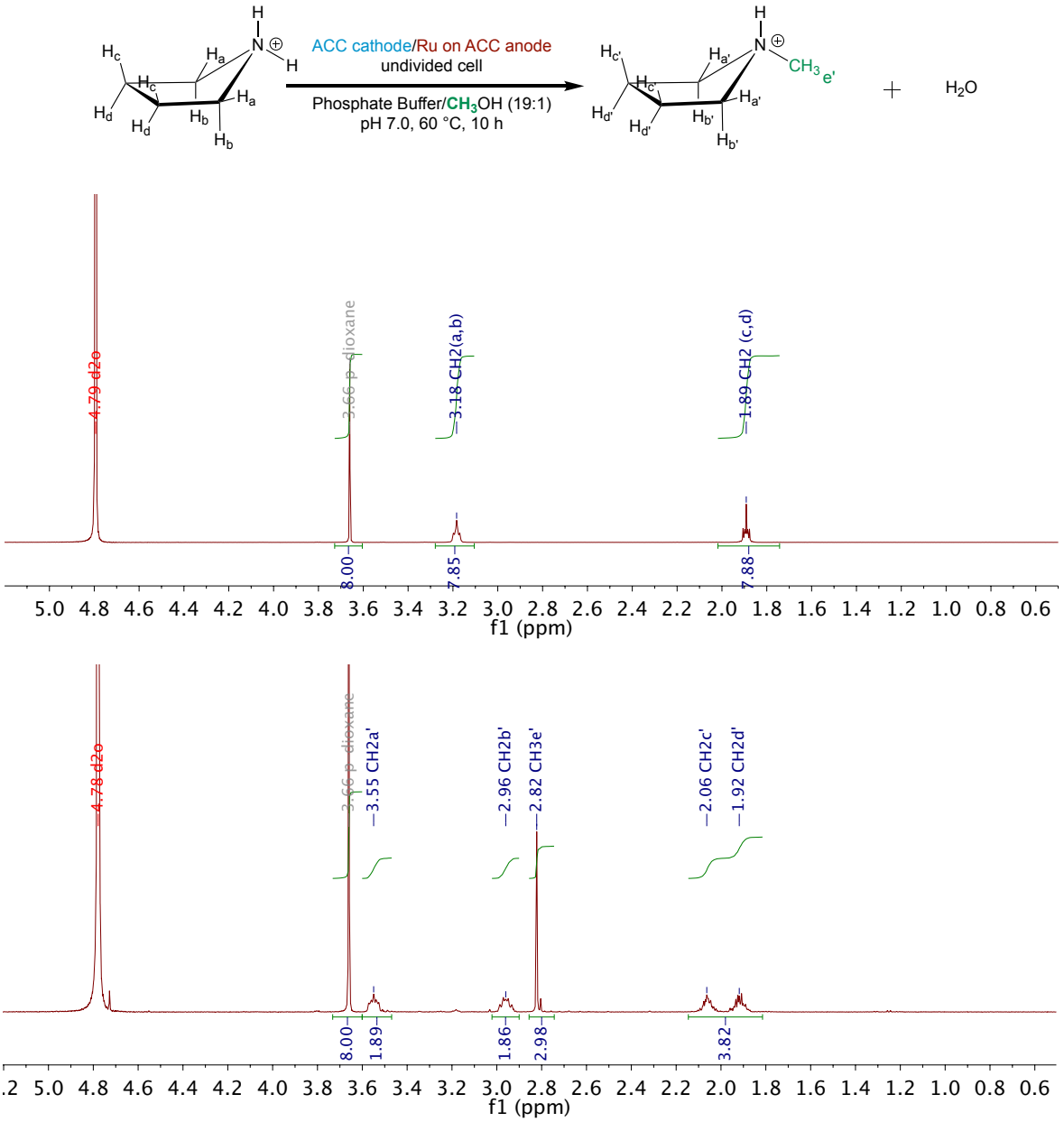

Figure 3.8. The reaction of pyrrolidine (top) with methanol at constant current of 2.2 mA/cm^2 yielded 85% *N*-methylpyrrolidine with 96% conversion (bottom)

N-methylpyrrolidine with 96% conversion (bottom).

^{1}H NMR: Reaction of pyrrolidine with ethanol

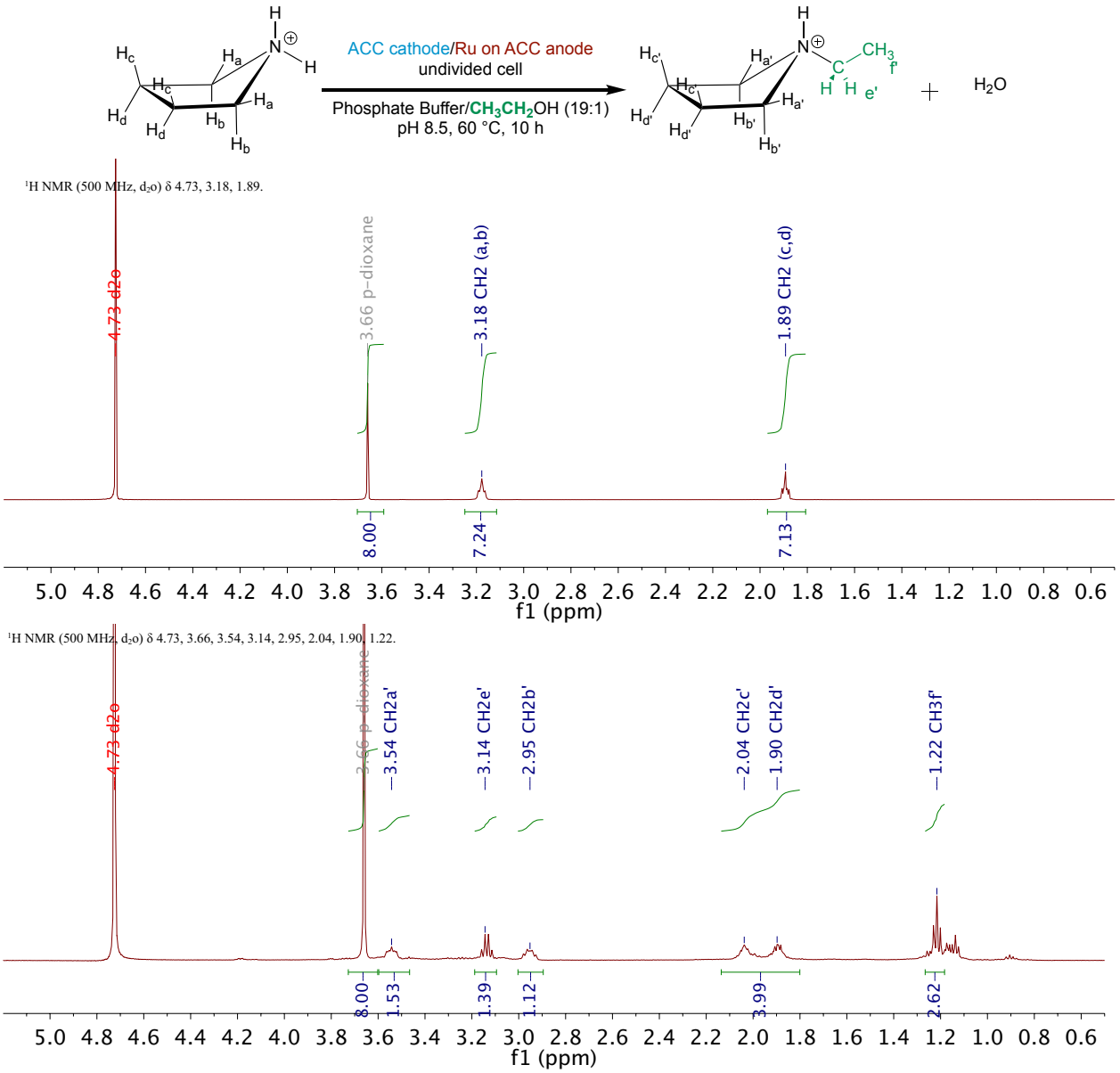

Figure 3.9. The end reaction of pyrrolidine (top) with ethanol at constant current of 2.2 mA/cm^2 yielded 89% *N*-ethylpyrrolidine with 93% conversion (bottom).

^{1}H NMR: Reaction of pyrrolidine with isopropyl alcohol

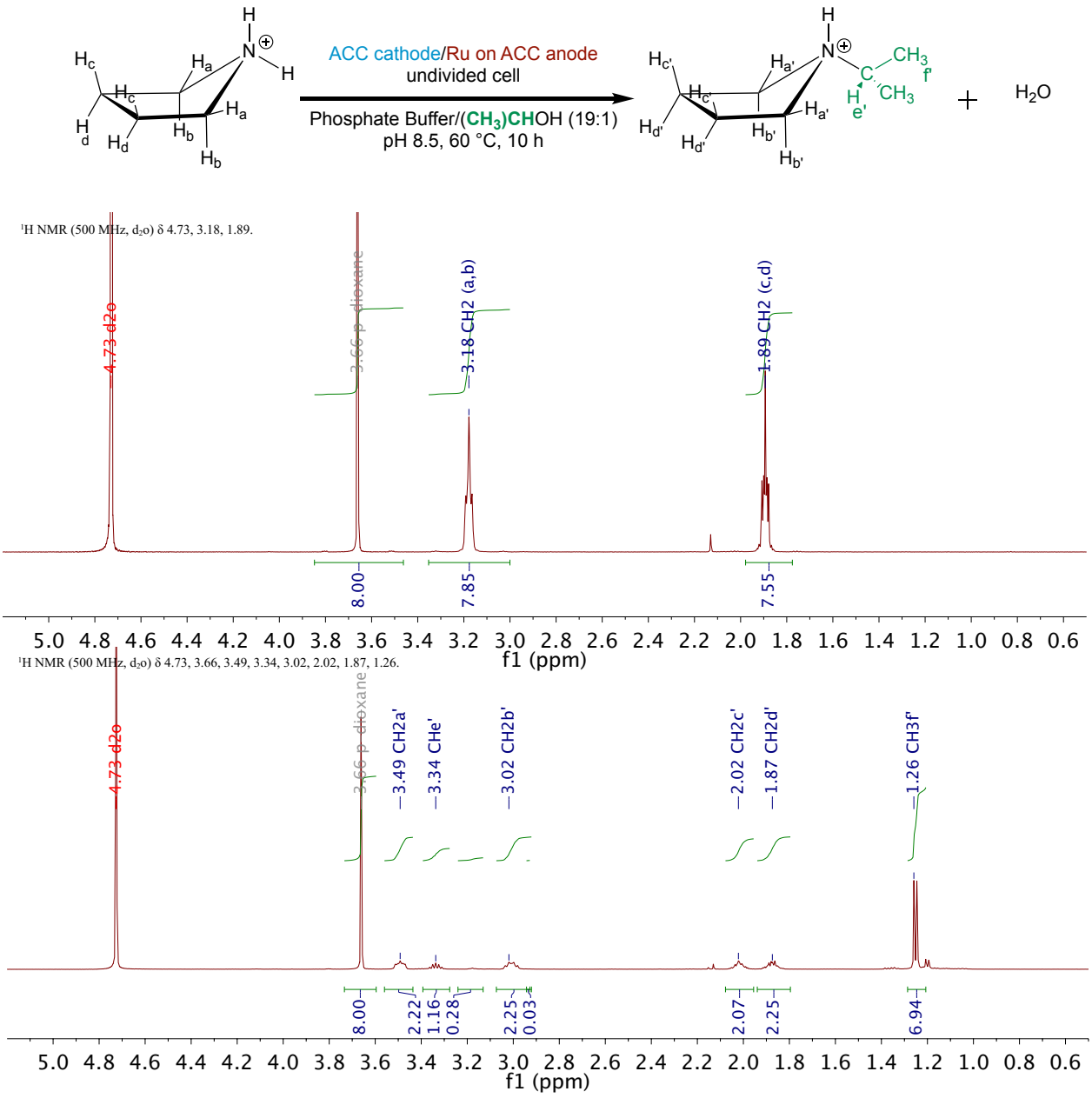

Figure 3.10. The end reaction of pyrrolidine (top) with isopropyl alcohol at constant current of 2.2 mA/cm^2 yielded 60% *N*-ethylpyrrolidine with 95% conversion (bottom).

[1]H NMR: Reaction of morpholine with methanol

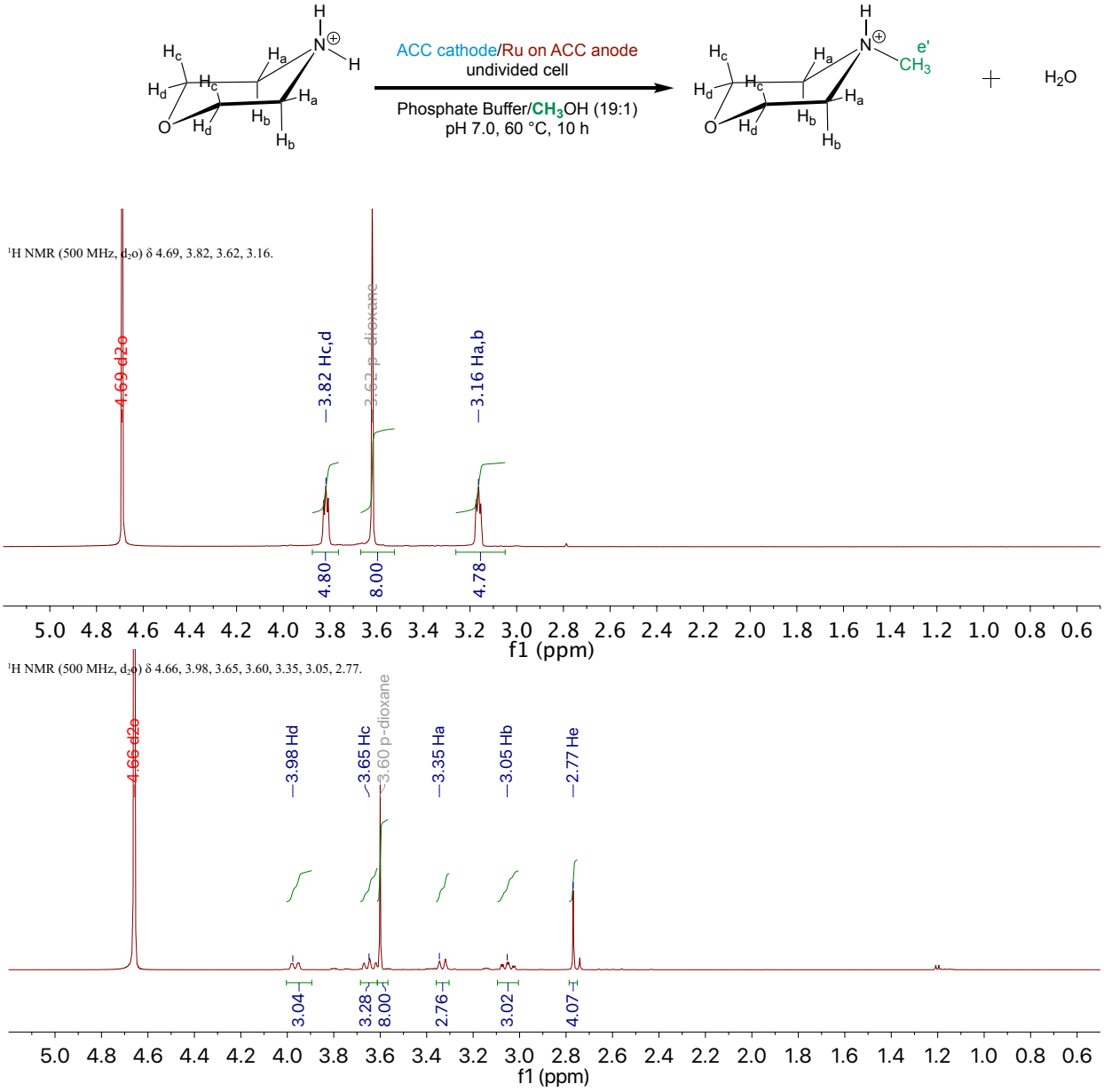

Figure 3.11. The reaction of morpholine (top) with methanol at constant current of 2.2 mA/cm^2 yielded 68% N-methylmorpholine with 87% conversion (bottom).

[1]HNMR: Reaction of morpholine with ethanol

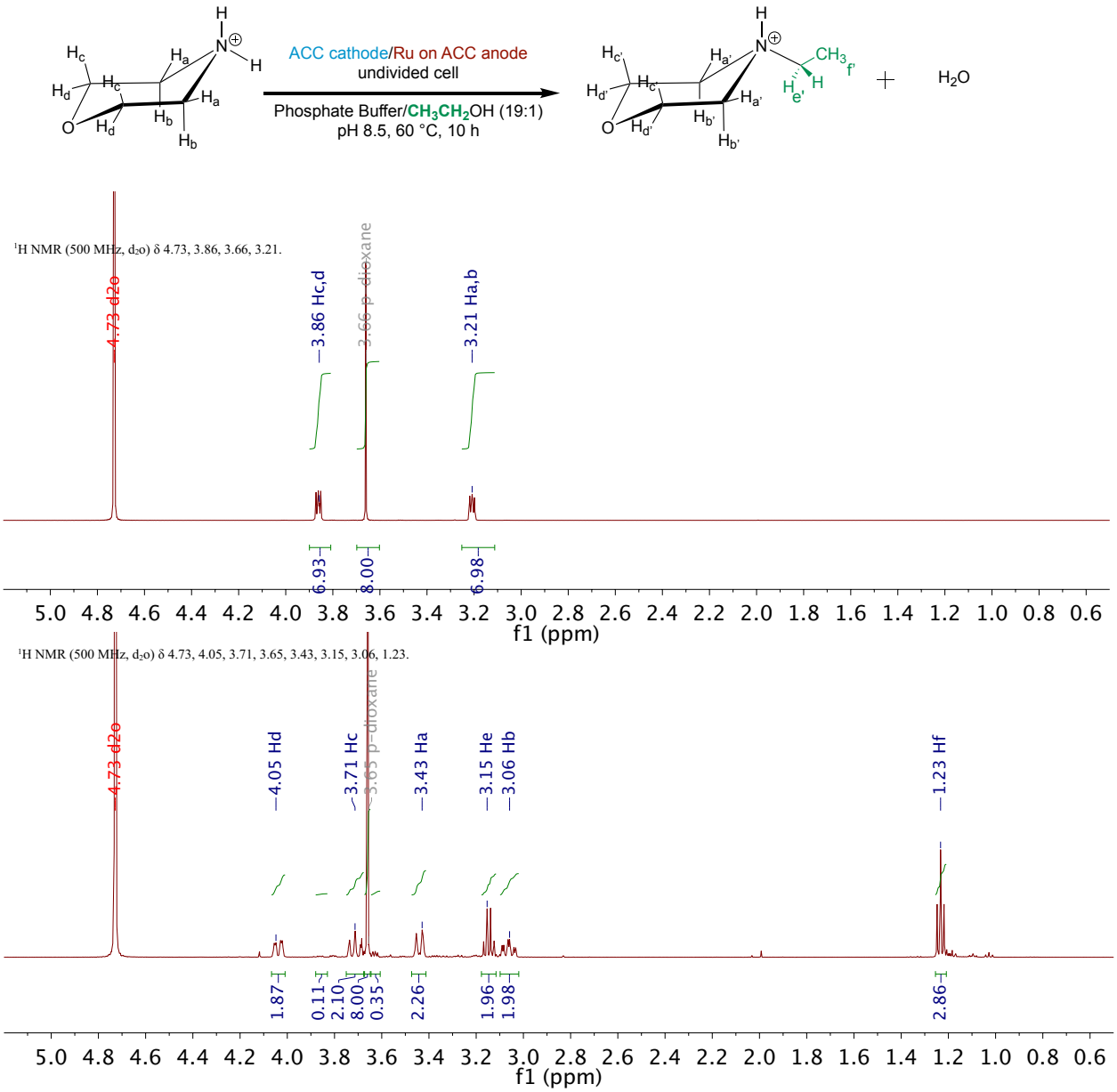

Figure 3.12. The reaction of morpholine (top) with ethanol at constant current of 2.2 mA/cm^2 yielded 69% *N*-ethylmorpholine with 98% conversion (bottom).

^{1}H NMR: Reaction of sarcosine with methanol

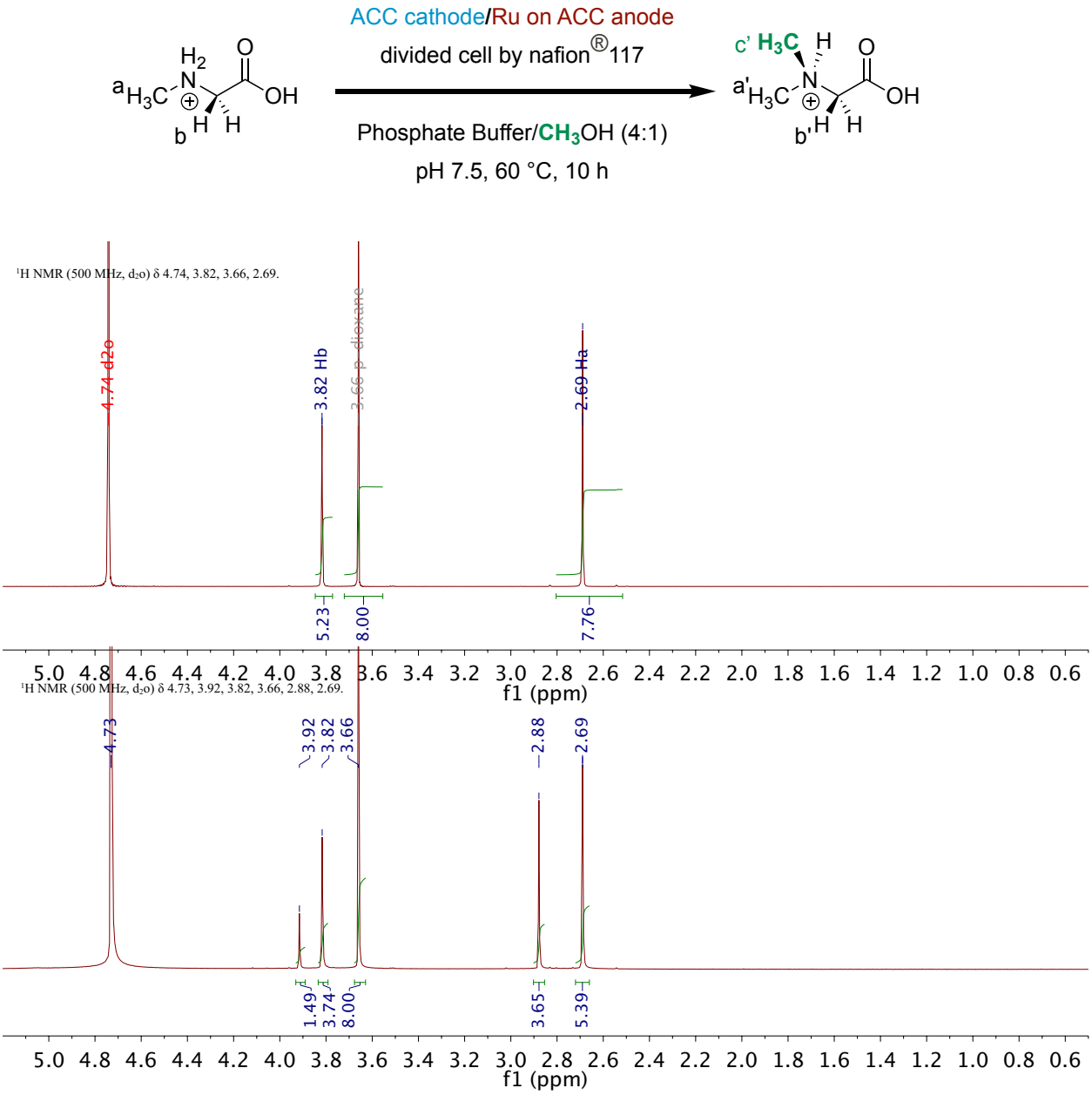

Figure 3.13. The reaction of sarcosine (top) with methanol at constant current of 2.2 mA/cm^2 yielded 62% *N*-methylsarcosine with 67% conversion (bottom).

^{1}H NMR: Reaction of sarcosine with ethanol

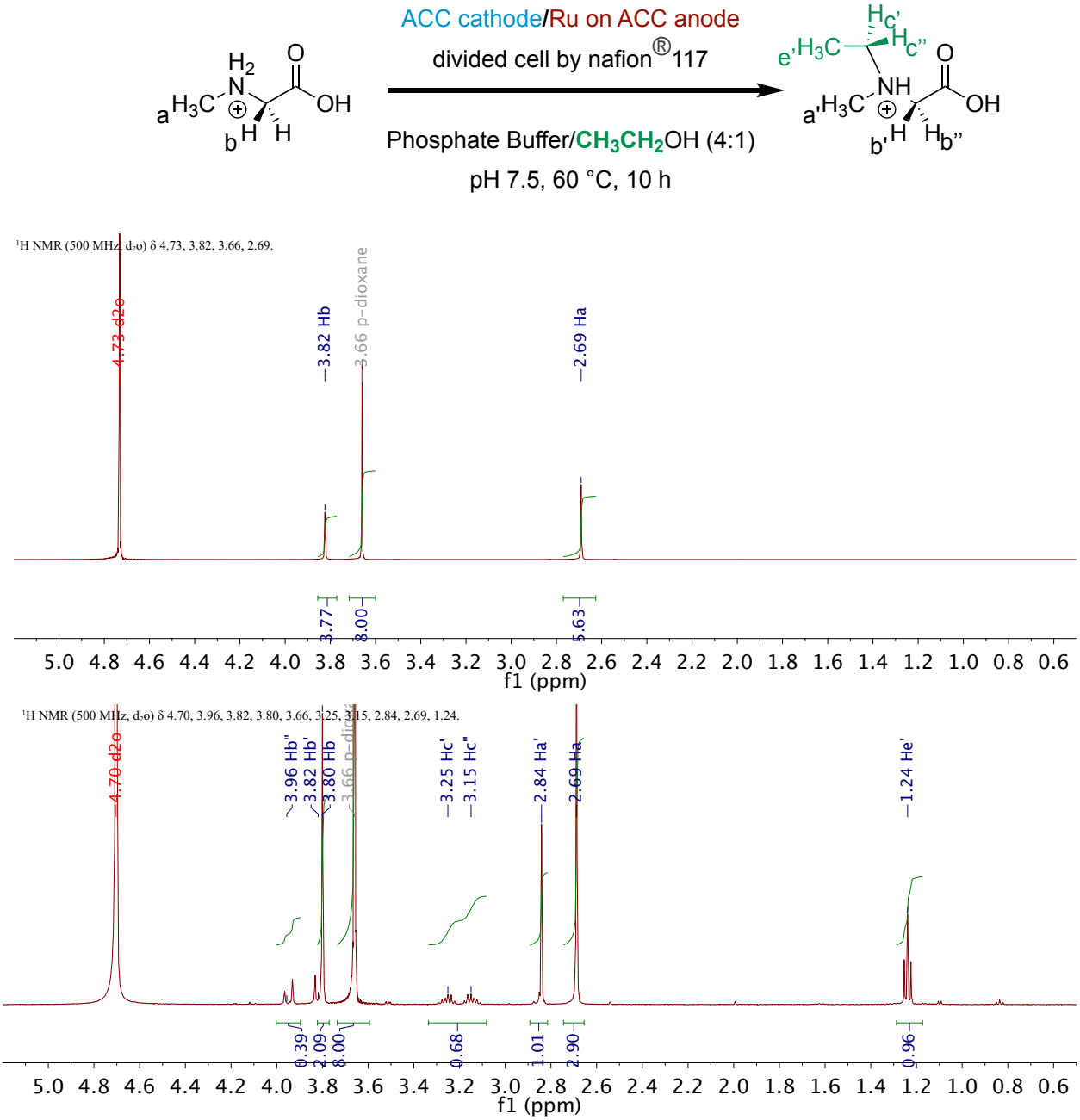

Figure 3.14. The reaction of sarcosine (top) with ethanol at constant current of 2.2 mA/cm^2 yielded 66% *N*-ethylsarcosine with 75% conversion (bottom).

^{1}H NMR: Reaction of ammonium acetate (generates ammonia in situ) with ethanol

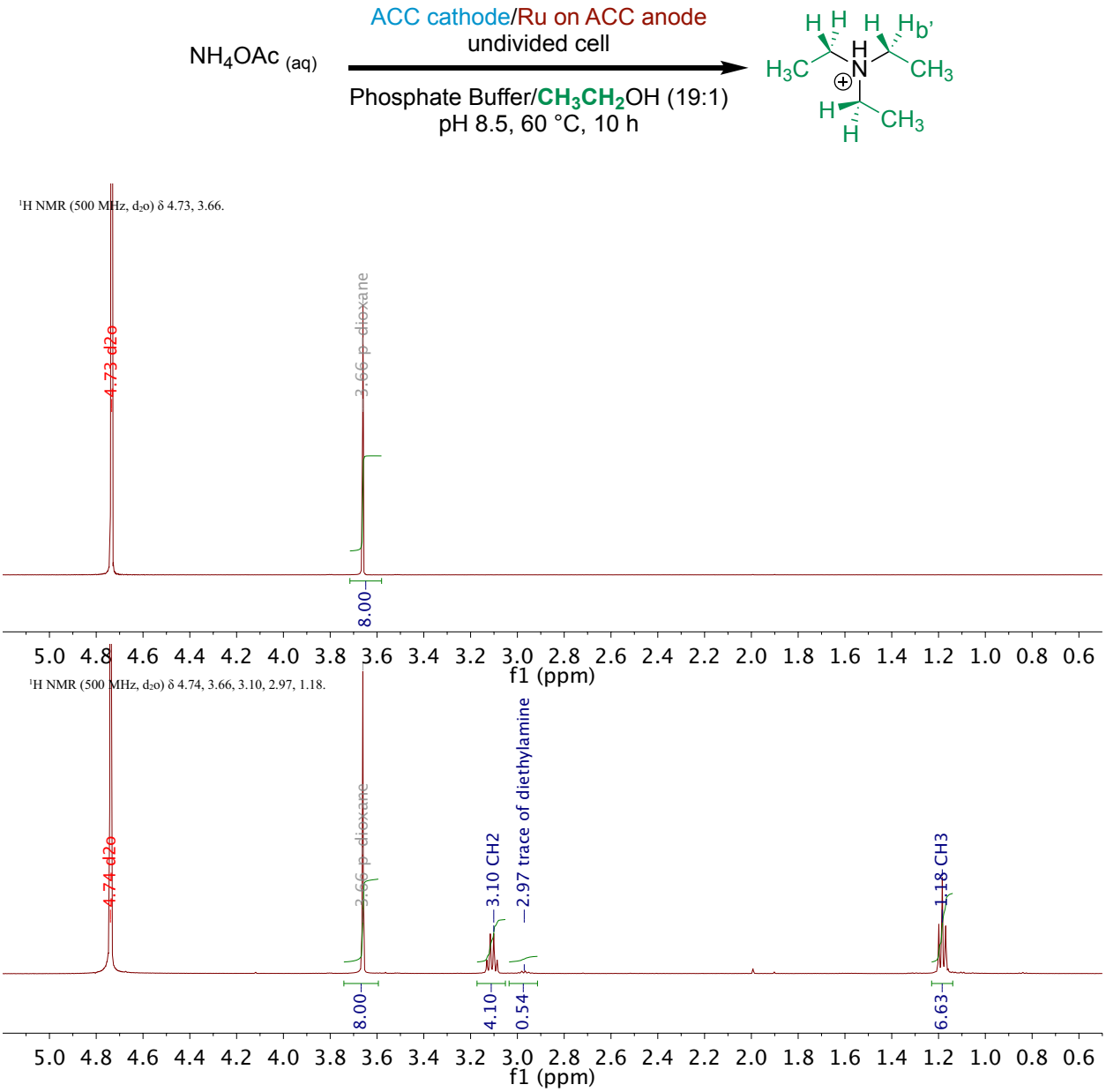

Figure 3.15. The reaction of ammonia acetate (ammonia) (top) with ethanol at constant current of 2.2 mA/cm^2 yielded 90% N-triethylamine with 92% conversion (bottom).

^{1}H NMR: Reaction of ethylamine with ethanol

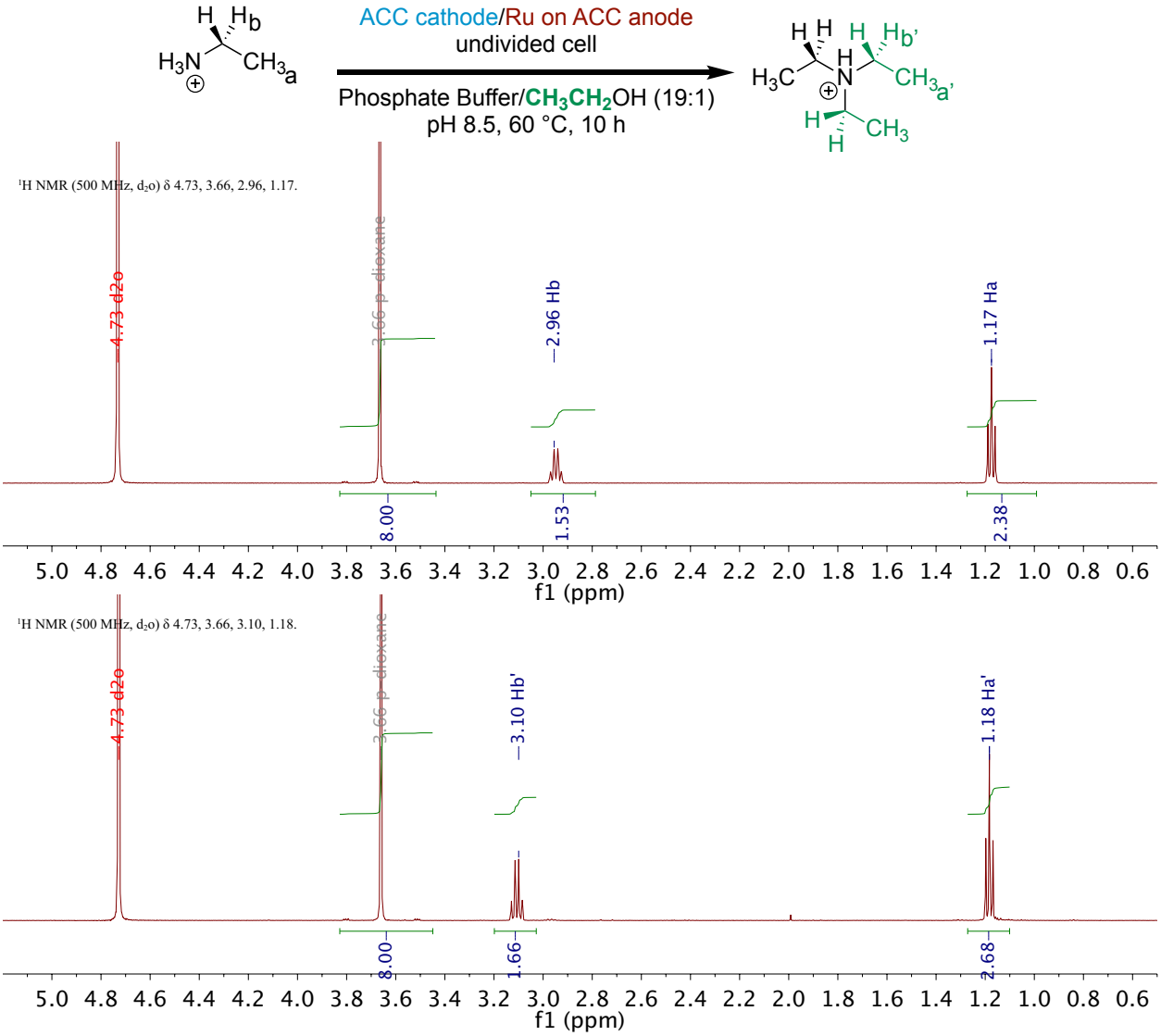

Figure 3.16. The reaction of ethylamine (top) with ethanol at constant current of 2.2 mA/cm^2 yielded 92% triethylamine and 97% conversion (bottom).

[1]H NMR: Reaction of diethylamine with ethanol

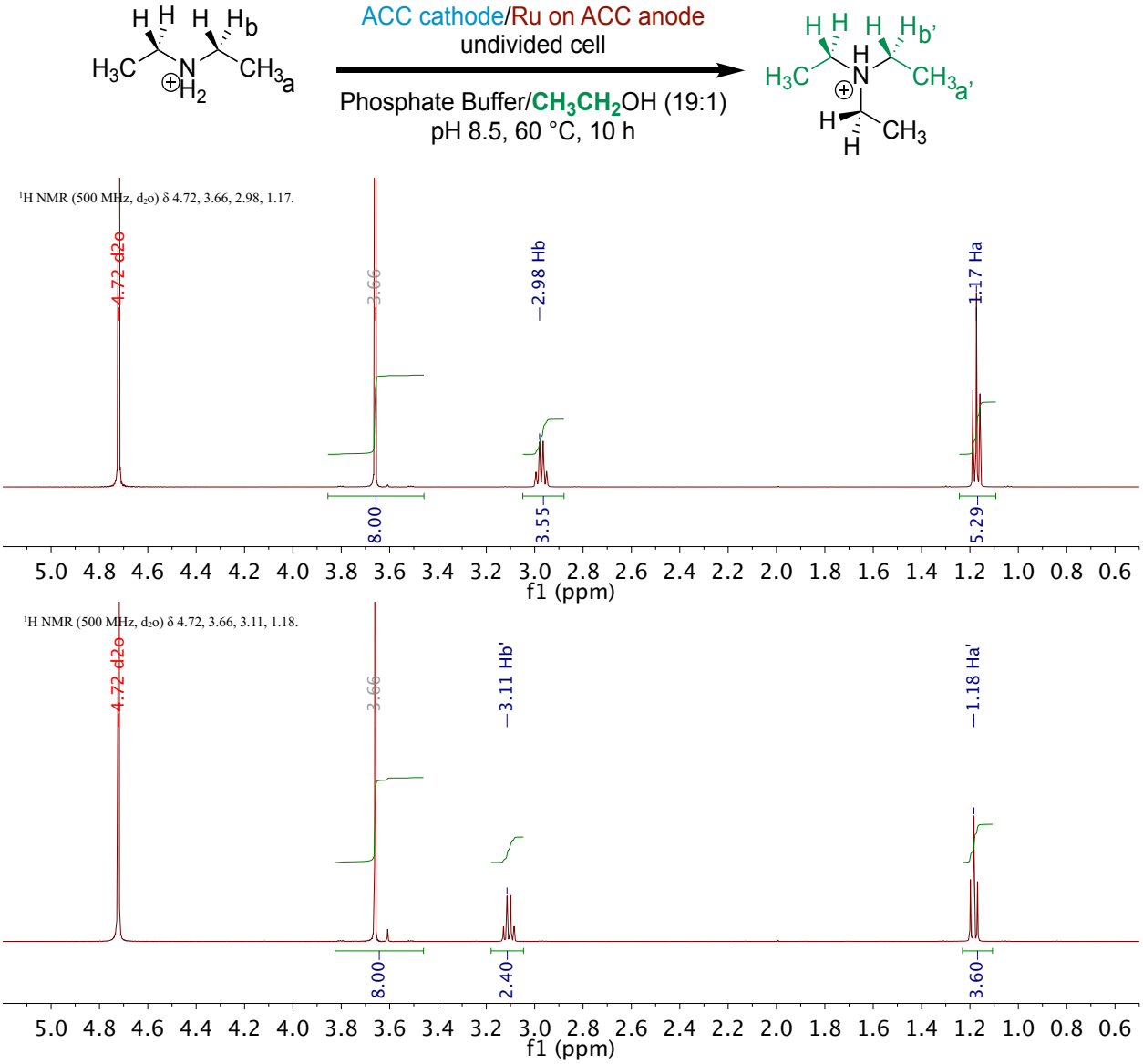

Figure 3.17. The reaction of diethylamine (top) with ethanol at constant current of 2.2 mA/cm^2 yielded 92% triethylamine and 100% conversion (bottom).

^{1}H NMR: Reaction of ammonium hydroxide with isopropyl alcohol

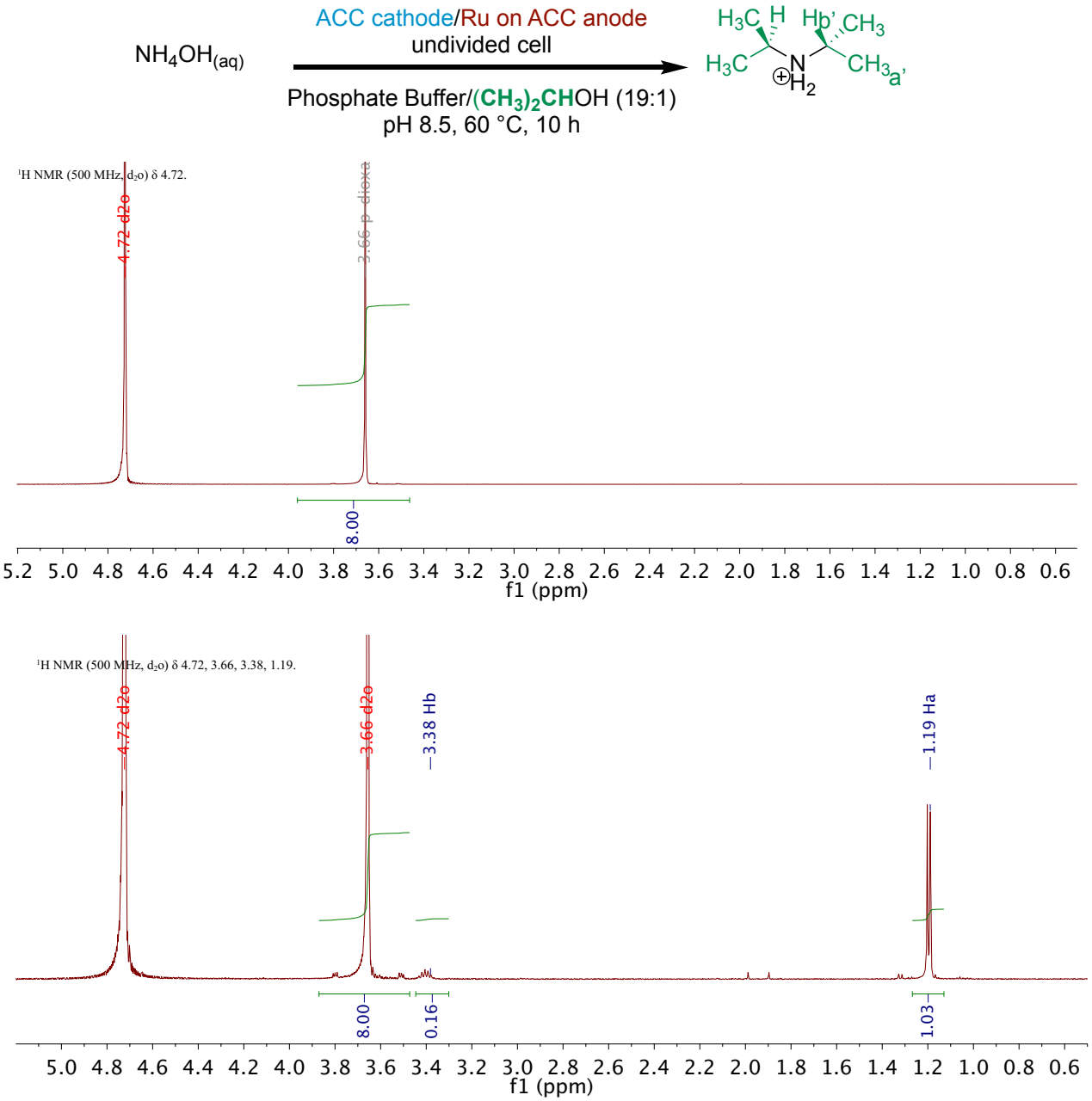

Figure 3.18. The end reaction of ammonium hydroxide (top) with isopropyl alcohol yielded 15% diisopropylamine at 60 °C (bottom).

[1]H NMR: Reaction of ammonium acetate with isopropyl alcohol

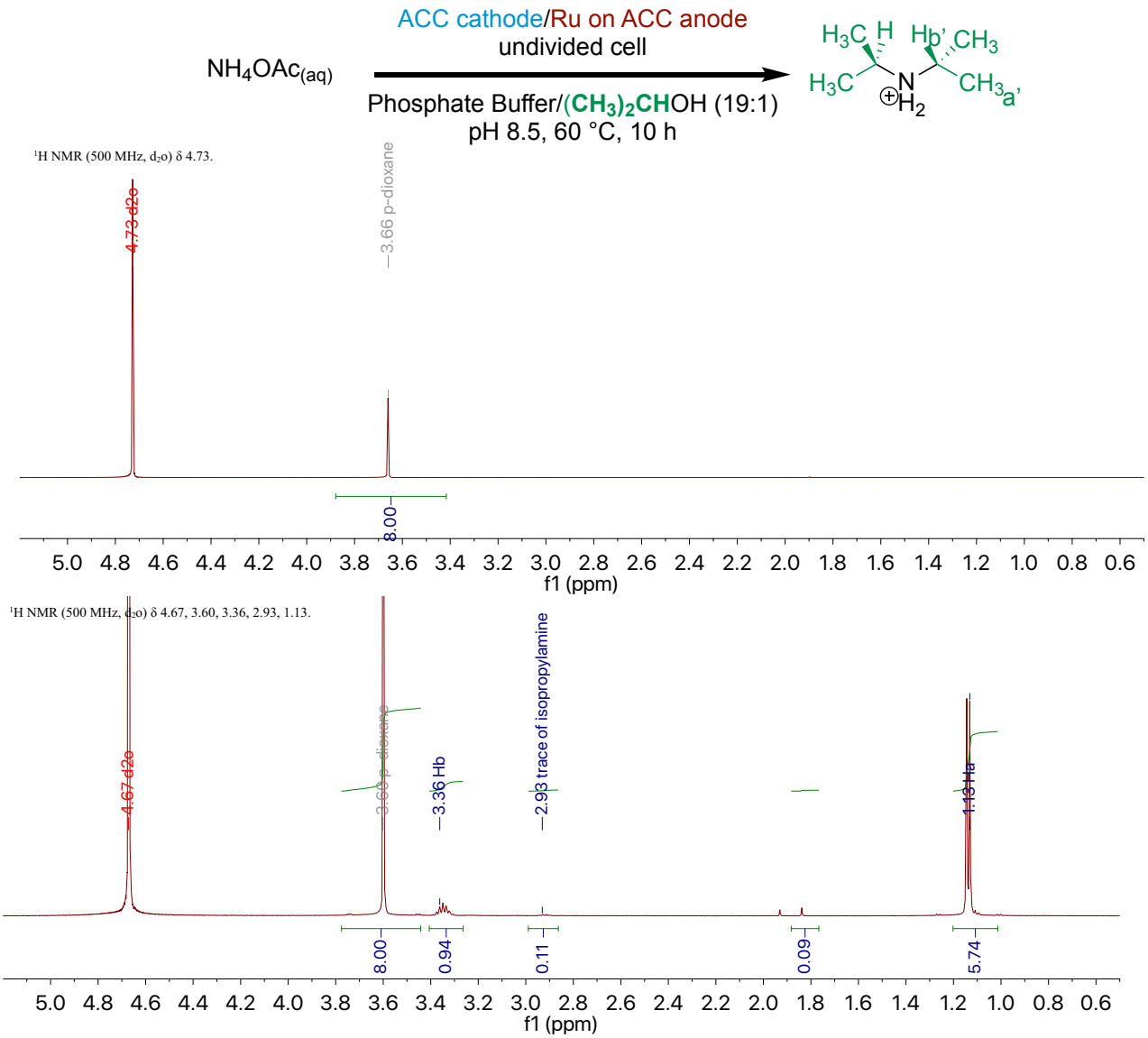

Figure 3.19. The end reaction of ammonium hydroxide (top) with isopropyl alcohol yielded 60 % diisopropylamine at 60 °C with trace of isopropylamine (bottom).

[1]H NMR: Reaction of diisopropylamine with methanol

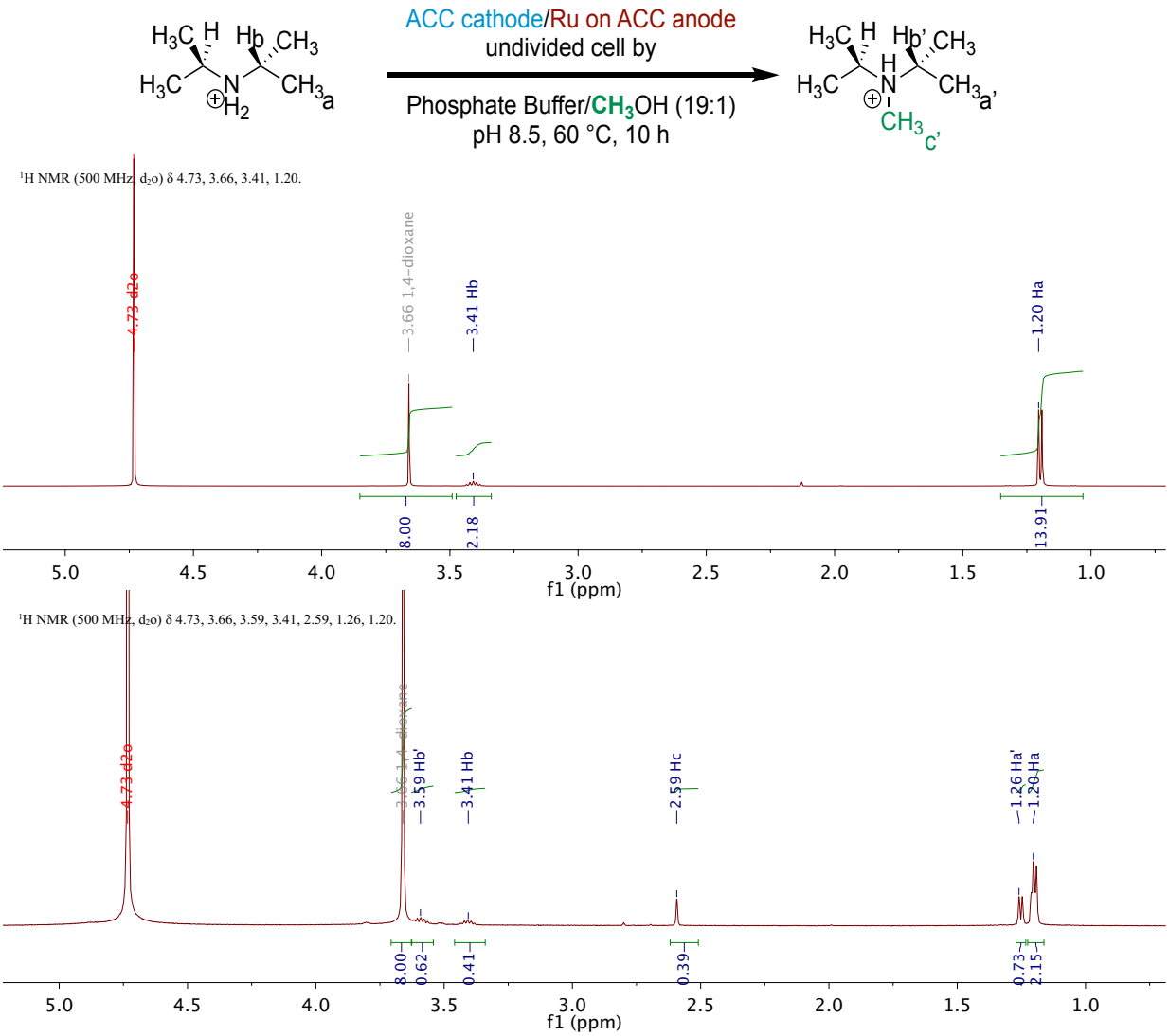

Figure 3.20. The reaction of diisopropylamine (top) with methanol at constant current of 2.2 mA/cm^2 yielded 30% *N*-methyldiisopropylamine and 34% conversion (bottom).

[1]H NMR: Reaction of diisopropylamine with ethanol

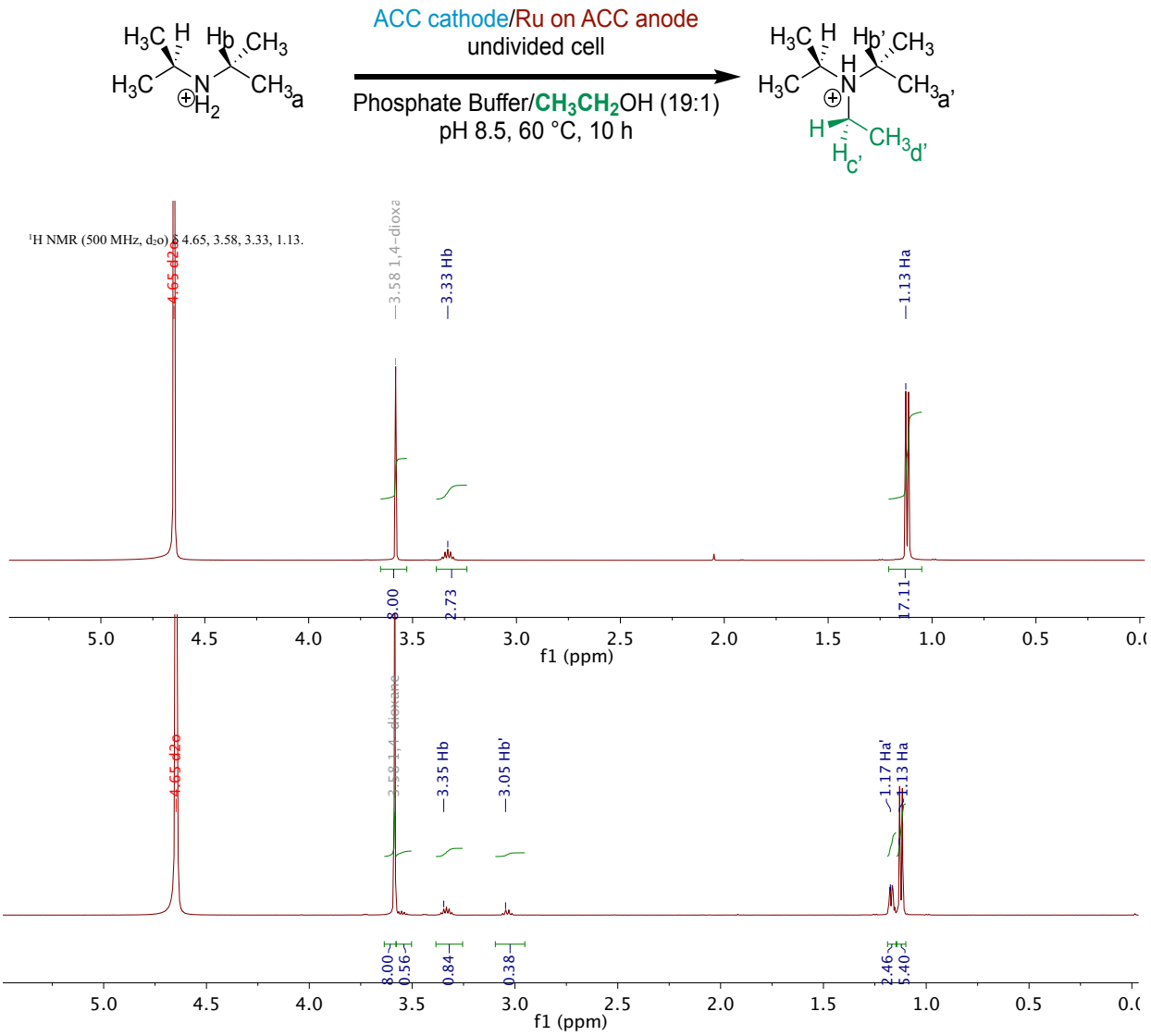

Figure 3.21. The reaction of diisopropylamine (top) with ethanol at constant current of 2.2 mA/cm^2 yielded 34% *N*-ethyldiisopropylamine, a.k.a. Hünig's base and 24% conversion (bottom).

[1]H NMR: Reaction of butylamine with ethanol

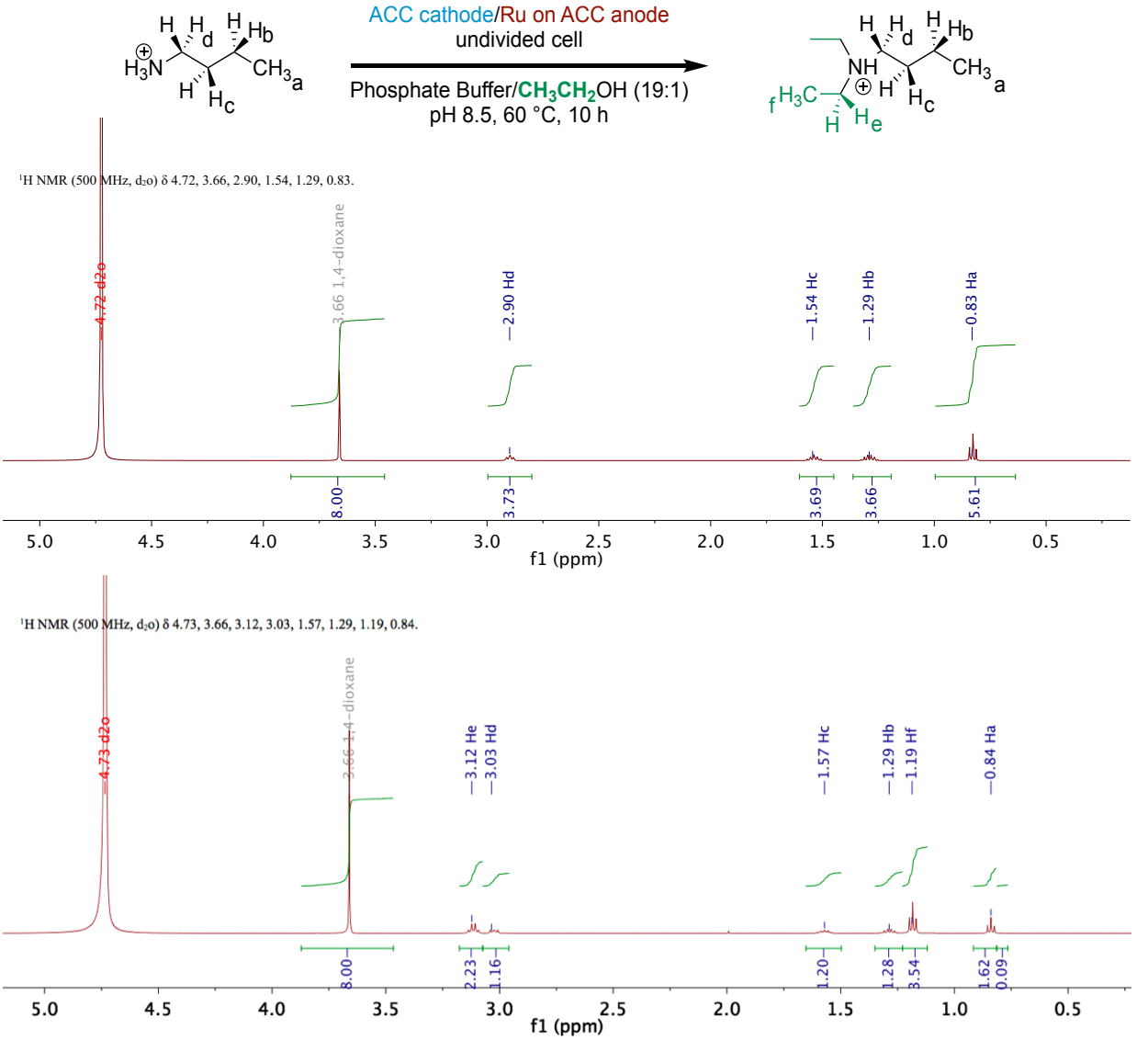

Figure 3.22. The reaction of *n*-butylamine (top)with ethanol at constant current of 2.2 mA/cm^2 yielded 90% *N,N*-diethylbutylamine and 100% conversion (bottom).

^{1}H NMR: Reaction of diethylamine with butanol

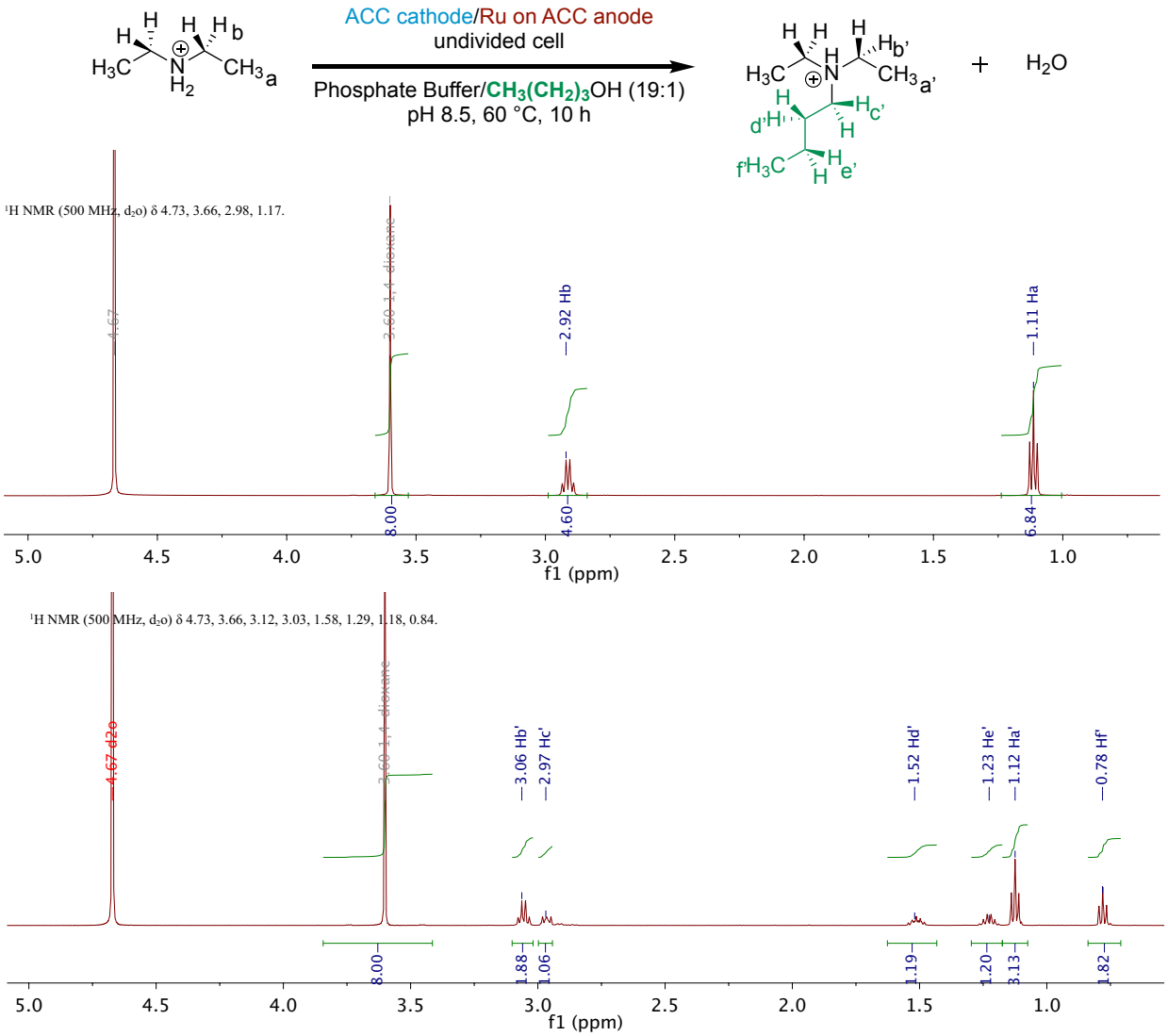

Figure 3.23. The reaction of diethylamine (top) with butanol at constant current of 2.2 mA/cm^2 yielded 90% *N,N*-diethylbutalamine and 100% conversion (bottom).

[1]HNMR: Reaction of pyrrolidine with 4-methylcyclohexanone (divided cell)

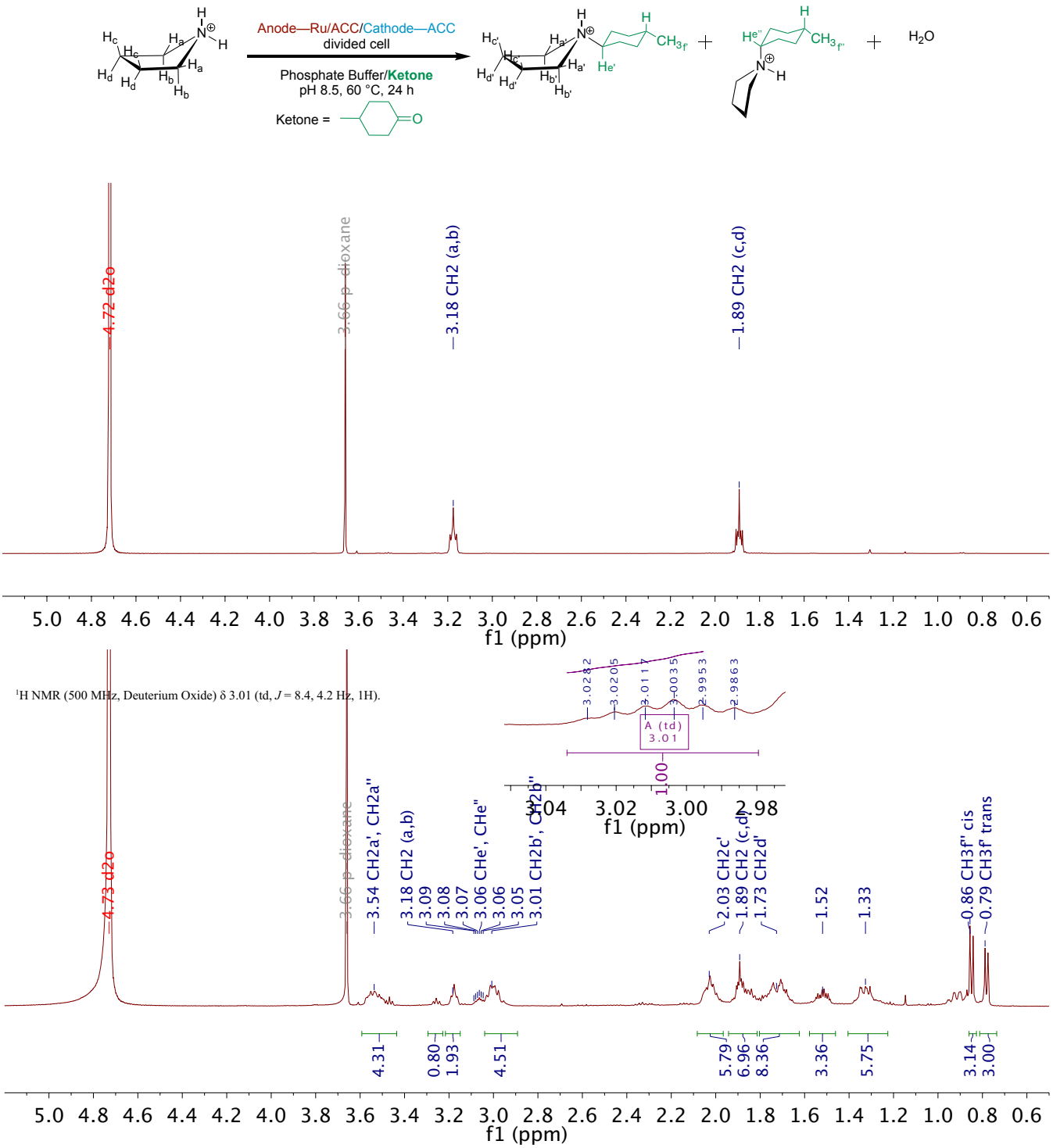

Figure 3.24. The reaction of pyrrolidine (top) with 4-methylcyclohexanone at constant current of 2.2 mA/cm^2 forming 1:1 ratio of cis/trans-4-methylcyclohexylpyrrolidine (bottom).

[1]H NMR: Reaction of pyrrolidine with *cis*-4-methylcyclohexanol (divided cell)

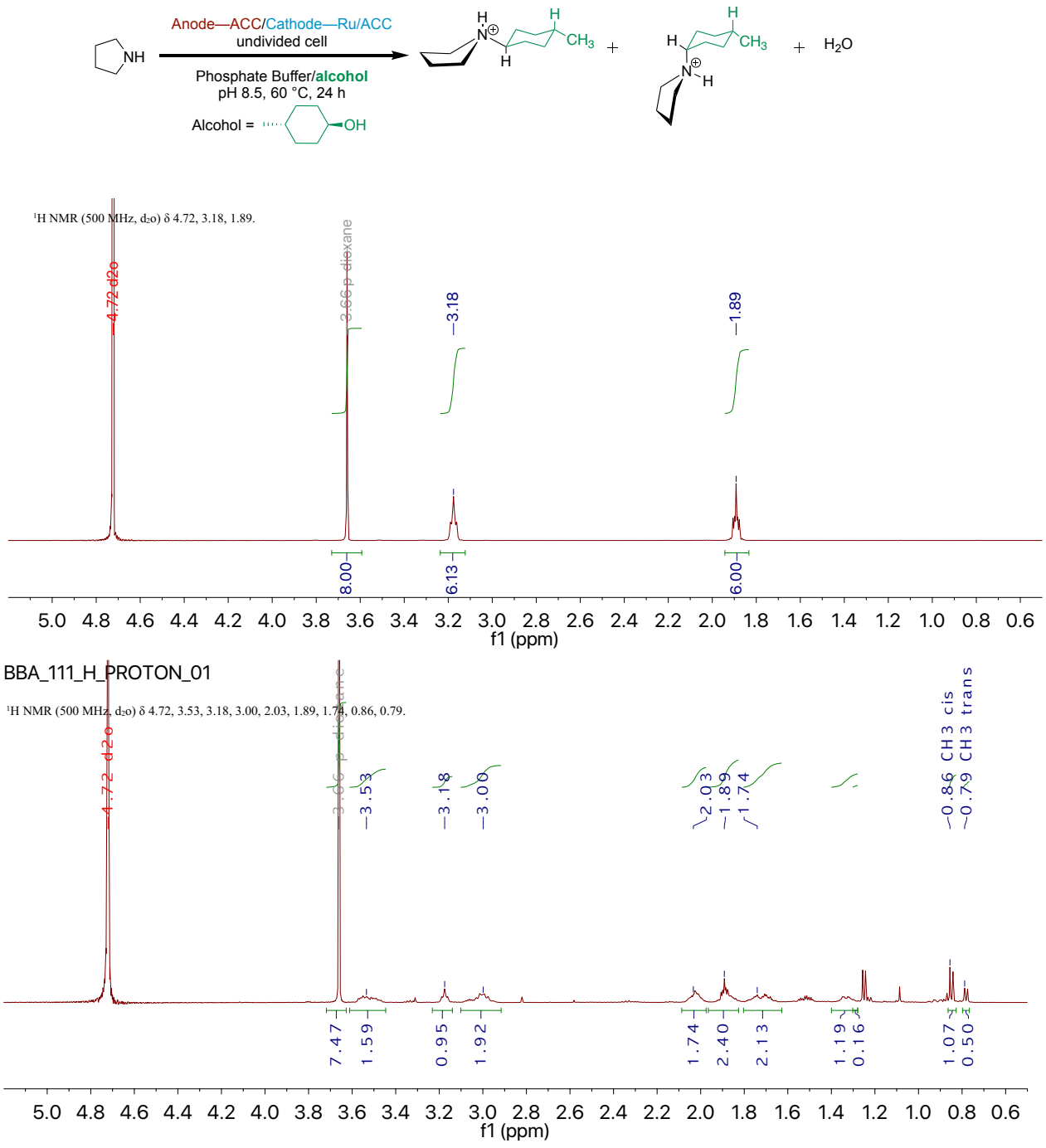

Figure 3.25. The reaction of pyrrolidine (top) with *cis*-4-methylcyclohexanol at constant current of 2.2 mA/cm^2 forming 2:1 ratio of cis/trans-4-methylcyclohexylpyrrolidine (bottom).

[1]H NMR: Reaction of pyrrolidine with 4-methylcyclohexanone (undivided cell)

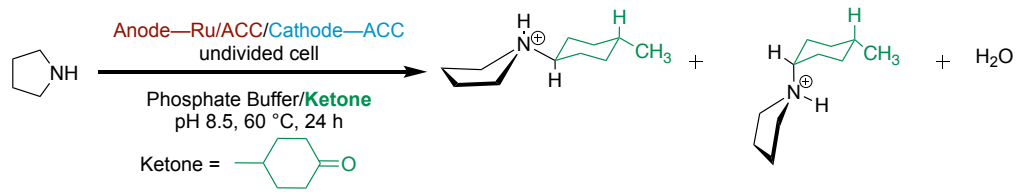

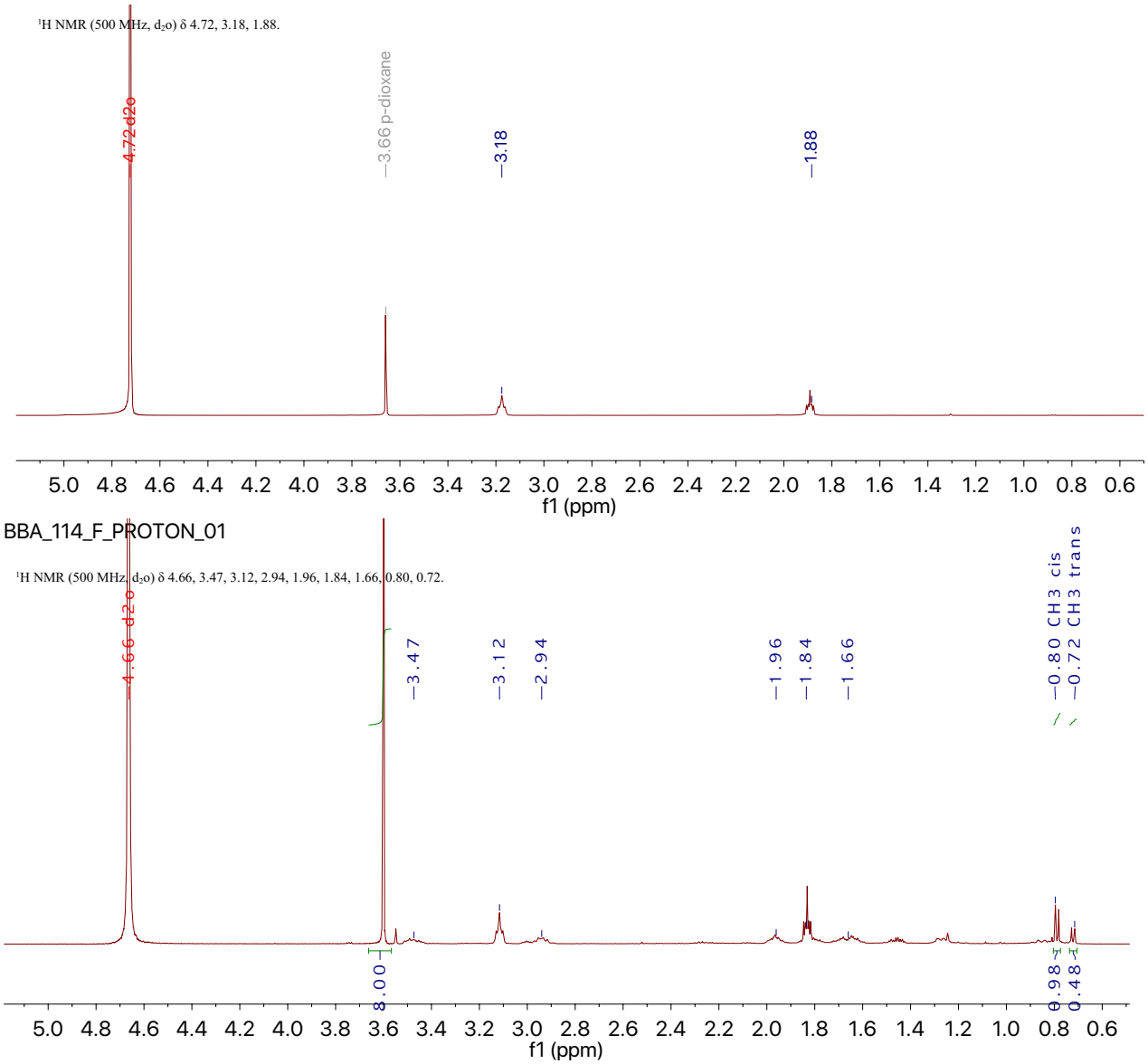

Figure 3.26. The reaction of pyrrolidine (top) with 4-methylcyclohexanone at constant current of 2.2 mA/cm^2 forming 2:1 ratio of cis/trans-4-methylcyclohexylpyrrolidine (bottom).

GC-MS of the Reaction of pyrrolidine with *cis*-4-methylcyclohexanol

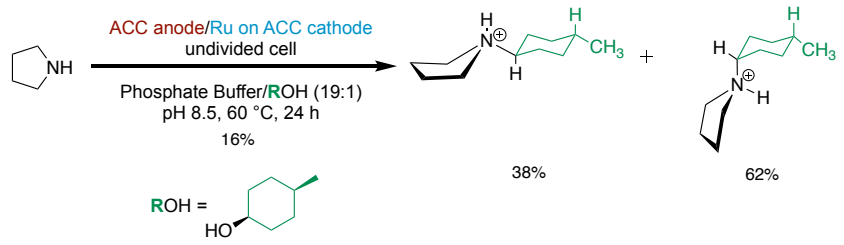

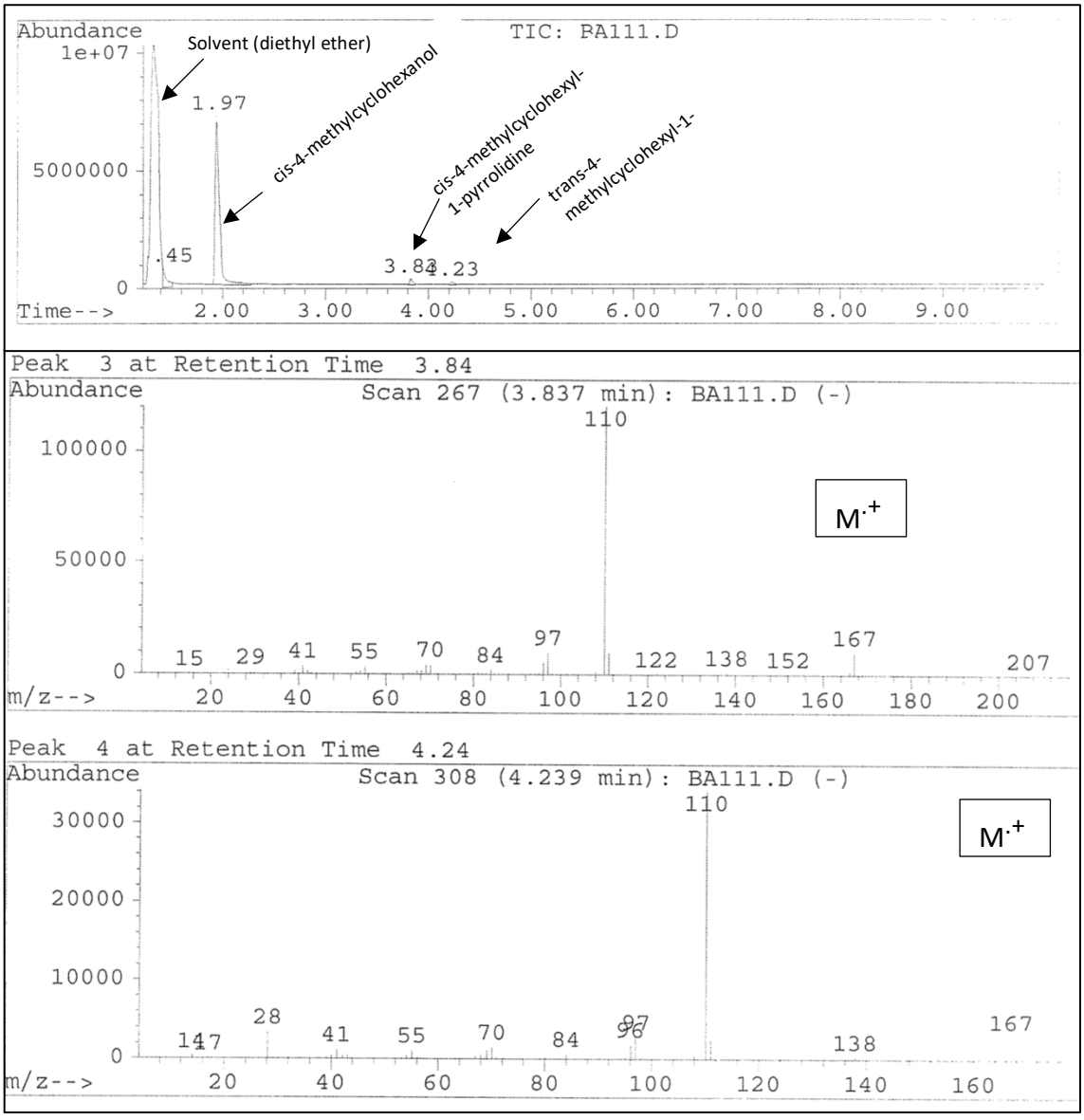

Figure 3.27. GC-MS of *cis* (mp = 137-137.5 ℃) and *trans*-4-methylcyclohexylpyrrolidine (190-192 ℃). [100]

Fragmentations of 4-methylcyclohexylpyrrolidine (deduced from spectra)

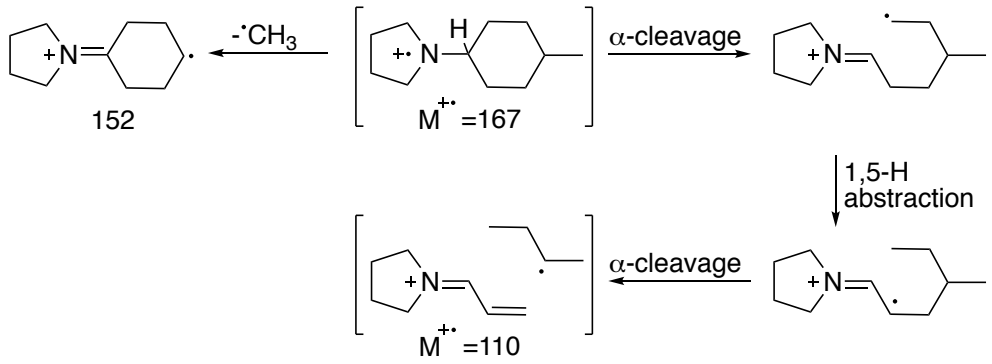

Figure 3.28. Proposed mass spectrometry fragmentation of 4-methylcyclohexylpyrrolidine

CHAPTER 4: REDUCTION OF CARBOXYLIC ACID FUNCTIONALITY IN AMINO ACIDS

Introduction

Carboxylic acids are more difficult to reduce than ketones and aldehydes due to the less reactive carbonyl electrophile. Strong reducing agents such as DIBAH and $LiAlH_4$ or borane (BH_3) are used to reduce carboxylic acids to aldehydes and alcohols respectively. The draw backs of such reactions are (1) these reducing reagents are pyrophoric and sensitive to water, (2) expensive and less cost effective on large scale and; (3) they generate wasteful salt byproducts. Jere et al. have achieved aqueous phase catalytic hydrogenation reduction of carboxylic group of amino acids (*L*-alanine) at 150 °C and 1000 psi using Ru/C powder as catalyst.[67,105] To check for the enantiopurity of the products as well as the stability of the α-H in the amino acid D_2 gas was used instead of H_2. Stereo-retentive H/D exchange was achieved at 100 °C at the α-H of the amino acid and amino alcohols were observed at 150 °C. Electrocatalytic hydrogenation (ECH) reduction analogue of this process was first applied to lactic acid and achieved reduction to both the aldehyde and the alcohol products using Ru/RVC (reticulated vitreous carbon) cathode in a closed cell separated by a frit.[106] These studies inspired the more recent work of Bhatia et al. on electrocatalytic stereo-retentive H/D exchange on carbon bearing —NH_2 and —OH groups.[68] It was envisioned that an amino or hydroxy group on the α-carbon of the carboxylic group could activate its reduction by acting as electron withdrawing group thermodynamically favoring a sp^3 center at the carbonyl carbon. This

project focus on an electrocatalytic version for amino acid reduction in aqueous phase conditions at temperatures below the boiling point of water and ambient pressure (1 atm). Several Ru catalysts including 5% Ru on Carbon trapped in ACC, Ru s sponge trapped in ACC and Ru^{3+} reduced onto ACC by electrodeposition were tried. The latter was found to be the most reactive and more selective for amino alcohol formation over amino aldehyde.

Experimental

Catalyst Preparation

The Zorflex® ACC (activated carbon cloth) FM100, which has high conductivity and large surface area, was used as a support to prepare different kinds of Ru catalyst/electrodes. ACC (3 cm x 1.5 cm) was washed in de-ionized (DI) water and then allowed to dry in an oven overnight at 105 °C.

5% Ruthenium on Carbon Trapped in ACC Electrode

0.1 g of 5% Ru/C powder was circulated in the cathodic half of a divided cell onto an ACC (3 cm x 1.5 cm) cathode at 80 mA (24.4 V) for 30 mins. Coupled with Pt anode and separated by Nafion® membrane, the amino acid substrates were added directly to the cathodic half for reduction. The chambers were charged with 0.20 M HCl or 0.29 M H_3PO_4 solutions.

Ruthenium Sponge Trapped in ACC Electrode

Similar to the preparation of the 5% Ru/C a divided cell was charged with 0.20 M HCl or H_3PO_4 solutions separated by Nafion membrane. 0.1 g Ru sponge was circulated with current flow of 80

mA to trap the spongy particles onto an ACC electrode. Again, the substrate was added to the cathodic chamber after 30 mins of circulation.

Electrodeposited Ru on ACC (Ru/ACC)

The Ru/ACC catalyst was developed by electroreduction/electrodeposition Ru(III) onto ACC as described in chapter 3. A solution of $Ru(NH_3)_6Cl_3$ (1.0089 g) dissolved in ammonium hydroxide (1.98 mL) and water (13.02 mL) was prepared and the dry ACC was soaked in it. The soaked ACC was then dried on the laboratory bench for 24 h and dried in a vacuum at room temperature for another 24 h. The Ru impregnated in ACC was then electrochemically reduced in the H-cell in 0.2 M HCl at a constant current of 150 mA for 30 mins (about 3 times the quantity of charge required). The solution showed three color changes in the progress of the reaction revealing the sequential reduction of Ru(III)-brownish yellow color, Ru(II)-pink color, Ru(I)-blue color and finally colorless Ru(0) which is entrapped in the ACC. The catalyst showed similar reactivity as the H_2 reduced counterpart described by Li et al.[91] and Bhatia et al. [68] Dr. Mahlet Garedew describes the optimum catalyst loading of 4% Ru on ACC for this process in her Ph.D. thesis.[90]

Reaction Procedure

The reaction was performed in a divided two-chamber (2-C) electrochemical cell with either 5% Ru on carbon/ACC, Ru sponge/ACC or Ru/ACC electrodeposited as cathode and Pt as anode with a Nafion®117 membrane as the separator. 20 mM *L*-alanine was used for the preliminary study which was charged into the cathodic half with 0.29 M H_3PO_4 solution in both chambers and run at a constant current of 70 –110 mA. The progress of the reaction was investigated by ^{1}H-NMR.

^{1}H NMR analysis—1 mL of the reaction mixture was taken every 2 h for 10 h and evaporated under a stream of N_2 gas to trap the product species as the ammonium salts. This salt was dissolved in 0.5 mL D_2O containing 20 mM p-dioxane as the internal standard.

Results and Discussion

Preliminary study was performed with *L*-alanine. Ru-carbon/ACC and Ru-sponge/ACC yielded 1.2% and 1.3% of alaninal respectively. The reaction with Ru/ACC electrode gave a 0.75% yield of *s*-alaninol and 0.5% of alaninal. The reaction was feasible with concentrated H_3PO_4 but surprisingly reactions performed with 0.2 M HCl or H_2SO_4 yielded no results. Though the reaction with Ru-sponge/ACC and Ru-C/ACC catalysts gave conversion to the aldehyde intermediate, the Ru/ACC was more efficient to further convert the aldehyde to the alcohol. Hence, the reaction procedure was then optimized for current density, temperature, and H_3PO_4 concentration for using the Ru/ACC cathode.

Reaction Optimizations with Ru/ACC Electrode

H_3PO_4 concentration: The acid concentration was studied at 70 °C from 0.025 M to 0.29 M. The reaction only gave the target product at acid concentrations ≥0.145 M. surprisingly, a species identified decarboxylated product was observed at lower acid concentration (< 0.145 M) (Table 4.1).

Current density: The current flow was initially studied at 70 mA but was further optimized to 10 mA (2.2 $mAcm^{-2}$), which was the amount of current needed to activate Ru as reported by Bhatia et al. in the stereoretentive H/D exchange study.

Temperature: The temperature of the system was investigated from 70 °C to 90 °C, with 70 °C being the most effective.

Surprisingly the reactions only worked with concentrated H_3PO_4 as solvent; no yields were observed when performed with concentrated HCl or H_2SO_4. The reduction of the amino acid requires that its stays protonated, so the excess amount of acid was necessary. Though in the catalytic hydrogenation process only ca. a 20% of excess of acid was required to keep the amino acid protonated throughout the reaction, here in the electrocatalytic system more excess acid was necessary since the acid protons are effectively being converted to hydrogen gas on the catalyst surface. Lowering the acid concentration to 0.2 M increased the yield and gave 8.3% alaninol. Further lowering of the acid concentration to 0.145 M lowered the overall yield to 5.5% of which 3% was alaninol and 2.5% alaninal. The 0.145 M acid concentration was chosen for further optimization. The current flow was lowered to 40 mA and that improved the yield to 17.5% alaninal. From our previous knowledge of the 2.2 mA/cm^{2}current density needed to activate the Ru catalyst, we explored the reaction at current flow of 10 mA (2.2 mA/cm^2) and observed a 21% yield of alaninal. The reaction was further explored at different temperatures of 80 °C and 90 °C which gave slightly lower yields of 16% and 11.5% respectively. It worth noting that at lower acid concentrations the decarboxylated product is observed giving ethylamine. This could be explained by the possible passage of the amino acid through the Nafion® membrane to the anode where oxidation is more likely to occur.

Table 4. 1. Effects of catalysts, acid Concentration, current density and temperature

Alanine Conc./mM	H_3PO_4 Conc./M	Catalyst	Current (mA)	Temp. °C	Yield %	
					Alcohol	Aldehyde
10	0.290	Ru sponge	70	70	0	1.3
10	0.290	(Ru/C) ACC	70	70	0	1.2
10	0.290	Ru/ACC	70	70	0.75	0.5
10	0.200	Ru/ACC	70	70	8.3	0
10	0.145	Ru/ACC	70	70	3	2.5
10	0.145	Ru/ACC	40	70	0	17.5
10	**0.145**	**Ru/ACC**	**10**	**70**	**0**	**21**
10	0.145	Ru/ACC	70	80	0	16
10	0.145	Ru/ACC	70	90	0	11.5
10	0.073	Ru/ACC	70	70	decarboxylation	
10	0.036	Ru/ACC	70	70	decarboxylation	
10	0.025	Ru/ACC	70	70	decarboxylation	

Mechanistic Investigation

In kinetic studies of aqueous classical hydrogenation by Pimparkar et al. it appeared that reduction of amino acids on ruthenium on carbon occurs at two separate sites. The adsorption of the protonated amino acid occurs on one sites (S_1) and the hydrogen dissociation occurs at the other (S_2).[107] The surface reaction energy and binding energy of carboxylic acid on palladium as molded by Neurock et al. suggested that acetic acid dissociates to form an acetyl surface intermediate which is then hydrogenated to form ethanol.[108] Thus the acid is adsorbed with the two oxygens while the dissociated hydrogen atoms on the metal and in the 3-fold coordinate interstices are used for the hydrogenation. The Langmuir–Hinshelwood (L–H) kinetic model studies on the aqueous-phase hydrogenation of alanine to alaninol by Jere et al.[105] suggested that protonated alanine and undissociated phosphoric acid compete for the same site. This could explain why the reaction worked at a certain optimum acid concentration of 0.145 M. The results indicated that at higher acid concentration of 0.29 M and lower concentrations below 0.145 M the reaction yields were much lower.

Conclusions and Outlook

The reduction of a carboxylic acid is certainly a difficult reaction both in the catalytic hydrogenation and in the chemical reduction process with strong reducing agents such as $LiAlH_4$ and BH_3. The electrocatalytic version is even more challenging due to its mildness. Though 21% conversion of alanine was achieved, much further study is needed to fully optimize the yield. Though phosphoric acid worked well, one potentially interesting direction to explore the used of CO_2 as the acid

source. CO_2 is fairly insoluble in acidic aqueous medium, but its solubility could be enhanced in with a buffer electrolyte such as phosphate solution.

Acknowledgements

I would like to thank the students who came along to contribute to this work; Mr. Chris Klap and Megan Moore for their dedication and hard work.

APPENDIX

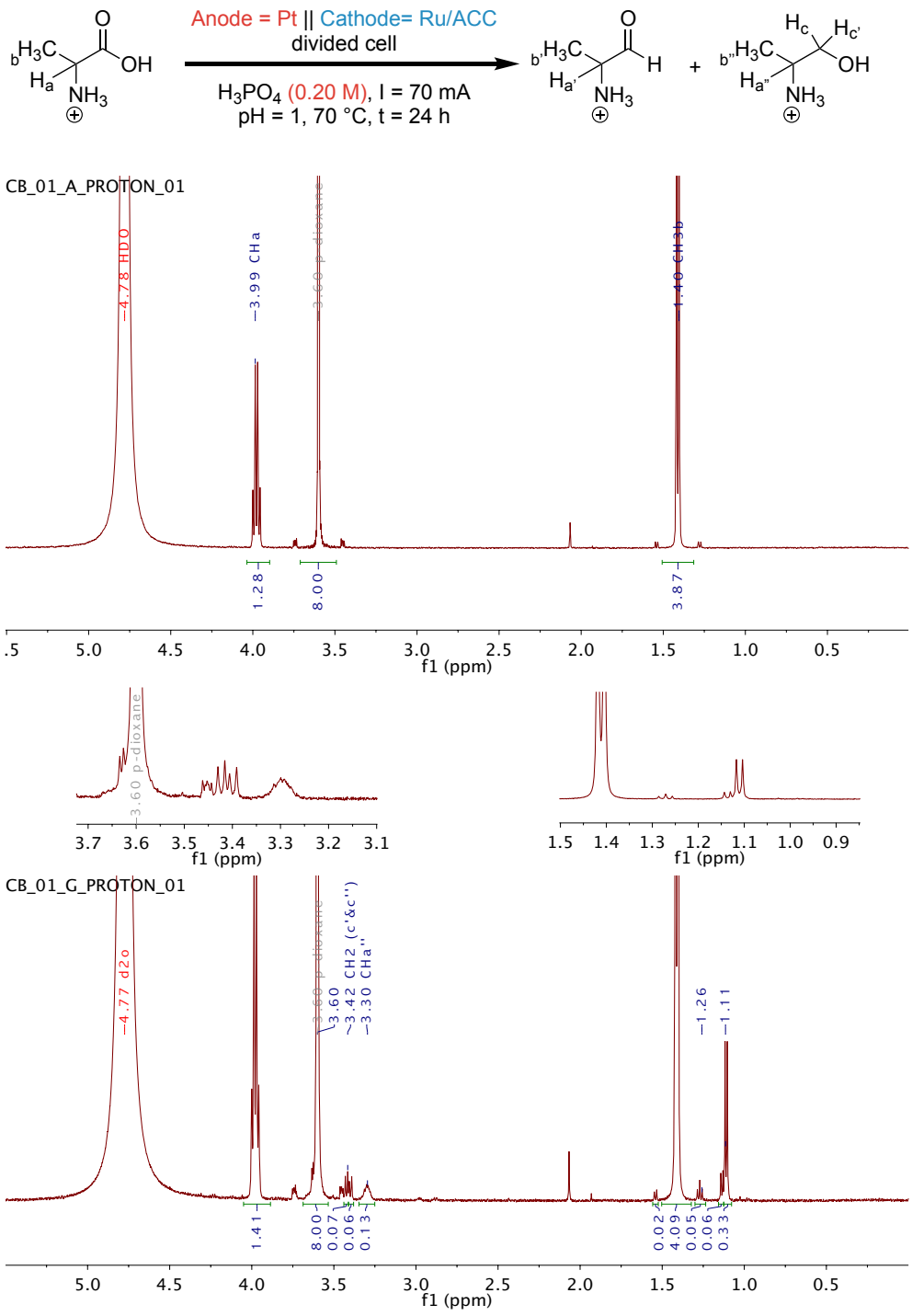

Figure 4. 1. ECH of l-alanine to *s*-alaninol on Ru/ACC in 0.20 M H_3PO_4 for 24 h.

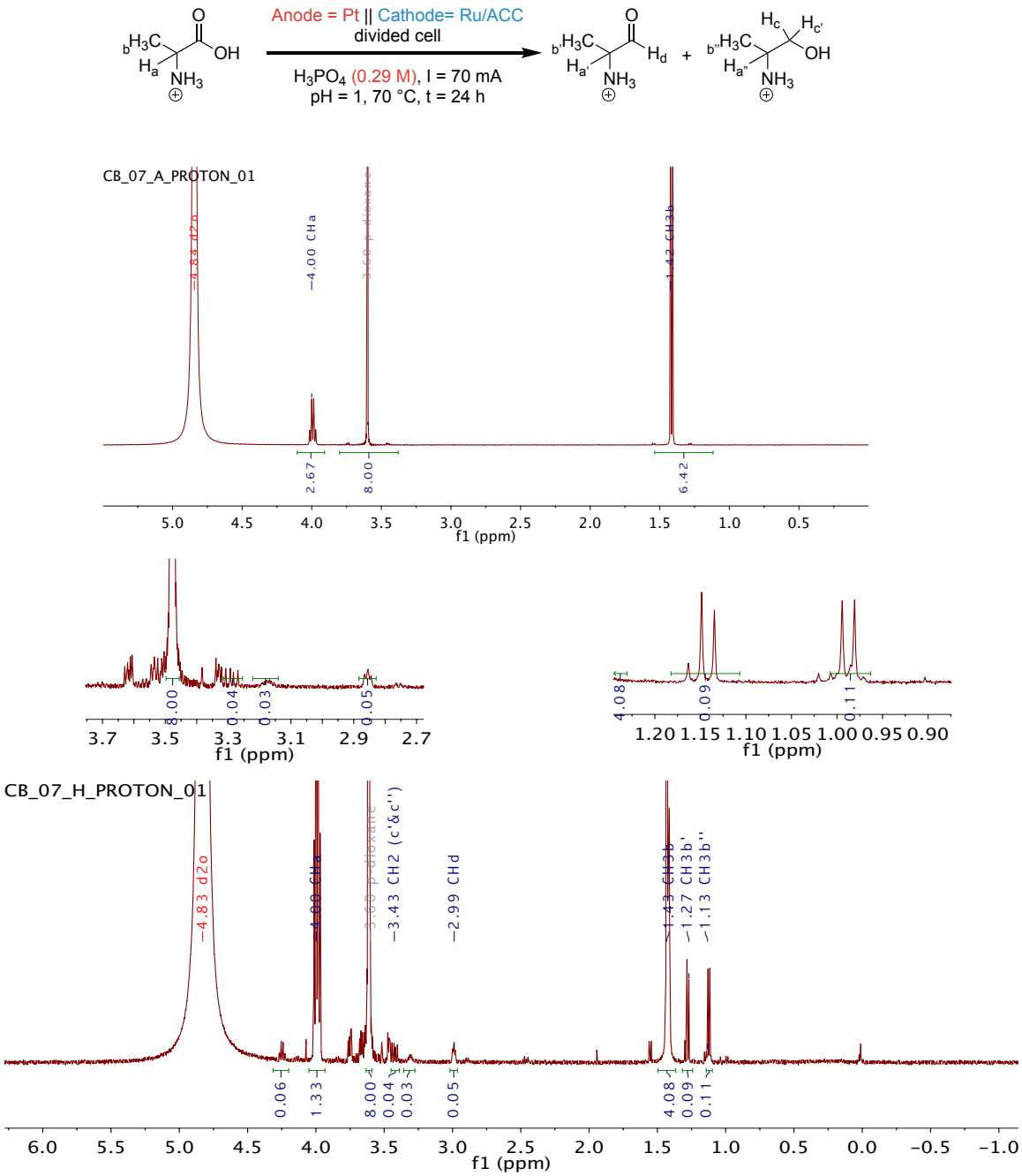

Figure 4. 2. ECH of l-alanine to *s*-alaninal (aldehyde) and *s*-alaninol on Ru/ACC in 0.29 M H_3PO_4 for 24 h.

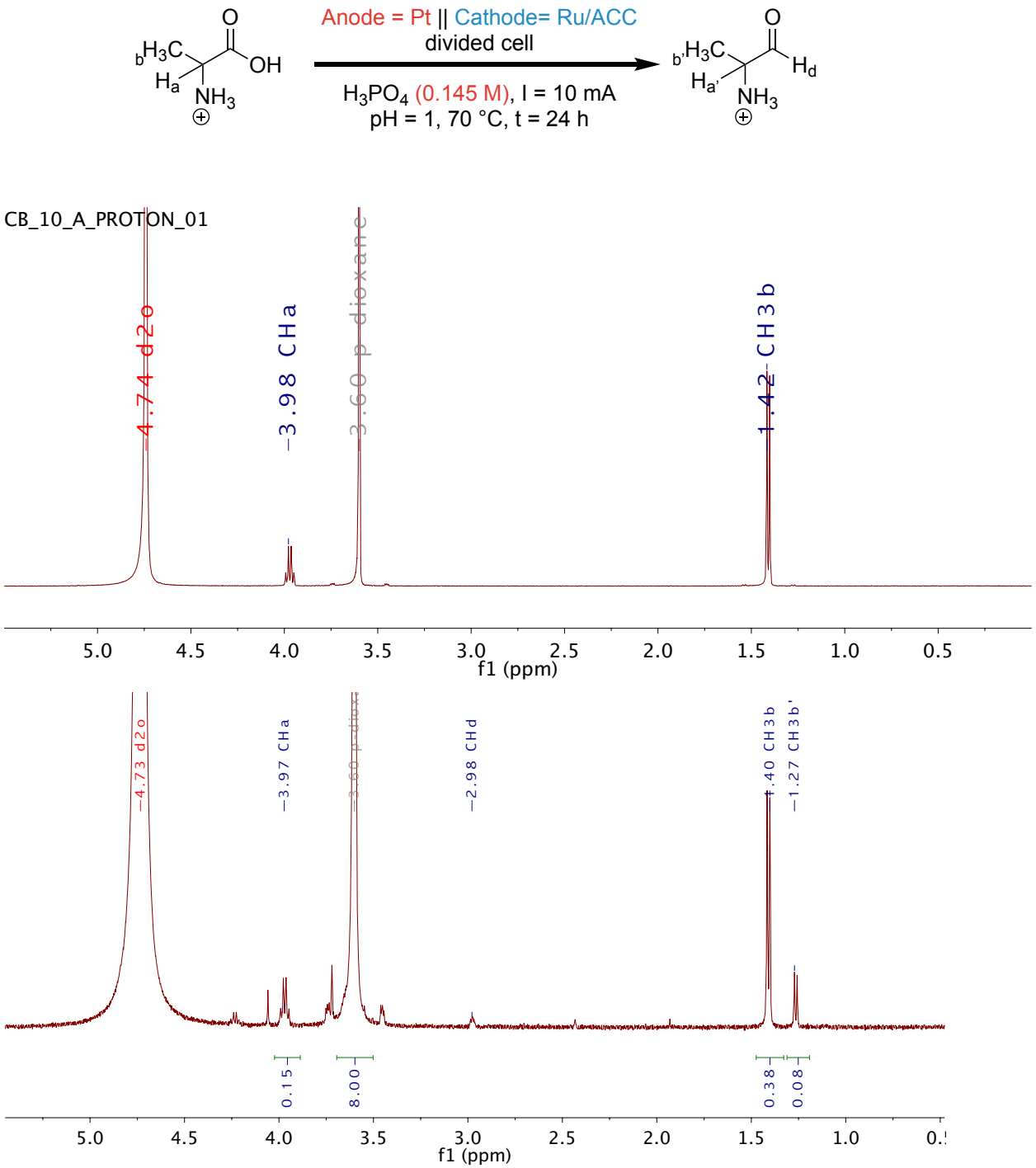

Figure 4. 3. ECH of l-alanine to s-alaninal (aldehyde) on Ru/ACC in 0.145 M H_3PO_4 at 10 mA for 24 h.

CHAPTER 5: ATTEMPTS TO REDUCE POLY- AND PER-FLUOROALKYL SUBSTANCES (PFAS) IN AQUEOUS MEDIUM AS AN APPROACH TO WATER PURIFICATION

Introduction

The electrocatalytic reduction of the carboxylic acid group in perfluoroalkyl substances (PFAS) could serve to convert these potentially dangerous and highly mobile chemicals into their alcoholic derivative. Supposedly, the alcoholic derivates could be excreted or metabolized just like ordinary edible alcohols though its health implications are known. PFAS are nonflammable and the longer chain members are water impermeable which makes them great candidates in domestic product developments such as dirt repellent in carpet, paint, and food packaging. Because of these desirable properties, PFAS have been used since the 1940s.[109] The numerous C–F bonds of PFAS make them chemically stable and persistent in the environment accumulating in the water bodies, foods and in living organisms. Many types of PFAS exist in the chemical industries but the most popularly used and studied for their connections with adverse health effects are perfluorooctanoic acid (PFOA) and perfluorooctane sulfonate (PFOS).[110] These PFAS have been found in several places in the environment such as in plants, drinking and waste water, and in animal and human bloodstreams to an due to bioaccumulation and dispersion.[111] The exposure of PFAS in human serum has connected PFOA to the changes in metabolic pathways, including altering biological

macromolecule (e.g. amino acid, carbohydrate, and lipid) metabolism. PFOA exposure was additionally associated with alterations in animal brains by influencing neurotransmitter concentrations, as seen by a study exposing mice to PFOA for 28 days.[112]

In the present study, ECH has been explored with molecules that could in principle be chemically related to PFAS molecules due to the electron deficient character of the α-C. Li et al. carried out electrohydrogenation on furfural to furfuryl alcohol. Similar to the situation with electrocatalytic lactic acid[106] or amino acid reduction, the α-C bearing the electronegative element N, O or F could have lowered the π^* orbital of the C=O through induction. The findings show that Ni and Fe are the most effective catalyst for the process.[113] These ECH studies show the possibility of electroreduction processes that could be extended to TFA reduction and larger PFAS molecules in the long run.

Model Compounds

TFA and hexafluoroacetone (HFA) were chosen as model compounds of PFAS molecules for this study due to their simplicity in analysis and characterization. TFA reduction, like that of any simple carboxylic acid, requires harsher conditions of highly pressurized hydrogen gas and elevated temperature in traditional catalytic hydrogenation method. ECH offers a potentially mild method which forms hydrogen from protons and electrons in water with the aid of heterogeneous catalysts. This method could incorporate the harvested hydrogens into TFA molecules achieving their reduction. ECH has the green advantage of running at temperatures below the boiling point of water and the ease of heterogenous catalyst removal. Computational simulations of lactic acid

suggested that the -Cα—OH of lactic acid favors conversion to sp^3 character from an sp^2 C=O, hence encouraging its reduction; The electron withdrawing Cα—OH pulls electrons from the C=O lowering its Π^* orbital to accept nucleophiles, electrons or hydrogen atoms. TFA and HFA, therefore, serve as matched candidates for this theory due to the electronegative Cα—F bonds.

Experimental

Catalyst Preparation

Again, electrodeposited Ru/ACC catalyst was developed using Zorflex® ACC FM100 as described in previous chapter. Here, the catalyst was used immediately with the same plating solution without any separate reaction process.

Reaction Procedure

A two compartment H-cell was mounted with a platinum anode and freshly soaked and air-dried Ru/ACC pre-catalyst in the cathodic chamber separated by a Nafion® 117 membrane. The Ru (III) is electrochemically reduced in 0.2 M HCl catholyte while the anolyte was charged with 0.2 sodium carbonate buffer solution with a pH of 8. The reduction process was conducted at a constant current of 150 mA for 30 mins (about 3 times the quantity of charge required). Again, the three color changes revealed the progress of reduction from Ru(III) to Ru(0) (i.e. Ru(III)-brownish yellow color, Ru(II)-pink color, Ru(I)-blue color and finally colorless Ru(0)) were tracked for the completion of the catalyst preparation at room temperature. After 30 mins run with 150 mA, only about ½ the

amount of acid (H^+) from the starting concentration was consumed. While the solution remained acidic with a pH of ca. 1, TFA or HFA was directly added to achieve a 20 mM solution in the cathode side. The reaction was continued to attempt reduction of the substrates at varying current density and temperature values.

Analysis

Wet-NMR study was chosen for the analysis of these studies. This was partly because conversion yields may be very small and wet-NMR provides the advantage of eliminating an extraction process while collected samples can be directly analyzed. Also, wet ^{1}H NMR was supported with ^{19}F-NMR as there are no source fluorine other than the substrate. The NMR tube containing samples directly from the reaction chamber was inserted with a sealed capillary tube containing 97 mM trifluoromethyl benzene (TFB) in DMSO-d6 of 11.53 uL. The capillary tube was then inserted into an NMR tube containing ca 110 uL of reaction sample making the internal standard (TFB) ca 10.1 mM. Initial studies quantifying a known amount (10 mM) of trifluoroethanol TFE gave a 9.5% error with ^{1}H-NMR and 2% error with ^{19}F-NMR. (see supplementary material)

Non-Deuterated (Wet) ^{1}H-NMR and ^{19}F-NMR

^{1}H NMR and ^{19}F NMR spectroscopy were optimized with relaxation time to 25 s to allow enough time for the aromatic protons to relax in time with the fast to relax TFE protons. The water peak was suppressed, and 16 scans were set for reasonable time for data accusation.

Results and Discussion

The reactions with TFA conversion did not yield the targeted products (TFE or the trifluoroacetaldehyde) despite several attempts with various different current density and temperature values. There were, however, traces of species that are unresolved in the NMR (see supplementary data).

The same reaction conditions were applied to the reduction of hexafluoroacetone and yielded possible three possible defluorinated derivatives which presently require further studies for identifications. As expected, the electronegative fluorine atom α to the carbonyl of HFA made it much easier to reduce this substrate.

Conclusion and Outlook

Though the reduction of the TFA was unsuccessful, the insight from the amino acid reduction showed that H_3PO_4 was the ideal solution for the carboxylic acid reduction; these findings may be

applied to the conversion of the TFA in future studies. The reduction of HFA may have opened another reactivity potential to electrocatalytic defluorination

Acknowledgements

A big thank you to Dr. Tayeb Kakeshpour for his help and training of my high school researchers, Ms. Megan Moore and Ms. Ridwan Sheikh-Omar for the NMR studies.

APPENDIX

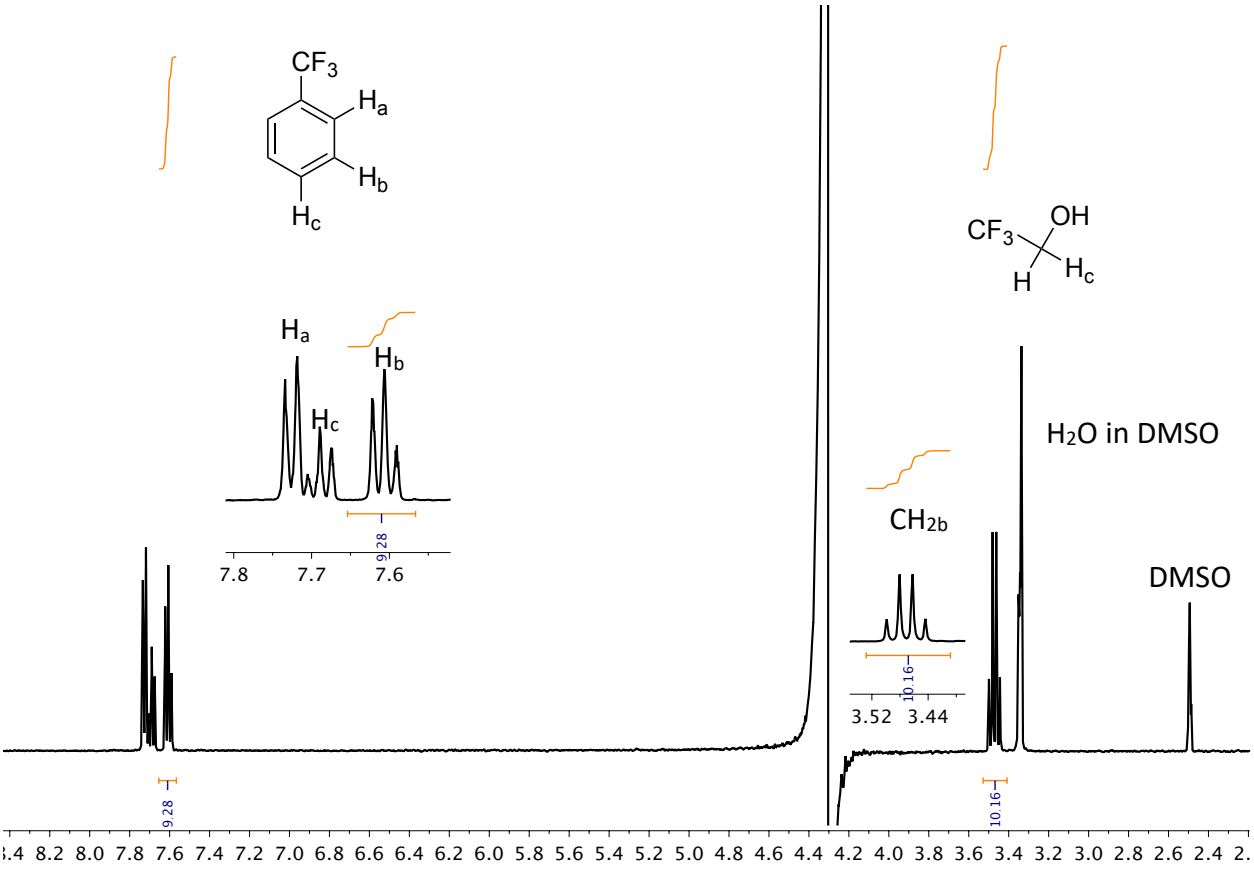

Figure 5. 1. Wet ^{1}H NMR spectrum external standard TFB in DMSO-*d6* in a capillary tube inserted into an NMR tube containing trifluoroethanol (TFE) in H_2O.

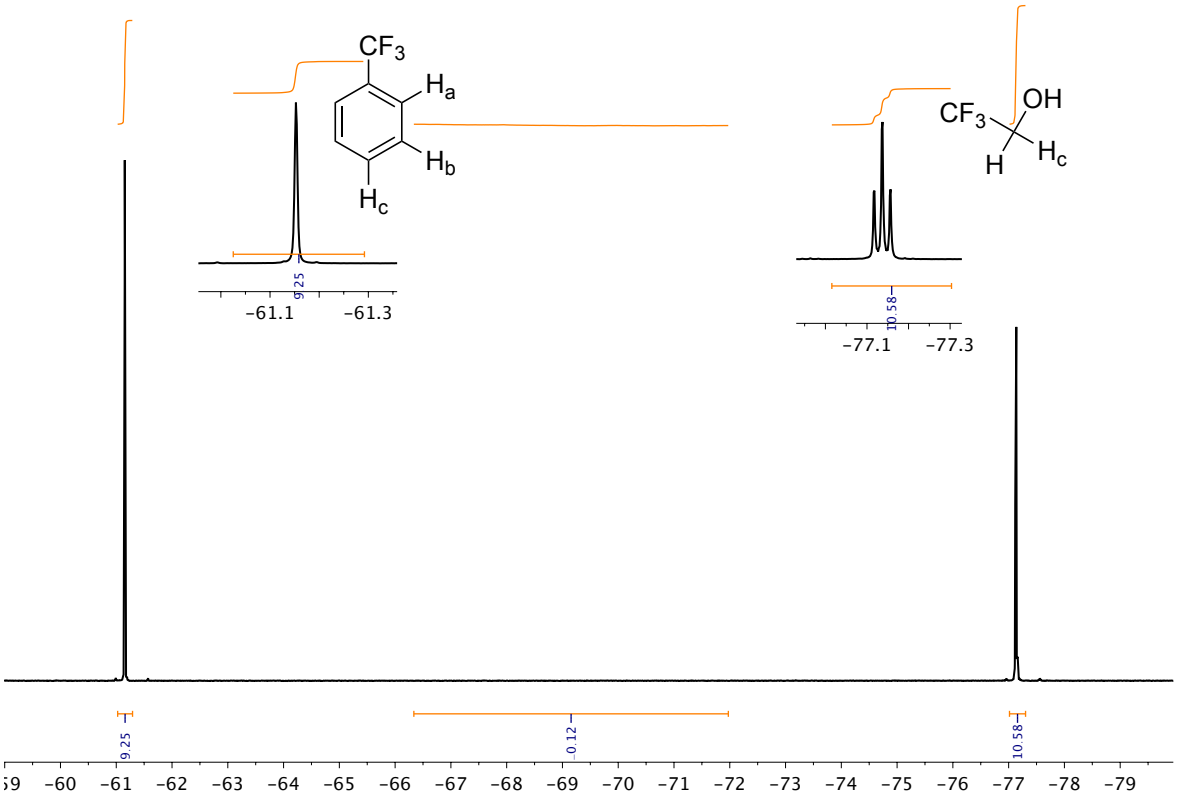

Figure 5. 2. The ^{19}F NMR spectrum showing qualitative and quantitative analysis of TFE with external standard TFB in a capillary tube inserted into the NMR sample.

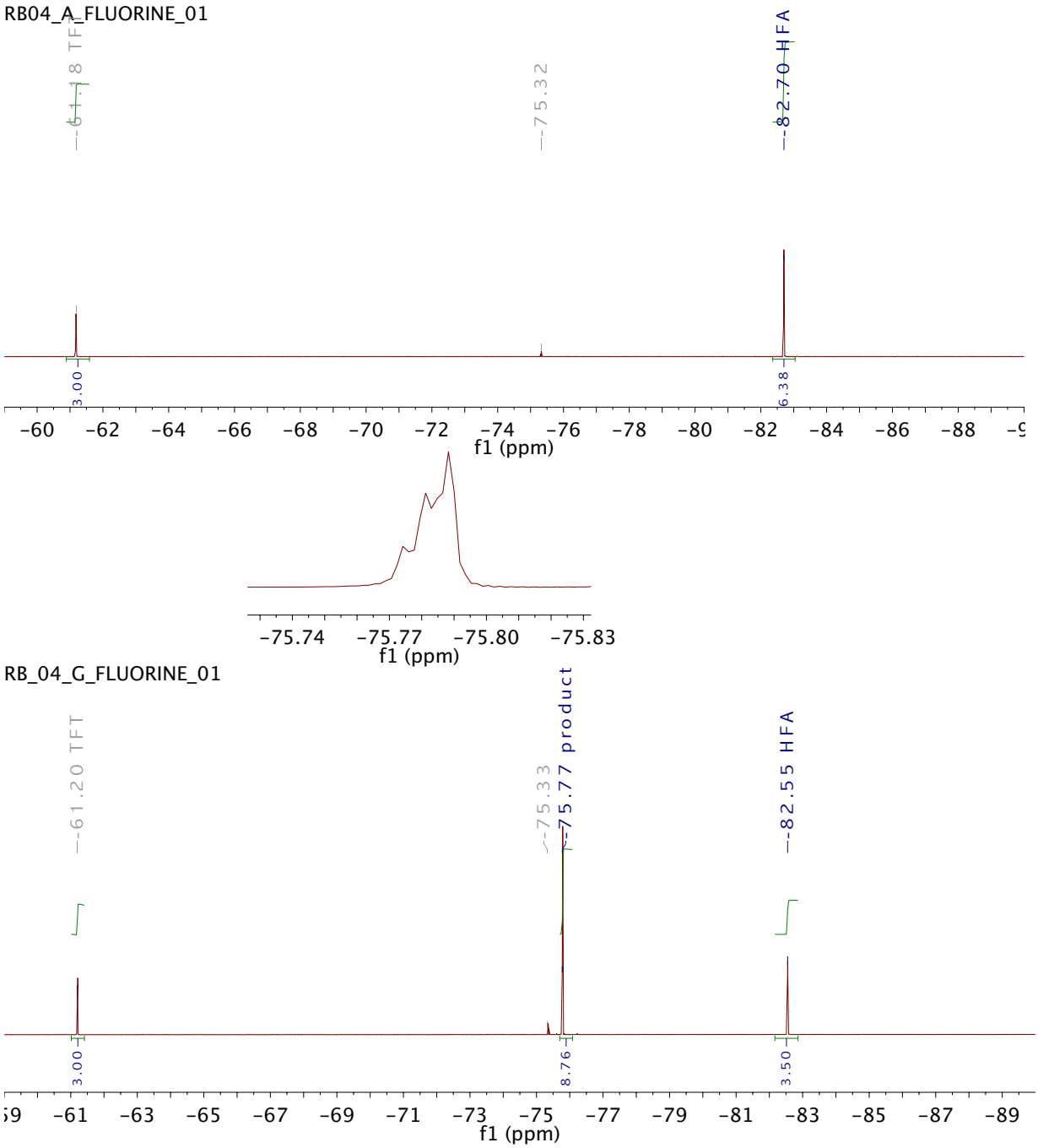

Figure 5. 3. 19F-NMR showing electrocatalytic reduction of hexafluoroacetone to possible defluorination. (top) Initial time 0h and the (bottom) final time 24 h at constant flow of current of 10 mA and temperature of 70 °C.

REFERENCES

REFERENCES

1 M. Faraday, *Experimental Researches in Electricity*, London, UK, Vol 1., 1839.

2 A. K. Vijh and B. E. Conway, *Chem. Rev.*, 1967, **67**, 623–664.

3 W. Zerong, in *Comprehensive Organic Name Reactions and Reagents*, John Wiley & Sons, Inc., Hoboken, NJ, USA, 2010, pp. 1443–1446.

4 F. J. Holzhäuser, J. B. Mensah and R. Palkovits, *Green Chem.*, 2020, **22**, 286–301.

5 A. Hickling and J. V Westwood, *J. Chem. Soc.*, 1938, 1039–1046.

6 M. Baizer and D. Danly, *J. Electrochem. Soc.*, 1975, **122**, C113.

7 H. Lund, *J. Electrochem. Soc.*, , DOI:10.1149/1.1462037.

8 N. L. Weinberg and H. R. Weinberg, *Chem. Rev.*, 1968, **68**, 449–523.

9 T. Mallat and A. Baiker, *Chem. Rev.*, 2004, **104**, 3037–3058.

10 B. Karimi, M. Rafiee, S. Alizadeh and H. Vali, *Green Chem.*, 2015, **17**, 991–1000.

11 M. Rafiee, B. Karimi and S. Alizadeh, *ChemElectroChem*, 2014, **1**, 455–462.

12 G. L. K. Hoh, D. O. Barlow, A. F. Chadwick, D. B. Lake and S. R. Sheeran, *J. Am. Oil Chem. Soc.*, 1963, **40**, 268–271.

13 I. Fried and D. Meyerstein, *Isr. J. Chem.*, 1970, **8**, 865–875.

14 Z. Fang, J. L. R. Smith and X. Qi, *Production of Platform Chemicals from Sustainable Resources*, Springer International Publishing, 2017.

15 J. V. B. Kanth and M. Periasamy, *J. Org. Chem.*, 1991, **56**, 5964–5965.

16 D. Bézier, S. Park and M. Brookhart, *Org. Lett.*, 2013, **15**, 496–499.

17 C. Mettler, *Berichte der Dtsch. Chem. Gesellschaft*, 1905, **38**, 1745–1753.

18 F. Fichter and I. Stein, *Helv. Chim. Acta*, 1929, **12**, 821–826.

19 H. Weil, *Berichte der Dtsch. Chem. Gesellschaft*, 1908, **41**, 4147–4148.

20 C. Mettler, *Berichte der Dtsch. Chem. Gesellschaft*, 1908, **41**, 4148–4150.

21 S. Ono and J. Nakaya, *Nippon kagaku zassi*, 1953, **74**, 907–911.

22 J. M. Chapuzet, R. Labrecque, M. Lavoie, E. Martel and J. Lessard, *J. Chim. Phys. Physico-Chimie Biol.*, 1996, **93**, 601–610.

23 D. Catarzi, L. Cecchi, V. Colotta, G. Filacchioni and F. Melani, *J. Heterocycl. Chem.*, 1992, **29**, 1161–1163.

24 J. Y. Becker and T. A. Koch, *Electrochim. Acta*, 1994, 39, 2067–2071.

25 S. N. Child, R. Raychev, N. Moss, B. Howchen, P. N. Horton, C. C. Prior, V. S. Oganesyan and J. Fielden, *Dalt. Trans.*, 2019, **48**, 9576–9580.

26 Q. Zhang, W. Zhu, J. Yao, X. Li and H. Zhou, *Org. Biomol. Chem.*, 2018, **16**, 8462–8466.

27 R. P. Anex, A. Aden, F. K. Kazi, J. Fortman, R. M. Swanson, M. M. Wright, J. A. Satrio, R. C. Brown, D. E. Daugaard, A. Platon, G. Kothandaraman, D. D. Hsu and A. Dutta, *Fuel*, 2010, **89**, 29–35.

28 C. A. Mullen and A. A. Boateng, *Energy and Fuels*, 2008, **22**, 2104–2109.

29 Y. Tang, W. Yu, L. Mo, H. Lou and X. Zheng, *Energy and Fuels*, 2008, **22**, 3484–3488.

30 Y. Wang, Y. Fang, T. He, H. Hu and J. Wu, *Catal. Commun.*, 2011, **12**, 1201–1205.

31 W. Wang, Y. Yang, H. Luo, H. Peng, B. He and W. Liu, *Catal. Commun.*, 2011, **12**, 1275–1279.

32 P. Wang, S. Zhan, H. Yu, X. Xue and N. Hong, *Bioresour. Technol.*, 2010, **101**, 3236–3241.

33 P. Pan, C. Hu, W. Yang, Y. Li, L. Dong, L. Zhu, D. Tong, R. Qing and Y. Fan, *Bioresour. Technol.*, 2010, **101**, 4593–4599.

34 Y. Lin, C. Zhang, M. Zhang and J. Zhang, *Energy and Fuels*, 2010, **24**, 5686–5695.

35 X. Xiwei, J. Enchen, M. Wang and L. Bosong, *Renew. Energy*, 2012, **39**, 126–131.

36 N. Sorek, T. H. Yeats, H. Szemenyei, H. Youngs and C. R. Somerville, *Bioscience*, 2014, **64**, 192–201.

37 T. A. Khan, J.-H. Lee, H.-J. Kim and J. Ralph, eds. H. Ariffin, S. M. Sapuan and M. A. B. T.-L. for F. B. Hassan, Elsevier, 2019, pp. 153–206.

38 X. Tian, Z. Fang, R. L. Smith, Z. Wu and M. Liu, in *Production of Biofuels and Chemicals from Lignin*, eds. Z. Fang and R. L. Smith Jr., Springer Singapore, Singapore, 2016, pp. 3–33.

39 A. Demirbas, *Energy Sources, Part A Recover. Util. Environ. Eff.*, 2017, **39**, 592–598.

40 Where Wood Works Harnessing the Energy of Woody Biomass in Colorado, https://static.colostate.edu/client-files/csfs/pdfs/Where-Wood-Works-2011.pdf.

41 M. Lynes, *International Energy*, 2016.

42 C. H. Lam, S. Das, N. C. Erickson, C. D. Hyzer, M. Garedew, J. E. Anderson, T. J. Wallington, M. A. Tamor, J. E. Jackson and C. M. Saffron, *Sustain. Energy Fuels*, 2017, **1**, 258–266.

43 C. H. Lam, C. B. Lowe, Z. Li, K. N. Longe, J. T. Rayburn, M. A. Caldwell, C. E. Houdek, J. B. Maguire, C. M. Saffron, D. J. Miller and J. E. Jackson, *Green Chem.*, 2015, **17**, 601–609.

44 C. H. Lam, C. B. Lowe, Z. Li, K. N. Longe, J. T. Rayburn, M. A. Caldwell, C. E. Houdek, J. B. Maguire, C. M. Saffron, D. J. Miller and J. E. Jackson, *Green Chem.*, 2015, **17**, 601–609.

45 L. Delle Site, A. Alavi and C. F. Abrams, *Phys. Rev. B - Condens. Matter Mater. Phys.*, 2003, **67**, 1–3.

46 A. Valavanidis, 2016, 1–33.

47 K. Parmar, *IRA-International J. Appl. Sci. (ISSN 2455-4499)*, 2017, **7**, 42.

48 F. H. Isikgor and C. R. Becer, *Polym. Chem.*, 2015, **6**, 4497–4559.

49 L. O. Ingram and J. B. Doran, *FEMS Microbiol. Rev.*, 1995, 16, 235–241.

50 L. J. Chapuzet Jean Marc, Andrzej Lasia, *Electrocatalysis*, 1998, 155–196.

51 U.S. Patent, 4731496, 1988, (U.S. Patent: 4731496).

52 D. Robin, M. Comtois, A. Martel, R. Lemieux, A. K. Cheong, G. Belot and J. Lessard, *Can. J. Chem.*, 1990, **68**, 1218–1227.

53 M. A. R. Matos, M. S. Miranda and V. M. F. Morais, *J. Chem. Eng. Data*, 2003, **48**, 669–679.

54 P. J. Linstrom and W. G. Mallard, *NIST Chemistry webBook, NIST Standard Reference Database Number 69*, 2014.

55 E. Fujimaki, A. Fujii, T. Ebata and N. Mikami, *J. Chem. Phys.*, 1999, **110**, 4238–4247.

56 M. W. Kanan, Y. Surendranath and D. G. Nocera, *Chem. Soc. Rev.*, 2009, **38**, 109–114.

57 M. A. Varfolomeev, D. I. Abaidullina, B. N. Solomonov, S. P. Verevkin and V. N. Emel, *J. Phys. Chem. B*, 2010, **114**, 16503–16516.

58 B. Appiagyei, S. Bhatia, G. L. Keeney, T. Dolmetsch and J. E. Jackson, *Green Chem.*, 2020, **22**, 860–869.

59 B. S. Sekhon, *J. Pharm. Technol. Res. Manag.*, 2013, **1**, 43–68.

60 J. Genovino, S. Lütz, D. Sames and B. B. Touré, *J. Am. Chem. Soc.*, 2013, **135**, 12346–12352.

61 R. Yadav, M. Ahmed, A. K. Singh and A. Sakthivel, *Sci. Rep.*, 2016, **6**, 1–9.

62 M. B. Smith and J. March, *March's advanced organic chemistry*, Wiley & Sons, New York, 5th edn., 2001.

63 M. Lersch and M. Tilset, *Chem. Rev.*, 2005, **105**, 2471–2526.

64 D. S. Surry and S. L. Buchwald, *Angew. Chemie - Int. Ed.*, 2008, **47**, 6338–6361.

65 C. A. Olsen, M. Witt, J. W. Jaroszewski and H. Franzyk, *Synlett*, 2004, **3**, 473–476.

66 S. Hünig and M. Kiessel, *Chem. Ber.*, 1958, **91**, 380–392.

67 F. T. Jere, D. J. Miller and J. E. Jackson, *Org. Lett.*, 2003, **5**, 527–530.

68 S. Bhatia, G. Spahlinger, N. Boukhumseen, Q. Boll, Z. Li and J. E. Jackson, *European J. Org. Chem.*, 2016, **2016**, 4230–4235.

69 A. V. Naumkin, A. Kraut-Vass, C. J. Powell and S. . Gaarenstroom, NIST Standard Reference Database 20 version 4.1, http://srdata.nist.gov/xps.

70 R. C. Rizzo, T. Aynechi, D. A. Case and I. D. Kuntz, *J. Chem. Theory Comput.*, 2006, **2**, 128–139.

71 J. U. Nef, *Justus Liebig's Ann. der Chemie*, 1901, **318**, 137–230.

72 R. Grigg, T. R. B. Mitchell, S. Sutthivaiyakit and N. Tongpenyai, *J. Chem. Soc. Chem. Commun.*, 1981, 611–612.

73 Y. Watanabe, Y. Morisaki, T. Kondo and T. Mitsudo Ta, *J. Org. Chem.*, 1996, **61**, 4214–4218.

74 M. H. S. a Hamid, C. L. Allen, G. W. Lamb, A. C. Maxwell, H. C. Maytum, A. J. a Watson and J. M. J. Williams, *J. Am. Chem. Soc.*, 2009, **131**, 1766–1774.

75 A. J. A. Watson, A. C. Maxwell and J. M. J. Williams, *J. Org. Chem.*, 2011, **76**, 2328–2331.

76 K. O. Marichev and J. M. Takacs, *ACS Catal.*, 2016, **6**, 2205–2210.

77 R. Kawahara, K. Fujita, R. Yamaguchi and S. Kyoto, *J. Am. Chem. Soc.*, 2010, **3**, 15108–15111.

78 W. Baumann, A. Spannenberg, J. Pfeffer, T. Haas, A. Köckritz, A. Martin and J. Deutsch, *Chem. - A Eur. J.*, 2013, **19**, 17702–17706.

79 A. B. Brown and E. E. Reid, *J. Am. Chem. Soc.*, 1924, **46**, 1836–1839.

80 Y. Zhang, X. Qi, X. Cui, F. Shi and Y. Deng, *Tetrahedron Lett.*, 2011, **52**, 1334–1338.

81 H. Liu, G. K. Chuah and S. Jaenicke, *J. Catal.*, 2012, **292**, 130–137.

82 K. Yamaguchi, J. He, T. Oishi and N. Mizuno, *Chem. - A Eur. J.*, 2010, **16**, 7199–7207.

83 J. He, K. Yamaguchi and N. Mizuno, *Chem. Lett.*, 2010, **39**, 1182–1183.

84 J. W. Kim, K. Yamaguchi and N. Mizuno, *J. Catal.*, 2009, **263**, 205–208.

85 A. Corma, J. Navas and M. J. Sabater, *Chem. Rev.*, 2018, **118**, 1410–1459.

86 K. I. Shimizu, *Catal. Sci. Technol.*, 2015, **5**, 1412–1427.

87 M. A. R. Jamil, A. S. Touchy, M. N. Rashed, K. W. Ting, S. M. A. H. Siddiki, T. Toyao, Z. Maeno and K. Shimizu, *J. Catal.*, 2019, **371**, 47–56.

88 B. G. Reed-Berendt, K. Polidano and L. C. Morrill, *Org. Biomol. Chem.*, 2019, **17**, 1595–1607.

89 B. Ohtani, K. Nakagawa, S. Nishimoto and T. Kagiya, *Chem. Soc. Japan*, 1986, 1917–1920.

90 M. Garedew, in *Ph.D. Dissertation, Michigan State University*, 2018, p. 69,94.

91 Z. Li, M. Garedew, C. H. Lam, J. E. Jackson, D. J. Miller and C. M. Saffron, *Green Chem.*, 2012, **14**, 2540.

92 M. A. Méndez, L. Alibabaei, J. J. Concepcion and T. J. Meyer, *ACS Catal.*, 2013, **3**, 1850–1854.

93 J. T. Kozlowski and R. J. Davis, *ACS Catal.*, 2013, **3**, 1588–1600.

94 R. Yamaguchi, S. Kawagoe, C. Asai and K. I. Fujita, *Org. Lett.*, 2008, **10**, 181–184.

95 A. Maczynski, D. G. Shaw, M. Goral and B. Wisniewska-Goclowska, *J. Phys. Chem. Ref. Data*, 2007, **36**, 59–132.

96 P. J. Stephens, F. J. Devlin, C. F. Chabalowski and M. J. Frisch, *J. Phys. Chem.*, 1994, **98**, 11623–11627.

97 W. J. Hehre, R. Ditchfield and J. A. Pople, *J. Chem. Phys.*, 1972, **56**, 2257–2261.

98 C. Adamo and V. Barone, *J. Chem. Phys.*, 1998, **108**, 664–675.

99 R. Krishnan, J. S. Binkley, R. Seeger and J. A. Pople, *J. Chem. Phys*, 1980, **72**, 650–654.

100 R. O. Hutchins, W. Y. Su, R. Sivakumar, F. Cistone and Y. P. Stercho, *J. Org. Chem.*, 1983, **48**, 3412–3422.

101 C. C. Chambers, G. D. Hawkins, C. J. Cramer and D. G. Truhlar, *J. Phys. Chem.*, 1996, **100**, 16385–16398.

102 D. H. Barich, J. B. Nicholas and J. F. Haw, *J. Phys. Chem. A*, 2001, **105**, 4708–4715.

103 J. R. Cheeseman, G. W. Trucks, T. A. Keith and M. J. Frisch, *J. Chem. Phys.*, 1996, **104**, 5497–5509.

104 A. V. Marenich, C. J. Cramer and D. G. Truhlar, *J. Phys. Chem. B*, 2009, **113**, 6378–6396.

105 F. T. Jere, J. E. Jackson and D. J. Miller, *Ind. Eng. Chem. Res.*, 2004, **43**, 3297–3303.

106 T. S. Dalavoy, J. E. Jackson, G. M. Swain, D. J. Miller, J. Li and J. Lipkowski, *J. Catal.*, 2007, **246**, 15–28.

107 K. P. Pimparkar, D. J. Miller and J. E. Jackson, *Ind. Eng. Chem. Res.*, 2008, **47**, 7648–7653.

108 V. Pallassana and M. Neurock, *J. Catal.*, 2002, **209**, 289–305.

109 Per and Polyfluoroalkyl Substances (PFAS).

110 M. Clara, C. Scheffknecht, S. Scharf, S. Weiss and O. Gans, *Water Sci. Technol.*, , DOI:10.2166/wst.2008.641.

111 These Chemicals Are Forever: Water Contamination from PFOA, PFOS, and other PFAS.

112 N. Yu, S. Wei, M. Li, J. Yang, K. Li, L. Jin, Y. Xie, J. P. Giesy, X. Zhang and H. Yu, *Sci. Rep.*, , DOI:10.1038/srep23963.

113 Z. Li, S. Kelkar, C. H. Lam, K. Luczek, J. E. Jackson, D. J. Miller and C. M. Saffron, *Electrochim. Acta*, , DOI:10.1016/j.electacta.2011.12.105.